UNIVERSITY OF CALIFORNIA, SAN DIEGO

Roles for Wnts and Their Receptors in Topographic Mapping and Laminar Termination

A dissertation submitted in partial satisfaction of the
requirements for the degree Doctor of Philosophy

in

Biology

by

Alisha Richman

Committee in charge:

Professor Yimin Zou, Chair
Professor Andrew Chisholm
Professor Yishi Jin
Professor Barbara Ranscht
Professor Mark Tuszynski

2011

The Dissertation of Alisha Richman is approved, and it is acceptable in quality and form for publication on microfilm and electronically:

Chair

University of California, San Diego

2011

TABLE OF CONTENTS

LIST OF ABBREVIATIONS

Terms

RGC = retinal ganglion cell

SGFS = stratum griseum et fibrosum superficiale (in which RGCs form synapses)

SO = stratum opticum (the outermost layer of the optic tectum)

Directions and Orientations

D = dorsal (referring to dorsal retina)

A = anterior (referring to anterior tectum or being oriented toward the anterior tectum)

L = lateral (referring to lateral tectum or being oriented toward the lateral tectum)

M = medial (referring to medial tectum or being oriented toward the medial tectum)

P = posterior (referring to posterior tectum or being oriented toward the posterior tectum)

V = ventral (referring to ventral retina)

AP = anteroposterior

DV = dorsoventral

ML = mediolateral

Techniques and Statistics

%IB = percentage of primary axons bearing interstitial branches

ABL = average (interstitial) branch length

IHC = immunohistochemistry

ISH = *in situ* hybridization

PAL = (average) primary axon length

LIST OF FIGURES

LIST OF TABLES

ACKNOWLEDGEMENTS

I would like to acknowledge Professor Yimin Zou for his support as my research advisor. His guidance and advice have been crucial to the development of this dissertation research.

Chapters 1 through 4, in part, have been submitted for publication of the material. Richman, Alisha; Zou, Yimin. The dissertation author was the primary investigator and author of this material.

VITA

2005 Bachelor of Arts, Yale University

2011 Doctor of Philosophy, University of California, San Diego

ABSTRACT OF THE DISSERTATION

Roles for Wnts and Their Receptors in Topographic Mapping and Laminar Termination

by

Alisha Richman

Doctor of Philosophy in Biology

University of California, 2011

Professor Yimin Zou, Chair

In topographic mapping, axons project to appropriate targets based upon their spatial positions, with adjacent cells projecting to adjacent targets. During development, retinal ganglion cells project to the optic tectum to map along the tectal surface based on the position of the originating soma in the retina. Retinotectal topographic map formation has been highly studied, but questions about the mechanisms of mapping along the mediolateral tectal axis remain. In this dissertation, I show that the activities and

interactions of two sets of gradients, Wnt3-Ryk and ephrinB1-EphB, are necessary to form an accurate mediolateral map. During map formation, I show that the front of the tectal Wnt3 gradient shifts laterally between E10 and E12, while the ephrinB1 gradient remains stable, generating a laterally-shifting intersection between these two gradients at which mapping forces are balanced. The timing of this gradient movement corresponds to the similarly timed medial-to-lateral development of retinal axons and interstitial branches in the tectum. By overexpressing Ryk and EphB2 and downregulating Ryk via *in ovo* electroporation, I demonstrate that Ryk and EphB2 provide opposing mapping forces within retinal interstitial branches, with Ryk repulsing these branches laterally while EphB2 attracts them medially. These mediolateral direction choices occur near branch initiation without later direction reversals, suggesting that branches respond to specific balance points in a time-limited manner, defining the mediolateral map. This concept of a moving series of balance points which drives opposing forces within growth cones to define topographic positions in a time-specific manner comprises the Moving Gradient Model of topographic mapping.

Interstitial branches invade the tectal surface to select specific deeper tectal laminae for arbor stabilization and synapse formation after map formation. The mechanisms by which these laminae are selected or targeted are largely unknown. In this dissertation, I show that six Frizzleds are expressed in RGC subsets, while five Wnts appear in specific tectal laminae during map formation and tectal laminar targeting. To study how these Frizzleds may affect laminar targeting, I employ *in ovo* retinal electroporation and AChRβ2 labeling to characterize small populations of retinal ganglion cells, as well as to overexpress Frizzled1 to observe targeting effects.

PART I: Wnt3-Ryk Signaling in Topographic Map Formation

INTRODUCTION

The nervous system exists as a series of neural circuits that communicate between various regions of the body to process, interpret, and respond to internal and external stimuli. These precise circuits are generated during development through a series of sequential processes, from the differentiation of neuronal subtypes, to migration of neurons to appropriate locations, to neurite initiation and outgrowth, to the guidance of axons to accurate targets for synapse formation. The molecular cues needed to generate correctly wired neural circuits are provided by both cell-autonomous activities and external signaling molecules, from cell adhesion molecules to secreted ligands. These molecules send signals through receptors in the neuronal growth cone in response to the environment, directing an axon toward or away from a series of intermediate targets in order to reach a site appropriate for synapse formation.

Body regions are systematically mapped onto the central nervous system in an orderly manner, such that signals from areas of the body that are next to each other, such as neighboring fingers, are similarly ordered in the spinal cord and brain. In order to accomplish this, corresponding molecular gradients of axon guidance molecules allow adjacent regions in an originating site to connect with adjacent regions in a targeted brain structure, generating a specific series of sites topographically projected from the body to the brain.

The retinotectal system is the best characterized system for understanding the formation of these topographic maps within the nervous system. To form an accurate map in the chick, retinal ganglion cell (RGC) axons must travel from the retina through the optic chiasm to the contralateral optic tectum, where they form long primary axons along the tectal surface. These primary axons express EphA3 in an increasing nasotemporal gradient in the retina, corresponding to a repulsive increasing anteroposterior gradient of ephrin A2 and A5 in the stratum opticum, the outermost layer of the tectum, driving more temporal primary axons away from higher posterior concentrations of these molecules to generate an anteroposterior tectal map (Nakamura and O'Leary, 1989; Nakamoto et al., 1996; Monschau et al., 1997; Feldheim et al., 2000; Yates et al., 2001). These primary axons sprout interstitial branches, which locate appropriate targets along the mediolateral axis in order to invade the tectum and form synapses in appropriate tectal laminae. These interstitial branches are guided by an increasingly dorsoventral gradient of EphB2 and EphB3 in the retina, which is medially attracted toward a decreasing mediolateral gradient of ephrinB1 in the tectum (Holash and Pasquale 1995; Kenny et al., 1995; Braisted et al., 1997; Hindges et al., 2002; McLaughlin et al., 2003b). However, with just one relative gradient, it would be expected that all axons would collapse to one side of the mapping surface; thus, the mapping activity of a single molecular gradient is insufficient to ensure accurate mapping (Gierer, 1987).

Until recently, Eph-ephrin gradients were the only identified guidance cues involved in retinotectal map formation. However, both theoretical models of retinotectal map formation and experimental results, such as the lateral mistargeting of interstitial

branch termination in EphB2/EphB3-deficient mice, suggested that map accuracy must be generated either through Eph-ephrin biphasic responses (Hindges et al., 2002; McLaughlin et al., 2003b) or via additional opposing gradient cues in the retina and tectum. In 2006, the Zou lab identified an increasing dorsoventral retinal gradient of the atypical receptor tyrosine kinase Ryk, corresponding to a decreasing mediolateral tectal gradient of Wnt3 (Schmitt et al., 2006). The orientation of these gradients would induce a laterally-repulsing Ryk-Wnt3 signal to counterbalance the medially-attractive EphB-ephrinB1 signal already characterized within the retinotectal system.

However, the implications of two opposing gradients have never been explored *in vivo*. Further, in characterizing the *in vivo* mapping activities of Wnt-Ryk gradients, I demonstrated that the Wnt3 gradient itself expands laterally during map formation. In this dissertation, I examine a Moving Gradient Model for mediolateral retinotectal mapping (Figure Intro.1), in which a laterally-expanding Wnt3 gradient intersects with a stable ephrinB1 gradient to generate a series of laterally-moving balance points, corresponding to the medial-to-lateral developmental progression of retinal axons in the tectum. Through the counterbalancing activities of Ryk and EphB2, retinal axon interstitial branches are able to respond to these balance points during a limited developmental time period, targeting appropriate termination zones for arbor formation in the chick optic tectum.

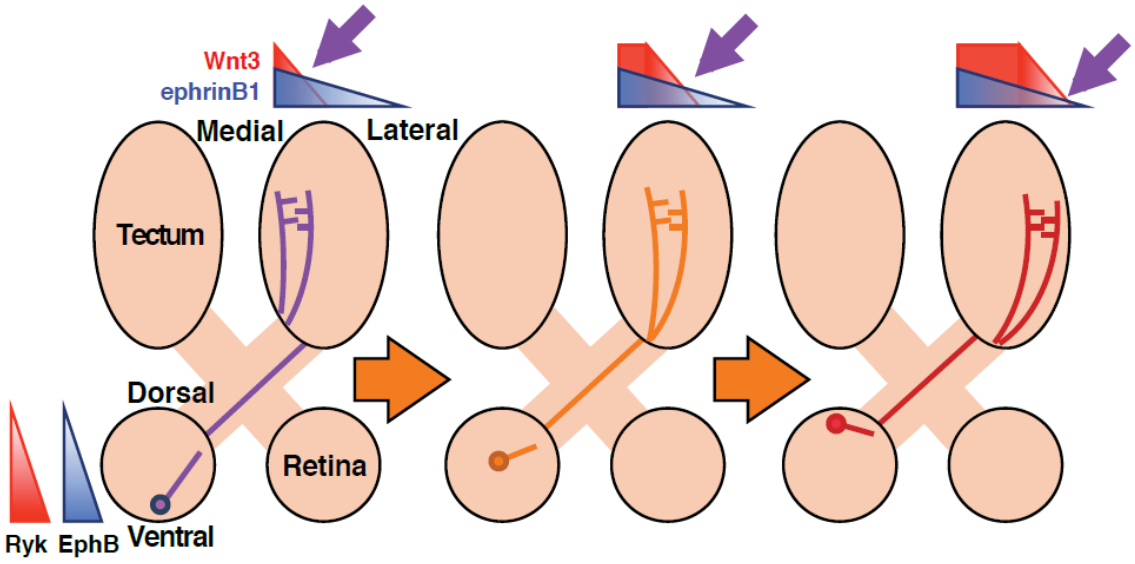

Figure Intro.1. A moving gradient model of mediolateral retinotectal mapping. In the moving gradient model, the lateral shift of a Wnt3 gradient in the context of a stable ephrinB1 gradient generates a laterally-moving series of balance points, where branches lateral of the balance point are attracted medially by higher ephrinB1 concentrations while branches medial of the balance point are repulsed laterally by higher Wnt3 concentrations. This laterally-moving balance coincides with the medial-to-lateral development of retinal axons and their interstitial branches along the tectal surface. Because these interstitial branches can only respond to the Wnt3-ephrinB1 gradient balance points during a limited period, the combination of these features creates a series of termination zones, each centered on a different balance point.

CHAPTER 1: BACKGROUND

Santiago Ramón y Cajal, the father of modern neuroscience, once remarked, "the retina has always [been] shown to be generous to me . . . the retina [is] the oldest and most tenacious of my laboratory loves . . ." (from translation in Piccolino et al, 1989). Indeed, Ramón y Cajal's detailed studies of retinal structure and development extended to chicken, owl, mouse, rabbit, cat, dog, and cow, as well as several invertebrates, frogs, and reptiles (Ramón y Cajal, 1892 [English version 1972] (bird studies); Puelles, 2009). In these studies, he could discern the retinal laminae, various retinal cell types (including the retinal ganglion cells (RGCs) with which this dissertation is concerned), and the connections between these cells as they developed and migrated to their appropriate positions within the retina. Ramón y Cajal also sketched and described the avian optic tectum in detail, noting the development and structure of the tectal laminae and providing the first labeling system for these laminae (Ramón y Cajal, 1889; Ramón y Cajal, 1891; Ramón y Cajal, 1911).

To understand the studies leading up to this dissertation, it is first necessary to understand the basic development of the retinotectal projection, the retinal ganglion cell axon which travels from the cell soma in the retina to appropriate targets in the brain. Fish and frog retinal axons have large growth cones which directly target appropriate topographic positions along the two tectal axes, the anteroposterior and mediolateral axes, simultaneously and without any observed targeting corrections (Stone, 1960; Attardi and Sperry, 1963; Sperry, 1963; Jacobson and Gaze, 1965; Gaze and Sharma, 1970; Harris et al, 1987). The retinal growth cone slows as it approaches its tectal target,

then undergoes back-branching, in which additional branches initiate directly behind the growth cone to develop, along with the growth cone itself, into the retinal arbor (Sakaguchi and Murphey, 1985; O'Rourke and Fraser, 1986; Fujisawa, 1987; Harris et al., 1987). In zebrafish it has been shown that this guidance process does not require competition between axons to generate appropriate topographic order: even if an eye contains only a single retinal ganglion cell, that RGC will target the appropriate location in the optic tectum regardless of the absence of other RGCs (Gosse et al., 2008).

Unlike in fish and frog, the targeting of retinotectal projections in chick and mouse is a multi-step process in which the anteroposterior and mediolateral axes are targeted via distinct morphological events. First, upon reaching the anterior end of the tectum (or superior colliculus), the retinal ganglion cell growth cone directs the primary axon posteriorly, extending beyond the appropriate anteroposterior targeting site (Nakamura and O'Leary, 1989; Simon and O'Leary, 1992a; Simon and O'Leary, 1992b; Yates et al., 2001). The primary axon then begins to sprout interstitial branches along its length, with the highest concentration of branches near the appropriate AP target (Nakamura and O'Leary, 1989; Simon and O'Leary, 1992b; Yates et al., 2001; Lom et al, 2002; Marotte et al., 2004; Marler et al., 2008). These branches travel along the mediolateral tectal axis to the approximate topographic target to invade the tectal (collicular) laminae and form arbors in this termination zone (Nakamura and O'Leary, 1989; Simon and O'Leary, 1992c; Hindges et al., 2002; McLaughlin et al., 2003b). At this point, the overextended primary axon is retracted or eliminated (Nakamura and O'Leary, 1989; Simon and O'Leary, 1990; Hindges et al., 2002; Hoopfer et al., 2006), retinal arbors are refined, and inappropriate arbors are retracted in response to retinal

activity (O'Leary et al., 1986; McLaughlin et al., 2003a; Torborg and Feller, 2005; Chandrasekaran et al., 2005).

Retinotectal studies have made great strides since Ramón y Cajal's early retinal monographs. During the past century, researchers have elucidated the developmental mechanisms behind many aspects of retinotectal development, discerning the nature of many of the developmental and morphological processes described above. Here, I will focus on studies regarding the morphological development of retinal axons during retinotopic mapping, the history of topographic mapping via molecular gradients, and the conceptualization and testing of gradient models to explain topographic mapping.

Interest in the developing (and regenerating) eye as a system for study

At the turn of the previous century, Hans Spemann published a groundbreaking paper on lens formation in the frog *Rana fusca*, showing that when the retinal primordium was entirely removed no eye developed, but that when the primordium was partially removed the development of the lens was dependent on whether the remaining primordium contacted the overlying ectoderm (Spemann, 1901). These results set off a wave of experiments, both within and between species, on the eyes of various animals, leading into the first forays into the amphibian retinotectal system (Lewis, 1904; King, 1905; Spemann, 1907). For example, a series of experiments in salamanders of the genus *Amblystoma* (also known as *Ambystoma*) using heteroplastic transplants of the eye of a larger salamander species into a smaller species (and vice versa) demonstrated that the transplanted eyes grew to the size appropriate to their originating species; the corresponding contralateral tectum and eye muscles in the host species also expanded or

contracted to match the size of the transplanted eye (Herrick, 1925; Harrison, 1925; Harrison, 1929; Twitty, 1929; Stone, 1930; Twitty and Schwind, 1931; Twitty, 1932). Among other features, this suggested a direct connection between eye or retinal size (in terms of cell number or connectivity) and tectal size, which had been similarly previously observed in limb transplants and their target ganglia in the same species (Detwiler, 1920; Harrison, 1924).

Roger Sperry's retinotectal studies and the chemoaffinity hypothesis

Entering graduate school in the 1940s, Roger Sperry became interested in the question of whether neuronal connectivity was important to animal behavior. Though he initially studied motor nerve transplants in adult rats, Sperry soon moved into the visual system of amphibians for better behavioral analysis and ease of neural access (Meyer, 1998; Sperry, 1940; Sperry, 1941; Sperry, 1942). In 1943, Sperry published two papers on visual manipulations on *Trituris viridescens*, the Eastern newt. In the first of these, Sperry rotated the newt's eye 180 degrees and used food presentation (providing a fly on a wire) to check the newt's responses (Sperry, 1943a). If the eye was simply rotated without affecting the optic nerve, or if the nerve was crushed and regrown after rotation, the newt behaved as though the world were upside-down; however, if the optic nerve was cut and regrown without rotating the eye, the newt behaved normally, suggesting that despite rotation, the eye renewed the original eye-brain connectivity to invert the newt's behavioral responses (Sperry, 1943a; Sperry, 1943b). Because the newt's behavioral response failed to readjust to the upright world over time after eye rotation, these studies

argued against a prevailing theory of the time which indicated that behavior itself drove proper connectivity, indicating instead that connectivity was the constant (Sperry, 1951).

Sperry then shifted his experiments into frogs, confirming his newt results in the new system both in adult frogs via food presentation tests and in tadpoles via optokinetic stimulation; even allowing modified tadpoles to age failed to reverse their eye rotation-induced inverted behavior (Sperry, 1944). From this point, Sperry also began to work more directly with the tectal half of the retinotectal system, combining tectal lesions with optic nerve regeneration experiments to demonstrate that loss of tectal targeting areas resulted in loss of vision in a specific part of the visual field, and that this loss was consistent based on the location of the lesion (Sperry, 1944). This, combined with the failure to change behaviors after eye rotation, convinced Sperry that there was a direct specificity of positional connections between eye and tectum, generated by an as yet unknown organizing force (Sperry, 1944). Sperry continued on this path in his next experiments, showing that uncrossing the optic nerves to connect them to the ipsilateral (rather than the usual contralateral) tecta led to these same inverted behavioral patterns, without any learned improvement in the frogs (Sperry, 1945). Even more telling, by removing one eye, rotating it, and transplanting it into the other eye socket (which retains nasotemporal orientation while reversing dorsoventral eye orientation), he observed that tadpoles and salamanders still showed inverted behavioral responses (Sperry, 1945). Histology of these opposite-side transplant tadpoles revealed that the retinal axons from these eyes were, in fact, targeting the contralateral rather than the ipsilateral tectum, the target of their original eye location, clearly indicating that certain retinal and tectal properties caused these axons to select spatially-appropriate targets within the

contralateral tectum; furthermore, given that dorsoventral but not anteroposterior orientation (and behavior) was affected, these organizational activities corresponded to two separately defined axes (Sperry, 1945).

While Sperry worked in other systems to test his ideas through the late 1940s and 1950s, his next major advance did not arrive until the 1960s with studies in fish. During this gap, in 1959, a group of electrophysiologists working on visual physiology reported that retinal axons did in fact return to appropriate retinotopic targets in the tectum after optic nerve regeneration based on electrophysiological recordings (Maturana et al., 1959). These results further strengthened the idea that certain cues between retina and tectum caused a topographically ordered set of projections from the former to the latter. Sperry and Arora responded on the anatomical side with a new study in cichlids, demonstrating that when the medial and lateral branches of the optic tract were separated from each other and regrouped by type, medial with medial and lateral with lateral, the inappropriately placed halves did not follow their new tracts but instead turned back and found the appropriate channels (Arora and Sperry, 1962). Arora refined these surgeries in greater detail with similar results in 1963. Sperry and a second colleague, Attardi, similarly responded with a new anatomical study in goldfish (Attardi and Sperry, 1963). To isolate subregions of the retina, Sperry and Attardi removed half of the goldfish retina (dorsal, ventral, nasal, or temporal), crushed the optic nerve, and labeled the new outgrowth and targeting of the retinal axons from the remaining retinal half into the contralateral tectum. This labeling confirmed their predications: not only did each retinal half target a specific, consistent half of the tectum (nasal retina to posterior tectum and

temporal to anterior, for example), but the optic fibers were also grouped to the correct parts of the optic tract itself prior to tectal innervation (Attardi and Sperry, 1963).

With these results in hand, Sperry set out to elaborate and unify his connectivity ideas in his "Chemoaffinity in the orderly growth of nerve fiber patterns and connections" (Sperry, 1963). In this article, he considered not only the individual neuron-level specificity of connections, but also the idea of position-determining gradients (delineated a good decade earlier by Sperry himself (Sperry, 1951)) creating orderly, direct topographic connections between structures. Indeed, Sperry pointed out his labeling work with Attardi as particularly key in confirming the chemoaffinity concept, as prior work, such as his work in frog and newt, relied heavily on indirect, behavioral measures and thus could not directly demonstrate that some targets or methods of organization for retinotectal projection were preferred over others despite apparently (from an anatomical perspective) equally permissive environments in the optic nerve and tectum.

Refining Sperry's hypothesis with the spatial flexibility of map formation

Despite a growing body of evidence, many expressed serious reservations about the chemoaffinity hypothesis and the general idea that retinal and tectal chemical gradients ordered retinotectal projections. Among these, some were openly skeptical of the chemoaffinity hypothesis on the whole, while others identified or confirmed principles that were either reinterpretive of or complementary to chemoaffinity for tectal map organization.

In 1959, Michael Gaze recorded action potentials from the tecta of adult frogs whose optic nerves had been severed as tadpoles to demonstrate that topographic order between eyes and tecta was restored regardless of whether the eye was rotated or upright, in support of Sperry's observations (Gaze, 1959). However, many of Gaze's studies went on to delineate inconsistencies in the development, growth, and regrowth of retinotectal projections in light of Sperry's chemoaffninity hypothesis, particularly with regard to neuronal environment conditions producing dissimilar effects during normal development and after optic nerve regeneration. Gaze in particular noted Stone's 1948 studies of eye rotation in a series of different ages of *Amblystoma*, in which the inverted behaviors studied by Sperry were only observed as a result of eye rotation at time points occurring after retinal topography had been established, suggesting the possibility of highly different conditions for developing and regenerating retinotectal projections (Stone, 1948; Gaze et al., 1963). Gaze expanded in part on the work of Székely, which showed that when the targeted tectal half was destroyed after innervation by double-nasal (rostrally-targeting) or double-temporal (caudally-targeting) eyes, the modified newts became blind (Székely, 1954). By generating embryonic frogs with double-nasal or double-temporal eyes and raising them until electrophysiology was possible, Gaze et al. determined that the topographic maps of these frogs appeared to cover an entire tectum worth of surface, and furthermore that the covered tectal surface did not represent an expansion of the normally targeted tectal half with the atrophy of the untargeted half, but rather was due to the retinal axons from these double-nasal or double-temporal eyes spreading across the normal, unmodified tectum (Gaze et al., 1963; Gaze et al., 1965 (related half-retinal studies in fish: Schmidt et al., 1978)).

While Sperry continued to argue for the direct, one-to-one specificity of chemical targeting in the retinotectal system, supporting the interpretation that the expansion of the appropriately labeled tectal half with atrophy of the untargeted half allowed for Gaze's full-tectal maps, Gaze and associates continued to provide further evidence that these double-nasal or double-temporal retinas targeted the full, normal tectal field (Sperry, 1965; Gaze et al., 1965; Straznicky and Gaze, 1971; Straznicky et al., 1979; Gaze and Straznicky, 1980; Straznicky and Gaze, 1982). In related experiments in fish, Gaze and Sharma demonstrated that when the posterior tectum was removed and the optic nerve severed and regenerated, the entire retinal map was organizationally compressed onto the remaining anterior tectal half, which did not grow to accommodate the increased innervation (Gaze and Sharma, 1970). Furthermore, when looking at the natural expansion of the tectum in frogs as they aged, corresponding to the peripheral addition of retinal ganglion cells in the adult frog eye, Gaze and colleagues noted that in order to appropriately place connections from these new peripheral RGCs, already present retinotectal connections shifted to provide accurate topographic targets (Gaze et al, 1974 (related topographic expansion in fish: Johns, 1977; Easter et al., 1981; Rusoff and Easter, 1983; Rusoff, 1984; Steurmer and Easter, 1984)). These experiments, taken together, indicated a degree of flexibility to the retinotectal topographic map which failed to conform to Sperry's narrow expectations of a direct correspondence between retinal and tectal positions based on specific cues. They argued instead for a degree of relativity or plasticity in mapping, given that the retinotectal projections appeared to expand and contract the map yet retain spatial order, based upon the tectal surface available, and that connections were shifted over time to add new retinal axons to topographically

appropriate locations. Overall, these notions suggested a sliding scale model of topographic mapping (Sperry, 1975).

Refining Sperry's hypothesis through the preordering of retinal inputs

A second area of dissent from the chemoaffinity hypothesis involved the idea that retinotopic order was generated not by chemical gradients but instead by the basic pre-ordering and maintenance of ordering of retinal axons during development. Several groups noted that the retinas of several fishes developed their retinal ganglion cells in a central-to-peripheral sequence (Horder and Martin, 1978; Scholes, 1979; Bunt, 1982; Rusoff, 1984). This developmental sequence, along with positioning along the retinotopic axes, was retained throughout the optic nerve as the retinal axons extended toward the tectum, although the methods of targeting along the tectal surface were not necessarily attributable to this developmental sequence (Attardi and Sperry, 1963; Scalia and Fite, 1974; Horder and Martin, 1978; Scholes, 1979; Bunt, 1982; Rusoff, 1984). Additionally, a ventral discontinuity in the fish optic nerve due to the ventral fusion of the retina in early development (and corresponding to the choroid fissure seen in such animals as cichlids and chickens) showed that the optic nerve conserved structural rather than topographic order; this suggested that the adjacency of neurons in topographic mapping was less relevant than the immediate physical presence of neighboring cells or axons in deriving order (Scholes, 1979; Bunt, 1982; Rusoff and Easter, 1983; Thor et al., 1990). Furthermore, this preordered arrival sequence for tectal targeting in fish appeared to reoccur in a less orderly manner after optic nerve regeneration, despite developmental

and anatomical studies indicating a role for both physical organization and chemical cues in this guidance (Bunt et al., 1978; Scholes 1979; Bunt, 1982; Rusoff, 1984).

However, while some organisms, such as the aforementioned fish, showed a strong degree of developmental order over chemoaffinity, others formed accurate retinotopic maps despite having variably disordered optic nerves, suggesting definite variation in the necessity of preordering and chemoaffinity for accurate optic nerve organization and retinotopic map formation by species (Udin and Fawcett, 1988). Frogs, for example, despite having much less distinctly ordered optic nerves, still developed an accurate retinotectal map, even when the frog's optic nerves were scrambled to disrupt any remaining axonal order (Sperry, 1944; Sperry, 1945; Fawcett, 1981; Reh et al., 1983; Scalia and Arango, 1983; Bunt and Horder, 1983). Similarly, this response to disordering of the optic nerves was also reminiscent of experiments in cichlids, an organism with fairly well-ordered optic nerves, in which appropriate mapping positions could still be generated despite surgeries to bisect and misdirect the halves of each optic nerve (Arora and Sperry, 1962; Arora, 1963). Traveling even further from a need for developmental order to form accurate maps, transplanting the eyes of axolotls (a salamander in the genus *Amblystoma*, though not the same species that Twitty, Harrison, and others studied in the 1920s and 1930s) into genetically eyeless individuals generated wildly exploring retinal axons that rarely entered the optic tract yet still targeted appropriate map positions provided they reached the tectum (Harris, 1982). Further work by Harris and Holt in *Xenopus* indicated that while *Xenopus* retinal axons were in fact initially ordered upon tectal arrival, this ordering was irrelevant to map formation (Holt and Harris, 1983; Holt, 1984; Harris, 1984). Similarly, a recent study in zebrafish demonstrated that neither

specific timing nor the collating presence of other retinal axons was necessary for appropriate topographic mapping of retinal ganglion cells transplanted into RGC-lacking *lakritz* (*atoh7*) mutant retina (Gosse et al., 2008).

In similar studies in warm-blooded animals, chicks also showed a fair degree of order in the organization of the optic nerve. This organization reflected the order of generation of retinal ganglion cells in the retina as well as their dorsoventral positioning origins prior to reaching the tectum, although leading retinal axons showed signs of increased disorder as they traversed the tectal surface during map formation (DeLong and Coulombre, 1965; Goldberg, 1974; Crossland et al., 1974; Rager and Rager, 1978; Rager and von Oeynhausen, 1979; Rager, 1980; Thanos and Bonhoeffer, 1983). At the tectum, however, it began to emerge that chicks might employ both chemical and sequential cues to provide direction and order. When retinal explants from different retinal quadrants were cultured on the tectal surface of developing chicks, they showed directional axonal growth responses consistent with both certain position-dependent responses in accordance with the chemoaffinity hypothesis (DeLong and Coulombre, 1967) as well as with more randomly directing axons along anteroposterior and dorsoventral grid patterns observed to occur along the tectal surface itself (Goldberg, 1974). Furthermore, when the optic chiasm was disrupted prior to the arrival of the axons in the optic nerve, over half the retinal axons targeted incorrect tectal positions, regardless of their topographic positions within the retina; most of these incorrectly targeting axons were removed over the course of map formation, leaving fewer, but solely accurately targeted, retinal axons to form the final map (Fujisawa et al., 1984). Detailed DiI tracing capable of clearly visualizing small groups of individual axons along their entire lengths confirmed that the

chick optic nerve retained a loose, imperfect spatial ordering of retinal axons (Nakamura and O'Leary, 1989). While these axons entered the tectum in a vaguely ordered manner, they showed frequent signs of obvious initial mistargeting and later correction to appropriate mapping positions, indicative of the involvement of both spatial and chemical cues ordering the chick retinotopic map (Nakamura and O'Leary, 1989).

By comparison, mice and rats showed fairly little ordering of their retinotopic projections, yet managed to form appropriate collicular maps (Bunt and Lund, 1982; Bunt et al., 1983; Simon and O'Leary, 1992b; Simon et al., 1994; Plas et al., 2005). In rats, virtually all sequential or ordered information from the retina appeared to be randomized at the optic chiasm, and retinal primary axons spread widely across the superior colliculus regardless of origin, while still coalescing to accurate mapping targets (Bunt and Lund, 1982; Bunt et al., 1983; Simon and O'Leary, 1992b; Simon et al., 1994). On the other hand, in mice, recent evidence suggested that dorsoventral, but not nasotemporal, order in the initially disorganized optic nerve was enforced at the optic chiasm, providing a degree of axial organization prior to collicular map formation (Plas et al., 2005). Thus, the importance of the roles played by retinal preordering of axons and gradient-directed chemoaffinity in mapping varies widely by species, yet both are clearly capable of generating topographic maps.

On retinal axon guidance and the identification of anteroposterior gradients

Frederich Bonhoeffer took a particular interest in how growth cones selected preferred substrates for growth and guidance, demonstrating that retinal cells could preferentially distinguish monolayers of retinal cells from tectal cells, and that temporal

retinal cells could distinguish anterior and posterior tectal monolayers (Bonhoeffer and Huf, 1980; Bonhoeffer and Huf, 1982). This was similarly observed with dissociated tectal cells or membranes preferably attaching to retinal explants from specific retinal regions, with a gradient-like degree of attachment preference (Halfter et al., 1981). In 1987, Walter and colleagues in the Bonhoeffer lab applied a new *in vitro* stripe assay, alternating anterior and posterior chick tectal membranes, to show that temporal but not nasal chick retinal axons showed a differential response to anterior and posterior tectum, with temporal axons showing preferential outgrowth on anterior tectal stripes while nasal axons displayed no preference (Walter et al., 1987a). Furthermore, when the membrane stripes were heated, this temporal axon preference for anterior membranes was no longer observed; this loss of preferential growth occurred when only posterior, but not only anterior, membranes were heated, indicating that these temporal axons were repulsed by posterior membranes rather than attracted by anterior ones (Walter et al., 1987b). While this had been strongly suggested *in vivo* by a number of studies in which the rotation of regions of the tectum resulted in the formation of a rotated map, the new assay provided an opportunity lacked by these *in vivo* studies: the ability to isolate and test possible anteroposterior mapping molecules directly (Yoon, 1973; Levine and Jacobson, 1974; Yoon, 1975; Itasaki et al, 1991; Itasaki and Nakamura, 1992).

Attempts to identify relevant mapping gradient molecules along the anteroposterior tectal axis had previously been made using other techniques. In the late 1980s, two groups identified an anteroposterior increasing gradient of the homeodomain transcription factor engrailed, first identified in fly segmentation, in the chick tectal primordium (Gardner et al., 1988; Patel et al., 1989). Nakamura and colleagues applied

this knowledge in the optic tectum, using quail brain explants to generate an inverted engrailed optic tectal gradient ectopically in the chick diencephalon (Itasaki et al., 1991; Itasaki and Nakamura, 1992). After confirming the gradient expression stability, normal development, and outward rotation (a common feature of chick tectal development (Goldberg, 1974)) of the false additional ectopic tectum, they used this system to show that inversion of the engrailed gradient produced an inversion of anteroposterior retinal axon targeting and thus AP map formation (Ichijo et al., 1990; Matsuno et al., 1991; Itasaki et al., 1991; Itasaki and Nakamura, 1992). Additionally, ectopic anterior expression of engrailed in chick tectum induced the expression of posterior tectal markers RAGS (ephrinA5) and ELF-1 (ephrinA2) in anterior tectum; this caused temporal axons to have difficulty targeting the anterior tectum while causing nasal axons to project diffusely over the depopulated tectal surface, suggesting engrailed affected AP patterning as an upstream regulator of guidance molecules (Logan et al., 1996; Friedman and O'Leary, 1996). Further study strongly suggested that the engrailed gradient itself was set up by FGF8 and Wnt1, after which engrailed proceeded to generate the RAGS and ELF-1 gradients, leading to appropriate map formation (Logan et al., 1996; Friedman and O'Leary, 1996; Rétaux and Harris, 1996; Lee et al., 1997; Shigetani et al., 1997; Sugiyama et al., 1998). More recently, engrailed has been shown to have a more direct role in guiding retinal axons as well, generating protein-expression-regulated repulsion *in vitro* and cooperating with ephrinA5 *in vivo* to position axons in *Xenopus* (Brunet et al., 2005; Wizenmann et al., 2009). Thus, the engrailed gradient in developing chick tectum has been shown to both generate later AP gradients prior to mapping and promote proper AP targeting through separate mechanisms during mapping.

However, it was RAGS (ephrinA5) and ELF-1 (ephrinA2), GPI-linked ligands regulated by engrailed, and the receptor MEK4 (EphA3) that took the spotlight as direct anteroposterior guidance factors in the mid-1990s. Hints of the involvement of ephrinAs in retinotopic mapping first appeared in 1990, when the Bonhoeffer lab demonstrated that phosphatidylinositol-specific phospholipase C (PI-PLC)-treated posterior membranes failed to repel temporal axons in their tectal stripe assay (Walter et al., 1990). They proceeded to raise antibodies against chick posterior tectal membranes, using them to isolate and identify a 33kD glycoprotein with high posterior expression, modifiable by PI-PLC, which induced temporal retinal growth cone collapse (Walter et al., 1990; Cox et al., 1990; Stahl et al., 1990). While this 33kD molecule was not fully identified and tested for several years, the isolation of PI-PLC-modifiable (likely GPI-linked) molecules proved fertile ground for identifying crucial anteroposterior guidance molecules in 1995, with the isolation of RAGS, a 25 kD GPI-linked protein capable of repelling retinal axons and expressed in a graded manner over the posterior half of the chick tectum (Kaprielian and Patterson, 1994; Drescher et al., 1995; Monschau et al., 1997). During this time period, a second GPI-linked member, ELF-1, isolated via binding to retinal axon receptor Mek4, was also demonstrated to repel and collapse retinal axon growth cones (Sajjadi et al., 1991; Sajjadi and Pasquale, 1993; Cheng and Flanagan, 1994; Shao et al., 1995; Cheng et al., 1995; Harris and Holt, 1995; Nakamoto et al., 1996; Monschau et al., 1997). ELF-1 and Mek4 were also shown to be expressed in complementary retinal and tectal gradients in chick, with ELF-1 appearing in a high-posterior, low-anterior tectal gradient while Mek4 was expressed in a high-temporal, low-nasal retinal gradient, fulfilling the initial suggested requirements for complementary gradients in topographic map

formation (Cheng et al., 1995; Monschau et al., 1997; Connor et al., 1998; Sperry, 1963). Soon afterward, ELF-1 was demonstrated to affect retinal axon mapping *in vivo* via overexpression in chick optic tectum, (Nakamoto et al., 1996). Ectopic expression of a truncated EphA3 in retina resulted in inappropriate posterior targeting of temporal retinal axons confirming that the chick retinal EphA3 gradient was required for accurate AP positioning as well (Feldheim et al., 2004).

Similarly, mouse superior colliculus was shown to have a high-posterior, low-anterior gradient of ephrinA5 (RAGS, AL-1, Lerk7) along with a slightly different, center-high, anterior-and-posterior-low gradient of ephrinA2 (ELF-1), corresponding to high-temporal, low-nasal gradients of EphA5 and EphA6 in the retina (Zhang et al., 1996; Frisén et al., 1998; Feldheim et al., 1998; Brown et al., 2000). Mouse retinal axons were repelled by transfected cells expressing ephrinA2 or A5 in a stripe assays *in vitro*, providing evidence that these gradients likely operated similarly in AP mapping in mouse and chick (Feldheim et al., 1998). *In vivo* in ephrinA5 knockout mice, some temporal retinal axons were shown to map to ectopically posterior termination zones or beyond the posterior superior colliculus and onto the inferior colliculus, while some nasal axons also showed abnormal anterior targeting (Frisén et al., 1998; Feldheim et al, 2000). EphrinA2 knockout mice displayed a different, weaker phenotype, with temporal axons targeting inappropriate posterior locations within the bounds of the superior colliculus and with no effect on nasal axons, suggesting that ephrinA5 and A2 might have different but overlapping roles in AP map formation (Feldheim et al., 2000). This was strongly confirmed when ephrinA2/A5 double knockout mice showed a strong synergistic effect on AP mapping as well as, surprisingly, on mediolateral mapping, showing multiple

incorrectly targeted arbors and frequently lacking any targeting whatsoever at appropriate targeting sites (Feldheim et al., 2000). By removing ephrinA3, which expressed evenly across the tectum, even the few remaining appropriate termination zones were abolished in ephrinA2/A3/A5 knockout mice, suggesting that ephrinAs are sufficient to control the entire anteroposterior map (Pfeiffenberger et al., 2006; Cang et al., 2008; Feldheim and O'Leary, 2011). On the receptor side, the knockdown of EphA5 in mice changed retinal axons' responsiveness to ephrinA gradients, with temporal axons targeting inappropriate posterior and nasal axons targeting inappropriate anterior positions (Feldheim et al., 2004). On the other hand, knock-in mice expressing EphA3, which is not present in mouse retina but does respond to ephrinA2 and A5, in 50% of RGCs across the retina showed more anterior targeting by those retinal axons expressing the ectopic EphA3 (Brown et al., 2000; Feldheim et al., 2004). Overall, these experiments clearly indicated that ephrinA-EphA gradients capably define the anteroposterior map, and that they do so via a relative rather than absolute graded response, filling spaces to cover the mapping surface (Feldheim et al., 1998; Frisén et al., 1998; Feldheim et al., 2000; Brown et al., 2000; Feldheim et al., 2004).

Additional redundant retinal and tectal gradients have also been shown to affect aspects of anteroposterior map formation. Among these is RGM, the 33kD GPI-linked protein previously referenced (Cox et al., 1990; Stahl et al., 1990), which has been shown to preferentially repel chick temporal axons and disrupt chick AP mapping via overexpression and knockdown, although initial attempts to show effects in knockout mice failed, perhaps due to redundancy of other RGM-family molecules (Müller et al., 1996; Monnier et al., 2002; Niederkofler et al., 2004; Matsunaga and Chetodal, 2004;

Matsunaga et al., 2006; Tassew et al., 2008). Odz3, several semaphorins, and L1 have also been suggested as anteroposterior guidance proteins (Oohashi et al, 1999; Campbell et al., 2001; Demyanenko and Maness, 2003; Liu et al., 2004).

In 2007, Luo and Flanagan summarized Sperry's criteria for topographic mapping gradients into three simple requirements, demonstrating the anteroposterior EphA-ephrinA gradients as the first guidance molecules to fulfill all qualifications (Luo and Flanagan, 2007; Sperry, 1963). First, the molecules had to be expressed in appropriate gradients; here, EphA3 was observed in chick and EphA5 and A6 in mouse retina in a high-temporal, low-nasal gradient, and ephrinA2 and A5 were seen in both chick tectum and mouse superior colliculus high posterior, low anterior gradients (Cheng et al., 1995; Drescher et al., 1995; Zhang et al., 1996; Frisén et al., 1998; Feldheim et al., 1998; Brown et al., 2000). Second, the identified molecules must be shown to operate on retinal axon guidance; stripe assays using modifications to both receptor and ligand levels showed changes in the repulsive responses and anteroposterior tectal stripe outgrowth choices of retinal axons (Drescher et al., 1995; Nakamoto et al., 1996; Feldheim et al., 1998). Third and finally, gain-of-function and loss-of-function experiments with both the suggested ligands and receptors must result in map targeting effects; indeed, these effects were observed in both chick and mouse as previously described (Nakamoto et al., 1996; Frisén et al., 1998; Brown et al., 2000; Feldheim et al., 2000; Feldheim et al., 2004). Taken together, these criteria can be used to consider the qualifications of other retinotectal gradients for topographic mapping.

On the appropriate initiation and development of interstitial branches

After the anteroposterior extension of primary axons, retinal axons sprout interstitial branches that travel along the mediolateral tectal axis in birds and mammals. Because retinal axons in fish and frogs target their retinal axon growth cones directly along both anteroposterior and mediolateral axes simultaneously rather than guiding along the two axes separately by forming interstitial branches after primary axon extension, additional mechanisms are necessary to explain this two-step process. This said, some features may, to varying degrees, be common to both types of mediolateral mapping, direct and via interstitial branching. Due to these notable differences in retinal axon behavior between species, to gain greater clarity regarding mediolateral retinotopic mapping, it is necessary to narrow one's observations to a more limited region of study. Chick and mouse are well characterized animal models that share several features in retinotectal mapping: both show signs of requiring some retinal axon preordering prior to map formation (DeLong and Coulombre, 1965; Goldberg, 1974; Crossland et al., 1974; Rager and Rager, 1978; Rager and von Oeynhausen, 1979; Rager, 1980; Thanos and Bonhoeffer, 1983; Plas et al., 2005), extend anteroposterior primary axons and mediolateral interstitial branches to map somewhat distinctly on the two tectal axes (Nakamura and O'Leary, 1989; Simon and O'Leary, 1990; Simon and O'Leary, 1992a; Simon and O'Leary, 1992b; Simon and O'Leary, 1992c; Yates et al., 2001; Hindges et al., 2002; McLaughlin et al., 2003b), and have been used extensively to study the roles of molecular gradients in retinotectal mapping (Cheng et al., 1995; Drescher et al., 1995; Zhang et al., 1996; Frisén et al., 1998; Feldheim et al., 1998; Brown et al., 2000; Feldheim et al., 2000; Feldheim et al., 2004). While they do not necessarily apply the

same molecules for every task, they appear to use similar receptors and ligands within the same families; for example, EphA3 serves as the main retinal ligand in anteroposterior mapping in chick, while EphA5 and A6 serve that purpose in mouse, but both do use EphA receptors with ephrinA2 and A5 ligand gradients (Cheng et al., 1995; Drescher et al., 1995; Zhang et al., 1996; Frisén et al., 1998; Feldheim et al., 1998; Brown et al., 2000; Feldheim et al., 2000; Feldheim et al., 2004). Thus, characterizing either or both of these systems directly should allow for a greater understanding of the overall mechanisms of mediolateral map formation in birds and mammals.

The connection between anteroposterior and mediolateral map formation is that while retinal primary axons in chick and mouse overshoot their AP targets and are later retracted to appropriate locations, they tend to initiate their mediolateral-targeting interstitial branches in the appropriate AP targeting areas. To consider this, it is necessary to return to the observation in anteroposterior studies that in ephrinA2/A5 double knockout mice, both anteroposterior and mediolateral mapping defects were observed, and that in ephrinA2/A3/A5 triple knockout mice, all aspects of appropriate mapping were almost entirely abolished (Feldheim et al., 2000; Pfeiffenberger et al., 2006; Cang et al., 2008; Feldheim and O'Leary, 2011). If anteroposterior and mediolateral mapping were controlled by entirely separate mechanisms, guiding along each axis without respect to the other, then neither defects in both axes in response to the manipulation of one axis nor a complete abolition of map order as a result of manipulating one axis should be possible; because, however, both of these results have been observed, it is clear that a link between the mediolateral and anteroposterior axes exists. Studies by the O'Leary lab indicated that the nature of the interface was likely in

the appropriate AP placement of these interstitial branches, such that they could appropriately respond to local mediolateral gradients (Roskies and O'Leary, 1994; Yates et al., 2001). Furthermore, this preferential interstitial branch placement depended on two factors: causing branches to preferentially initiate at appropriate AP locations on the primary axon, and inhibiting branches from forming in inappropriate locations both anterior and posterior to the correct location (O'Leary et al., 1999; Yates et al., 2001; Yates et al., 2004). These could possibly be explained by the gradients and countergradients of EphAs and ephrinAs. Stripe assays showed that temporal retinal axons were more likely to form branches on anterior tectal membranes, and that this specificity was removed when membranes were treated with EphA3-Fc, allowing these axons to branch equally on both anterior and posterior membranes, indicating that the retinal EphA3- tectal ephrinA gradients were sufficient to limit branching posterior to the appropriate branching location (Yates et al., 2001). Similarly, when ephrinA5 was inactivated using chromophore-assisted laser inactivation in chick, increased branching and ectopic posterior arbors were observed, supporting ephrinA5's role in limiting inappropriate posterior branches (Sakurai et al., 2002). Computer modeling indicated that a second repulsive gradient should limit anterior activity (Yates et al., 2004). EphA7, expressed solely in a high-anterior, low-posterior gradient in the tectum corresponding to high nasal, low temporal retinal gradients of ephrinA2 and A5, was suggested to provide this activity (Marcus et al., 1996; Zhang et al., 1996; Rashid et al., 2005). Retinal axons were repulsed by stripes of EphA7 in stripe assays, and EphA7 knockout mice showed nasal axons with ectopic anterior termination and inappropriately long or wide arbors while temporal axons appeared mostly unaffected, suggesting that

EphA7 was sufficient to play a role in the appropriate outgrowth and branching of retinal axons; further, the orientation of the EphA7 tectal gradient and the knockout effects on nasal rather than temporal axons also strongly suggested EphA7 acted to limit inappropriate branching and termination anterior to the correct AP location, as predicted (Rashid et al., 2005).

While ephrinA and EphA gradients and countergradients were sufficient to explain how interstitial branching was limited to appropriate AP regions along the primary axons, they did not account for the induction of branching in those appropriate locations. BDNF and TrkB, which are evenly expressed in the tectum and retina, respectively, were suggested to provide these functions, as increasing BDNF levels in *Xenopus* tadpoles increased retinal axon branching and arborization, while supplying BDNF antibodies reduced arbor complexity (Cohen-Cory and Fraser, 1995). Recently it was shown that TrkB signaling could be enhanced through cis-interactions (with both molecules present on the axon rather than on axon and surface/tectum) with ephrinA5 on retinal axons while BDNF-induced branching was suppressed through dosage-dependent responses to EphA7, suggesting an additional mechanism to limit ectopic anterior branching normally produced via BDNF-promoted retinal axon branching (Marler et al., 2008). This EphA7 branch inhibition was demonstrated to be mediated through cis-interactions between ephrinA6 and TrkB in a complex with neurotrophin receptor p75(NTR) (Poopalasundaram et al., 2011). Thus, branching is inhibited in inappropriate locations by gradients and countergradients of EphAs and ephrinAs as well as through the interaction of these gradients with TrkB and p75(NTR), causing TrkB-BDNF-induced

branches to appear only at appropriate AP regions along retinal axons, where they can then respond to mediolateral gradients to form retinal arbors.

On the identification and testing of mediolateral guidance gradients

Even before the development of the Bonhoeffer stripe assay, there were clear signs that the dorsoventral retinal axis corresponded to the mediolateral tectal axis. In the 1970s, members of the Roth lab used dissociated retinal cells and membranes to show that, as earlier suggested by *in vivo* experiments, dorsal retinal cells preferentially attached to the lateral chick tectum, while ventral retinal cells preferred the medial tectum (Sperry, 1944; Sperry, 1945; Gaze 1959; Maturana, 1959; Arora and Sperry, 1962; Attardi and Sperry, 1963; Barbera et al., 1973; Marchase et al., 1977). This was similarly demonstrated with dissociated retinal cells and tectal cells, rather than tectal halves (Gottlieb and Arington, 1979). These results strongly suggested a direct molecular interaction was mediated between the two axes in a graded manner.

However, in contrast to the results seen with the direct interaction of retinal and tectal cells and membranes, many of the same groups that characterized anteroposterior gradient responses with retinal explant cultures found that their assays failed to yield results when tested for mediolaterally-controlled chick retinal axon attachment and outgrowth. Several attempts at mediolateral tectal membrane choice assays, described in the same papers as the anteroposterior tests, showed that outgrowing RGC axons in dorsal retinal cultures failed to display a preference for growing on lateral tectal membranes, and ventral retinal cultures lacked a preference for growing on medial tectal membranes or membrane stripes (Bonhoeffer and Huf, 1982; Walter et al., 1987a;

Hindges et al., 2002). Even so, using *in situ* hybridization, immunohistochemistry, and Fc-bound receptors to check for binding, it was demonstrated that EphB1, B2, and B3 were present in chick and mouse retinal axons and growth cones during times relevant to culture and mapping, and that ephrinBs in the outer tectum were able to bind EphB2-Fc (Holash and Pasquale, 1995; Henkemeyer et al., 1996; Braisted et al., 1997; Holash et al., 1997; Connor et al., 1998; Birgbauer et al., 2000). Furthermore, stripe assays done with *Xenopus* axons clearly demonstrated that under these conditions, mediolateral preference could be clearly identified as an attractive response of more ventral growth cones to EphBs in the *Xenopus* optic tectum, as it was abolished by the addition of anti-EphB antibodies (Nakagawa et al., 2000; Mann et al., 2002). These results combined suggested that while stripe assays had proved effective for identifying anteroposterior gradients relevant to chick and mouse, the lack of response seen when looking for mediolateral responses with the chick-based Bonhoeffer stripe assay was likely not due to errors in the execution or oddities of signaling crosstalk in chick retinal axons but rather might be due to other features, such as that only interstitial branches could respond to mediolateral gradient molecules. As the Bonhoeffer stripe assay is initiated and completed prior to interstitial branch formation (Bonhoeffer and Huf, 1980; Walter et al., 1987a), the observed lack of mediolateral response is therefore irrelevant to later studies, especially given that these assays still worked for mediolateral gradients in model organisms with directly-targeting retinal axons, like *Xenopus* (Mann et al., 2002).

Despite these oddities, many groups, encouraged by EphA and ephrinA gradients along the retinal nasotemporal and tectal anteroposterior axes and aware of the promiscuous binding of Eph-ephrin family molecules, continued their Eph-ephrin studies,

identifying a series of orthogonal gradients of EphBs and ephrinBs in complementary patterns in the dorsoventral retinal and mediolateral tectal axes (Holash and Pasquale, 1995; Henkemeyer et al., 1996; Braisted et al., 1997; Connor et al. 1998; Birgbauer et al., 2000; Hindges et al., 2002; Gale et al., 1996). In both chick and mouse, EphB2 (Cek5) and EphB3 (Cek10) are expressed in a high ventral, low dorsal gradient in the retina (as, interestingly, is EphA4 (Cek8) in chick), with EphB4 expressed in a similar gradient in mouse and EphB1 (Cek6) expressed evenly throughout the ganglion cell layer in chick and mouse (Holash and Pasquale, 1995; Connor et al., 1998; Birgbauer et al., 2000; Hindges et al., 2002). EphrinB1 is expressed in a complementary high medial, low lateral gradient in both chick tectum (in the ventricular epithelium at E3 through E13, disappearing by E14 as the ventricular epithelium also disappears) and mouse superior colliculus; however, ephrinB2 is absent in mouse SC and limited to deeper tectal laminae in chick, appearing at E10 in these laminae (Braisted et al., 1997; LaVail and Cowan, 1971a; Hindges et al., 2002). Furthermore, it has been demonstrated in chick that while ephrinB1 is generated in the ventricular epithelium, it is trafficked to the tectal surface along radial glial cells, where it can be encountered by arriving retinal axons (Braisted et al., 1997). Interestingly, much as with the EphAs and ephrin As, EphBs and ephrinBs were also shown to be expressed in complementary opposing gradients in both retina and tectum, with ephrinB1 and B2 expressed in high dorsal, low ventral gradients in the retina of both chick (from E3 through E14, localizing to RGCs as they develop and migrate to the ganglion cell layer and then remaining in RGCs in the ganglion cell layer) and mouse (Marcus et al., 1996; Braisted et al., 1997; Holash et al., 1997; Birgbauer et al., 2000; Hindges et al., 2002). EphB2 and B3 are present in the ventricular epithelium of the chick

tectum, with EphB2 and B3 expressed in high lateral, low medial gradients in mouse superior colliculus; EphB1 is present in both chick and mouse, but localized to non-mapping-relevant tectal/collicular regions (Holash and Pasquale, 1995; Connor et al., 1998; Hindges et al., 2002). These mediolateral axis gradients and countergradients, present in both chick and mouse, were expressed in the proper patterns and during the appropriate time periods to be relevant to the formation of the mediolateral retinotopic map.

In vivo manipulations of these mediolateral gradients led to more complex explanations for the formation of the mediolateral tectal axis. In the first of these studies, the O'Leary lab used EphB2/EphB3 deficient (+/-, -/-) or double knockout (-/-, -/-) mice to demonstrate ectopic lateral termination zones for ventral but not dorsal RGCs, although dorsal RGCs may have been affected in an unobserved manner due to their natural tendency to target laterally (Hindges et al., 2002). Furthermore, the EphB2/EphB3 double knockout mice showed a stronger lateral mistargeting phenotype than the doubly deficient mice, suggesting a dosage-dependent effect of EphBs on appropriate medially-attractive guidance (Hindges et al., 2002). This appeared to be confirmed by later studies with EphB1/EphB2/EphB3 deficient and knockout mice demonstrating that, overall, the number of null alleles present generated similar phenotypic severity in targeting regardless of the specific EphB null allele, rather than each EphB showing a related but slightly differing role in mediolateral mapping (Hindges et al., 2002; McLaughlin et al., 2009). Even so, both the occurrence of lateralization rather than randomization in response to EphB knockdown and the fact that EphB1/B2/B3 triple knockout mice still showed some topographic organization

suggested the presence of additional mapping molecules or mechanisms to generate the mediolateral map; Hinges and colleagues specifically predicted, based on mapping models, that a lateral-directive gradient opposing the medial-attractive EphB-ephrinB signaling forces must exist within this axis (Hindges et al., 2002; McLaughlin et al., 2009). More detailed studies of EphB2 function in the mouse retinotectal system clarified some of the activity of EphB2 in mapping, delineating that only EphB2 forward (ki/ki), and not reverse, signaling was involved in appropriate ML targeting and that the kinase domain, but not the PDZ domain, was necessary for this process (Hindges et al., 2002; Thakar and Henkemeyer, 2010). Additionally, EphB2 ki/ki, EphB3 -/- mice showed stronger phenotypic penetrance than standard EphB2/B3 double knockout mice; this was also observed in EphB1 forward signaling mutants on the EphB3 knockout background, suggesting that forward signaling alone, rather than any components of reverse signaling generated by the retinal ephrinB and tectal EphB countergradients, was relevant to mediolateral mapping decisions (Hindges et al., 2002; McLaughlin et al., 2009; Thakar and Henkemeyer, 2010).

Manipulations of the ephrinB gradients were also performed in both mouse and chick in order to sort out the nature of the lateral-directive behavior of both normal and EphB-deficient interstitial branches. In 2003, the O'Leary lab ectopically overexpressed ephrinB1 in the chick optic tectum using avian viral vector RCAS, then traced RGC axons from areas neighboring the ectopic ephrinB1 regions using DiI to observe interstitial branch response (McLaughlin et al., 2003b). Under these conditions, RGC axons targeting areas near the ectopic overexpression sites showed more dense termination zones, splitting of termination zones, and shaping away from areas of

ephrinB1 overexpression, suggesting that high concentrations of ephrinB1 produced a repulsive rather than attractive response in retinal axons (McLaughlin et al., 2003b). This targeting response implicated that EphB-ephrinB1signaling generated bifunctional activity to direct mediolateral guidance (McLaughlin et al., 2003b). However, the observed ectopic levels of ephrinB1 determined by EphB2-Fc binding appeared to have equal or stronger effects than the high wild-type medial tectal concentrations of ephrinB1; yet in the wild-type medial tectum, repulsive ephrinB1 interactions were not observed, making it unclear how this bifunctionality, if it occurs naturally *in vivo*, would operate (McLaughlin et al., 2003b). Further studies have failed to clarify this issue, other than to suggest that the small gradient differences across regions combining to form termination zones cause axons to make mediolateral direction choice decisions dependent on the ephrinB1 gradient alone, perhaps using EphB1-ephrinB1 binding to generate repulsive guidance (McLaughlin et al., 2003b; McLaughlin et al., 2009). Studies from the Henkemeyer lab in knockout mice, however, suggest a slightly different nuance, showing that ephrinB1 knockout mice show lateralization effects in ventral RGCs as previously suggested with EphB knockout mice; additionally, ephrinB2, which is expressed in a spreading dorsoventral countergradient in the retina, may use reverse signaling to assist in the appropriate mapping of dorsal RGCs, while both ephrinB1 and B2 are relevant to the accurate mapping of ventral RGCs (Thakar and Henkemeyer 2010). In order to fulfill the Luo and Flanagan (Sperry) criteria for mapping gradients, EphB gain-of-function studies in mouse are still needed, EphB gain-of-function and loss-of-function studies in chick would be advisable, and ephrinB2 gain-of function studies are strongly suggested by the Thakar and Henkemeyer results, preferably in both mouse

and chick systems, given the differing results between systems (Sperry, 1963; Luo and Flanagan, 2007; McLaughlin et al., 2003b; Thakar and Henkemeyer, 2010). Still, the incomplete studies on both EphBs and ephrinBs in this system indicate both that a lateral force, whether through ephrinB1 or otherwise, is required but not fully identified and that further characterization of the mediolateral axis is needed for full comprehension of mediolateral map formation.

On lateral-directive countergradients and the two-gradient (dual gradient) model

While transcription factors cVax in chick (and Vax2 in mouse) ventral retina and Tbx5 in dorsal retina were shown to affect dorsoventral development of the retina upstream of mediolateral guidance molecules (similar to engrailed in the AP axis) (Mui et al., 2005; Mühleisen et al., 2006; Golz et al., 2008; Alfano et al., 2011), no complementary or redundant ML axis guidance molecules were identified until 2006, with the demonstration that a high ventral, low dorsal retinal gradient of Ryk corresponded to a high medial, low lateral gradient of Wnt3, both in the same orientation as the forward signaling EphB-ephrinB1 gradients, in both chick and mouse (Schmitt et al., 2006). In retinal explant culture, retinal axon outgrowth was shown to have position- and concentration-dependent responses to Wnt3, with outgrowth decreasing as ventral retinal positioning or Wnt3 concentration increased and the reverse in the opposing direction, though with an interesting mild stimulation of outgrowth seen at the dorsalmost retinal positions (Schmitt et al., 2006). This suggested that while Wnt3 generally had a repulsive or outgrowth-diminishing effect on retinal axons, at these dorsalmost retinal positions under low Wnt3 concentrations, it might have a biphasic attractive or

outgrowth-inducing effect, much as suggested for EphB-ephrinB1 signaling (Schmitt et al., 2006). Furthermore, ectopic tectal overexpression of Wnt3 repulsed retinal axons laterally from the appropriate termination site, while downregulation of Ryk with a dominant negative construct resulted in more medially-directed branches and a wider, more medial termination zone, indicating that both the ligand and receptor affected mediolateral mapping *in vivo* (Schmitt et al., 2006).

Because Ryk provides a lateral-repulsive guidance cue while the EphBs provide a medial-attractive cue along the mediolateral axis, the possibility exists that the two gradients could provide competing opposing guidance forces to determine accurate mapping positions, an idea described in the two-gradient or dual gradient model. Developed through a series of papers by Alfred Gierer in the 1980s, the dual gradient (or two-gradient or countergradient) model suggests that through the use of gradients with two opposing forces, or a single gradient to which an axon can respond in both an attractive and a repulsive manner simultaneously, axonal growth cones seek out areas at which they experience the lowest 'potential', or at which the opposing responses are approximately equal (Gierer, 1981; Gierer, 1983; Gierer, 1987). While Gierer's computational models of this dual gradient competition predicted aspects of guidance and branching in a manner similar to those observed in the normally developing retinotectal system, the this model could not be tested *in vivo* until recently. Using the Ryk-Wnt3 and EphB-ephrinB1 gradients along the mediolateral axis, it would be possible to demonstrate whether Gierer's dual gradient hypothesis acts along this axis by comparing branch direction choices as a result of modulating receptor or ligand levels (demonstrating a

medial versus lateral shift indicative that the two gradients compete against each other to define map positions).

On the goals of these dissertation studies

The presence of similarly aligned Ryk-Wnt3 and EphB-ephrinB1 gradients with opposing guidance activities in the chick retinotectal system provides several opportunities to improve upon our understanding both of the activities of the molecules involved as well as on the formation of the mediolateral map and, overall, of the formation of topographic maps.

On the level of understanding the role and activity of Ryk-Wnt3 signaling in the mediolateral axis, Ryk has been shown to act via a mechanism of repulsion with outgrowth in response to the ligand Wnt5a both *in vitro* and *in vivo* in the corpus callosum (Li et al., 2009; Li et al., 2010; Hutchins et al., 2011). While initial studies showed that downregulation of Ryk resulted in increased medial branch direction choice, the effects of Ryk-induced repulsive guidance activities have not been completely studied in this system and are insufficient to confirm Ryk's role in mediolateral mapping in accordance with the Luo and Flanagan criteria (Schmitt et al., 2006), nor has the possibility of Ryk's outgrowth function in this system been studied (Hutchins et al., 2011). Additionally, both Ryk and Wnt3 gradients have not been fully characterized during development, unlike several of the EphB and ephrinB gradients (Braisted et al., 1997; Connor et al., 1998), nor has Wnt3 involvement in mapping been clearly delineated.

On the level of the formation of the mediolateral map, Ryk-Wnt3 and EphB-ephrinB1 gradients, with their opposing mapping forces, present an opportunity to test aspects of Gierer's dual gradient model. By modulating receptor levels, it should be possible to confirm, on the level of branch direction choice, that Ryk and EphBs oppose each other in map formation, with Ryk providing lateral and EphBs providing medial guidance to developing interstitial branches. As retinal axon outgrowth was affected by endogenous levels of Wnt3 *in vitro*, whereas retinal axons were repelled by ectopic overexpression of ephrinB1 above endogenous levels *in vivo*, comparing the activities of these two gradients, rather than focusing on the biphasic activity of EphB-ephrinB1 signaling, is more likely to provide strong grounds for the study of this model (Schmitt et al., 2006; McLaughlin et al., 2003b).

Lastly, on the level of topographic mapping, in addition to deciphering the dual gradient model, there remain clear signs that aspects of development separate from molecular gradients play a role in map formation in multiple organisms. As it is known in chick that retinal axons in the mediolateral but not anteroposterior axis shown signs of preordering prior to map formation, it may be possible to combine the study of gradient development and the characterization of axon and branch development in light of the two competing gradients to clarify the role of developmental preordering in this system, as well as to delineate the interaction of developmental preordering and competing gradients in the formation of an accurate topographic map. As these two components are frequently described (along with axon-axon competition and spontaneous and ordered neural activity) as probable requirements in map formation, by elucidating their roles

within this system, it may be possible to better understand the fundamentals of formation of topographic maps in many parts of the nervous system.

Chapter 1, in part, has been submitted for publication of the material. Richman, Alisha; Zou, Yimin. The dissertation author was the primary investigator and author of this material.

CHAPTER 2: MATERIALS AND METHODS

Maintenance of embryonic chicks

Fertilized White Leghorn chicken eggs were obtained from McIntyre Poultry & Fertile Eggs (Lakeside, CA). Eggs were stored at 4C for up to 7 days prior to initiating further development. To initiate development, eggs were placed in a humidified 37C hatching incubator (1550 Hatcher, GQF, Savannah, GA) with the long axis of the egg facing upward; the day on which eggs were placed into the incubator is considered embryonic day 0 (E0). Once the eggs reached E3 or E4, a syringe (3 mL Luer-lock syringe, BD Biosciences, Franklin Lakes, NJ) bearing an 18-gauge needle (BD 305196 18-gauge x 1½ inch needle, BD Biosciences, Franklin Lakes, NJ) was inserted into the wider end of each egg to remove approximately 4 milliliters of albumen (egg white) from the lower part of the egg; this resulted in the contents of the egg sinking slightly toward the bottom of the egg, generating an upper air space useful for access during later manipulations. Eggs were then returned to the incubator to continue developing until the appropriate age for experimentation.

Fixation and preparation of tissues for *in situ* hybridization

For *in situ* hybridization, whole chick left tecta were dissected from live embryos at E10 through E13 in chilled 1x PBS using lightly blunted forceps. Similarly, meninges and remaining skull and epithelial tissue were removed from the dissected tecta. After this, tecta were transferred to pre-chilled 4C 4% paraformaldehyde (PFA) in DEPC-treated water in a 15-milliliter conical tube (VWR International, West Chester, PA) and

kept at 4C overnight for fixation. (DEPC-treated water was made by adding 1 milliliter of DEPC (diethylpyrocarbonate, D5758, Sigma-Aldrich Corporation, St. Louis, MO) to 1 liter of milliQ-filtered water (Thermo Scientific Barnstead NANOpure Water Purification System, Thermo Fischer Scientific, Waltham, MA), then sealing and shaking the water for one minute to distribute the DEPC. After the resultant solution was allowed to sit open overnight in a fume hood to ensure complete diffusion and autoclaved, paraformaldehyde was added to the appropriate concentration (4% by mass), heated to 65C to ensure complete dissolution, and then chilled to 4C for experimental use.) After overnight fixation, the paraformaldehyde was removed from the fixed tecta. The tissues were rinsed once with 1x PBS to remove any remaining PFA residue, then transferred into 30% sucrose in 1x PBS solution and kept at 4C until the tissue was observed to reach the density of the sucrose solution, sinking to the bottom of the conical. At this point, half of the sucrose solution was removed and replaced with OCT medium (Tissue-Tek OCT Compound, Ted Pella, Inc., Redding, CA). The new solution was mixed by vortexing (Vortex Genie 2, Scientific Industries, Bohemia, NY) and tilting the tube back and forth to obtain an even consistency, then the tissue-containing conical was returned to 4C for a minimum of two hours (to a maximum of overnight) to equilibrate to the solution. After this, the tissue was embedded in OCT in small cryostat molds (22mm x 22mm truncated square Peel-A-Way molds, Polysciences, Inc., Warrington, PA). Tecta were oriented with the ventral (ventricular) side toward the bottom of the mold and the posterior end toward the protrusions. Molds were then placed in crushed dry ice with 100% ethanol for quick, even freezing and stored at -80C.

In situ hybridization of chick retinal and tectal tissues

Tissues were sectioned at a thickness of 20 microns using a cryostat (Leica CM3050 S cryostat, Leica Microsystems, Wetzlar, Germany). Tectal tissue blocks were oriented such that the medial, lateral, and dorsal (opposite ventricular opening) sides of the tectum were present and the ventricular opening and the nucleus mesencephalicus lateralis, pars dorsalis (or MLd, an auditory nucleus located in the deeper tectal laminae on the lateral side of the tectum) could be observed; only sections in which the ventricular opening could be observed, with the addition of a few immediately before or after the opening, were used. Tissue sections were mounted directly onto Superfrost Plus slides (Fisherbrand Superfrost Plus slides, Thermo Fisher Scientific, Waltham, MA) after sectioning and allowed to air dry for at least 20 minutes prior to beginning the *in situ* hybridization process. For the appropriate direct comparison of gradient strength and position, retinas or tecta of each age (E10-E13) were mounted on the same slides, with 3-5 sections of each age per slide to ensure redundancy in case of tissue damage or loss.

During the first day of the *in situ* hybridization (ISH) process, tissues were prepared for the hybridization process, and this process was initiated in the prepared tissues. After drying the tissue-covered slides, the slides were placed in 4%PFA in 1x PBS treated with DEPC (DEPC-PBS) for ten minutes at room temperature, then washed in 1x PBS-DEPC three times, three minutes per wash. To minimize non-specific hybridization, the slides were then placed in a freshly made acetylation solution for 10 minutes, after which the slides were again washed in 1x PBS-DEPC three times, five minutes per wash. To acclimate the slides for hybridization, they were then placed into a 20x saline sodium citrate (SSC) buffer treated with DEPC for fifteen minutes, after which

excess fluid was wiped from the backs of the slides using a Kimwipe. The slides were then placed into a pre-warmed (to 58C) hybridization chamber humidified using a 4x SSC/ 50% formamide solution on Whatman chromatography paper (Whatman 3MM CHR chromatography paper, GE Healthcare, Little Chalfont, UK). Six-hundred microliters of pre-warmed hybridization buffer were added to each slide, and the chamber was placed in a 58C hybridization oven for pre-hybridization. During this time, riboprobes were prepared by mixing 1.2 microliters of the relevant 400ng/mL riboprobe stock with 1.2 microliters of 10 mM EDTA per slide, then denaturing the probe mixture at 80C for five minutes. After this, 300 microliters of hybridization buffer per slide was added to the mixture. At this point, the hybridization buffer was removed from the slides and the probe solution was added to the appropriate slide (at 300 microliters per slide), after which each slide was covered with a HybriSlip (247459, Research Products International, Mt. Prospect, IL) to ensure an even distribution of probe across the slide surface and prevent prove solution from leaking off the slide. The slides were returned to the hybridization chamber and thence to the hybridization oven at 58C for 40 hours in order to allow the probes to hybridize with mRNA in the tissue sections.

During the second day of the ISH process (the third day overall), nonspecifically-bound riboprobes were detached from and probe-targeting antibodies were added to the tissue. After hybridization, the HybriSlips and probe solution were removed from the slides, and the slides were placed in pre-heated 0.2x SSC (without DEPC) at 65C for two incubations of 90 minutes each in order to detach non-specifically bound probes. The slides were then washed in room temperature 0.2x SSC for 10 minutes, after which they were transferred to B1 solution (0.1M Tris (pH 7.5), 0.15M NaCl) for five minutes.

During this time, B2 solution (B1 plus 1% blocking solution (a 1:10 dilution of 10% Boehringer Mannheim blocking reagent power (11 096 176 001, Roche Diagnostics GmbH, Mannheim, Germany) in pH 7.5 maleic acid buffer)) with anti-digoxygenin-AP (alkaline phosphatase) (1:5000, 11 093 274 910, Roche Applied Science, Mannheim, Germany) was generated. B1 was removed from the slides, which were then covered in B2 (1 milliliter per slide) and transferred to a 4C cold room overnight.

During the third day of the ISH process (the fourth day overall) the slides were developed and processed to reveal mRNA expression patterns. After the overnight incubation in anti-digoxygenin-AP antibodies, the slides were washed five times, ten minutes per wash in B1 at room temperature. The slides were then transferred to B3 (0.1M Tris (pH 9.5), 0.1M NaCl, 50mM $MgCl_2$) for five minutes to begin activating the alkaline phosphatase, during which time the colorimetric developing solution was generated (20 microliters of NBT/BCIP (11 681 451 001, Roche Applied Science, Mannheim, Germany) in 980 microliters of B3 per slide). The slides were then removed from the B3 and placed in an aluminum foil-covered slide box, at which time the NBT/BCIP developing solution was added. Slides were monitored every 15 to 30 minutes for visibility of a purple NBT/BCIP precipitate. One the colorimetric reaction was considered to be sufficiently dark for clear visualization, slides were transferred to 1x TE for 10 minutes, then rinsed in water and allowed to dry in a dark, room temperature location overnight. Slides were mounted using Poly-Mount (#08381, Polysciences, Inc., Warrington, PA) and 22mm x 50mm glass coverslips.

In some experiments, to remove nonspecific precipitate, an ethanol-xylene dehydration series was used prior to mounting. For this dehydration series, slides were

placed into 30% ethanol, then 50% ethanol, 75% ethanol, 95% ethanol, and 100% ethanol for up to 2 minutes each, then transferred to xylene for two washes of up to one minute each. Slides were monitored during this process to prevent excessive signal removal.

Probes employed for *in situ* hybridization

Most probes were generated from bacterial stocks created by previous members of the Zou lab. All probes were constructed from 200-900bp regions of the relevant genes and, in some instances, their 3' UTRs, cloned into a pCRII-TOPO vector (Invitrogen, Carlsbad, CA). Probes were tagged with digoxygenin during transcription for labeling during *in situ* hybridization.

Gradient Western blot – Tectal surface lysate preparation

Gradient Western blot assays were performed using a variant of techniques described in Schmitt et al., 2006. To generate tectal gradient lysates, left tecta from embryonic day 8 (E8) through E13 were dissected from live chick embryos using a pair of lightly blunted forceps, and any skull tissue and remaining attached meninges were removed. Only three to four tecta were dissected per lysate-generating session to minimize time for possible protein degradation.

Tecta were stored in pre-chilled 1x phosphate-buffered saline on ice while a solution of 4% low melting point agarose (Apex 20-103, Genesee Scientific Corporation, San Diego, CA) in 1x PBS was heated to boiling twice in succession in a microwave oven. The agarose solution was then poured into a square pre-chilled cryostat mold (22mm x 22mm truncated square Peel-A-Way mold, Polysciences, Inc., Warrington, PA)

on ice and stirred with a thermometer until a temperature of 35C was reached. (The melting/freezing point of the low melting point agarose is 27 to 29C.) At this point, the three to four tecta were added directly to the agarose solution and stirred into the solution with a small spatula to allow equilibration in the solution and thus better attach the tecta to the agarose during solidification. Once the agarose temperature decreased to approximately 31C, the tecta were then aligned in the thickening solution using the spatula, with their posterior ends facing the bottom of the mold and their lateral sides facing the left of the mold, where the direction-indicating protrusions on the mold are oriented toward the experimenter. Tecta were spaced as though the mold were divided into four equal quadrants as seen from above, and the posterior ends were posed to sit 2-4 millimeters above the bottom of the mold. The agarose was allowed to solidify with the tecta in this position.

Tecta were then sectioned using a vibratome (Leica VT 1000S, Leica Microsystems, Wetzlar, Germany). The tectal agarose block was trimmed with a flat razor blade and attached to the vibratome specimen disk with superglue, with the posterior ends now oriented upward and the dorsal tectum oriented toward the vibratome blade. Tecta were sectioned at 150 micron intervals; only tectal slices in which the tectal ventricle and, in tecta aged E10 through E13, the nucleus mesencephalicus lateralis, pars dorsal was present were selected for storage in pre-chilled 1x PBS on ice. These sections were then dissected in chilled 1x PBS on a dissecting scope (Zeiss Stemi SV6 or Zeiss Stemi 2000, Carl Zeiss Microimaging, LLC, Oberkochen, Germany). The tectal surface from approximately SGFS-G to the surface of the stratum opticum was separated from each tectal slice using a bent, sharpened tungsten pin with a cutting edge of 4 millimeters.

Each of these surface strips was then divided into five equal pieces by length via cutting with the same tungsten pin. These pieces were collected and grouped into individual proteinase-free eppendorf tubes of chilled 1x PBS based on position (medial-most to lateral-most) for each tectum.

As soon as all sections were dissected and organized, the eppendorf tubes had their contents spun down in a microcentrifuge (Thermo Forma MicroCentrifuge, Thermo Fisher Scientific, Waltham, MA) at 13,000rpm for one minute. The 1x PBS was then removed and 100 microliters of homogenization buffer (10mM Tris (pH 7.4), 1mM spermidine, 1.5mM $CaCl_2$) was added. The tissue samples were then homogenized with twenty twisting strokes of a tissue grinder (749520-0090, Kimble Chase, Vineland, NJ), and spun at 3.2 rpm for 5 minutes to concentrate the nuclei and other large debris in the pellet, leaving the membranes (which should contain the proteins of interest) and the cytoplasm in the supernatant. The supernatant was then transferred to new proteinase-free eppendorf tubes, and protein concentration was determined using a Bio-Rad Quick Start Bradford protein assay (500-0202, Bio-Rad Laboratories, Hercules, CA). A 6x SDS sample buffer was then added to each sample for a final concentration of 1x buffer, and the tubes were boiled in water in a tabletop heat block for 7-8 minutes. These tubes were then either used directly in protein gels for gradient analysis or were stored in a -80C freezer (Thermo Forma 906, Thermo Fisher Scientific, Waltham, MA) and later re-boiled for 7-8 minutes for use. Once re-boiled, any solution not used in experiments was discarded; samples were never further refrozen for repeated use.

Gradient Western blot – SDS-PAGE, transfer, and Western blotting

For SDS-PAGE, 8% or 10% SDS-PAGE gels were created using stock solutions; these concentrations allow for a clear separation of the bands of interest (Wnt3 at 37kD or ephrinB1 at 40kD), and the loading control α-tubulin at 50kD. Protein lysates were loaded into wells from medial-most to lateral-most in sequence order, with approximately 10-20 micrograms of protein loaded per well, based on Bradford analysis concentrations. To confirm protein size and track SDS-PAGE progress, 6 microliters of protein ladder (161-0374, Bio-Rad Laboratories, Hercules, CA) was loaded on the medial end of the well sequence.

After SDS-PAGE gels were run sufficiently to observe separation of the relevant ladder bands, the process was stopped, and the protein bands were transferred onto a membrane (Immobilon-P transfer membrane, EMD Millipore Corporation, Billerica, MA) using a protein-blotting transfer tank (Bio-Rad Mini Trans-Blot cell, Bio-Rad Laboratories, Hercules, CA) at 4C for 105 minutes at a constant 350 milliamps. To confirm smooth and complete transfer of proteins, the resultant nitrocellulose membrane was then placed in Ponceau solution for 10 minutes. The Ponceau solution was recycled into a common stock, and any remaining solution was rinsed away with water to reveal red protein bands of approximately even strength.

For Western blotting, the membrane was blocked for 60 minutes in a 5% milk (20-241 nonfat dry milk (blotting grade), Apex BioResearch Products, San Diego, CA) in 1x Tris-buffered saline (TBS) solution, then incubated at 4C in an antibody solution containing 5% milk in 1x TBS, mouse anti-α-tubulin (1: 20,000, Sigma T8023, Sigma-Aldrich, St. Louis, MO), and either rabbit anti-Wnt3 (1:100, Invitrogen 38-2700

(formerly Zymed), Invitrogen Corporation, Carlsbad, CA) or rabbit anti-ephrinB1 (1:500, sc-1011, Santa Cruz Biotechnology, Inc., Santa Cruz, CA) for 48 hours. The blots were rinsed three times with 5% milk in TBS and twice with 1x TBS alone for 15 minutes per wash, then incubated in 5% milk in TBS containing donkey anti-mouse IgG horseradish peroxidase (HRP) (1:1000, sc-2134, Santa Cruz Biotechnology, Inc., Santa Cruz, CA) and donkey anti-rabbit IgG HRP (1:1000, sc-2077, Santa Cruz Biotechnology, Inc., Santa Cruz, CA) for two hours at room temperature (approximately 24C). After this, the blots were again rinsed three times with 5% milk in 1x TBS followed by two rinses in 1x TBS alone for 15 minutes per wash, then excess fluid was removed via light touching at the corners with a Kimwipe. The HRP was then used to activate a luminescent reaction using a SuperSignal West Pico chemiluminescence kit (34080, Thermo Fisher Scientific, Waltham, MA) by laying the membranes protein surface down on a 1:1 solution of SuperSignal West Pico chemiluminescent substrate and hydrogen peroxide for 5 minutes. After this, excess fluid was again removed via light touching at the corners, the membranes were mounted in sheet protectors within a film developing casette (Kodak BioMax cassette, Eastman Kodak Company, Rochester, NY) and taken to a darkroom. The luminal reaction was recorded using film (E3018, Denville Scientific Inc., Metuchen, NJ) and developed using a commercial developer (Konica SRX-101A, Konica-Minolta Holdings, Inc., Marunouchi, Japan). Films were developed in which either the α-tubulin loading control bands or the ligand (Wnt3 or ephrinB1) bands were within their linear exposure range to ensure clarity for later image processing.

Chick retinal explant culture and immunohistochemistry

Retinal explant cultures were developed based on a technique from Hansen et al., 2004. First, retinas were dissected from E6 chick embryos using sharp forceps in chilled L-15 media, then dorsal and ventral retinal regions were cut into squares of 0.5 millimeter per side using a sharpened tungsten pin. The retinal explant squares were placed onto poly-D-lysine (PDL) and laminin-coated coverslips with the ganglion cell layer (the inner retina) facing downward for better growth and attachment.

Glass coverslips were prepared by first irradiating the coverslips (12-545-82 Fisherbrand 1.2mm-diameter circular cover glass, Thermo Fisher Corporation, Waltham, MA) for 20 minutes, then placing them into four-well plates (Nalge Nunc 176740, Thermo Fisher Scientific, Waltham, MA). The coverslipped wells were then exposed to a PDL solution (1:100 PDL (P6407, Sigma-Aldrich, St. Louis, MO) in filtered 1x PBS) for one hour in a 37C, 5% CO_2, humidified incubator (Steri-Cult CO_2 Incubator, Thermo Fisher, Waltham, MA) and rinsed three times with autoclaved filtered water. Next, a laminin solution (4ug/mL laminin (23017015, Invitrogen, Carlsbad, CA) in autoclaved filtered water) was added to the wells and the plate was again placed in a 37C humidified incubator for one hour, then again rinsed three times with autoclaved filtered water.

After the retinal explants attached to the surface of the coated coverslips, 300 microliters of a retinal culture media (80 uL 1M glucose, 10uL penicillin-streptomycin (Gibco Pen Strep, Invitrogen, Carlsbad, CA), 10uL Glutamax (Gibco GlutaMAX, Invitrogen, Carlsbad, CA), 10 uL B-27 supplement (Invitrogen, Carlsbad, CA), 1 ul NT-3 (R&D Systems, Minneapolis, MN), and 1 uL NGF (R&D Systems, Minneapolis, MN) filled to 1 mL with Neurobasal medium (for a total of 1 mL media per four-well plate),

filtered once with a 25mm syringe filter (0.45um 25mm sterile syringe filter, 09-719B, Thermo Fisher, Waltham, MA) were added to each well, and the explants were cultures for 24 hours in a 37C humidified incubator. The cultures were then fixed with pre-warmed 4% PFA in PBS added directly to the culture medium (for a 2% PFA final concentration) at 37C for 20 minutes.

After one hour in a 2% horse serum in 1x PBS buffering solution, immunohistochemistry was performed using rabbit anti-Ryk polyclonal antibodies (1:200, Zou lab (Schmitt et al., 2006)) and either goat anti-EphB1 (1: 200, sc-9319, Santa Cruz Biotechnology, Santa Cruz, CA) or goat anti-EphB2 (1:200, sc-1763, Santa Cruz Biotechnology, Santa Cruz, CA) antibodies in a 0.5% Triton X-100 (1610407, Bio-Rad Laboratories, Hercules, CA) and 0.5% horse serum (26050088, Invitrogen, Carlsbad, CA) in 1x PBS solution at 4C overnight. The coverslips were washed three times, ten minutes each, with 1x PBS, then exposed to a secondary antibody solution comprised of anti-rabbit AlexaFluor555 (1:500, A31572, Invitrogen, Carlsbad, CA) and anti-goat AlexaFluor488 (1:1000, A11055, Invitrogen, Carlsbad, CA) with 0.5% Triton X-100 and 0.5% horse serum in 1x PBS for two hours at room temperature in a dark box. The coverslips were washed three times, ten minutes each, in a dark box in 1x PBS, then mounted with Fluoromount-G (SouthernBiotech, Birmingham, AL) for visualization on a Zeiss inverted confocal microscope (Zeiss LSM 510 (on an Axio Observer Z1 inverted microscope), Carl Zeiss Microimaging, LLC, Oberkochen, Germany).

Generation of Ryk shRNA construct for retinal electroporation

A Ryk shRNA construct targeting a region common to both chick and mouse Ryk was generated by inserting the sequence ACCCAACAATGCAACACCC into the pSUPER.neo+GFP vector for expression (OligoEngine, Seattle, WA, USA). The Ryk shRNA scramble sequence GAAACCACCCATCCACACA was similarly inserted. Down regulation of Ryk protein expression was tested through co-transfection in Cos7 cells with RykHA overexpression to assess specific targeting The resultant down regulation was observed via Western blot; an anti-HA antibody (1:1000, Sigma, St. Louis, MO) was used to label the Ryk band, and GAPDH was used as a loading control (1:1000,MAB374, Chemicon, Rosemont, IL).

***In ovo* retinal electroporation**

On E7, eggs were checked for the survival, health, and location of their embryos by placing them up to a brightly shining gooseneck lamp, a procedure known as candling. Eggs were selected for electroporation if the interior membranes appeared continuous and the chorioallantoic membrane showed bright red blood vessels and had detached from the egg surface, generating an appropriate manipulation space for the electroporation.

To access the embryo, a piece of clear heavy-duty packaging tape (Scotch 3500 High-Performance Packaging Tape, 3M Company, Preston, MN) was smoothed onto the egg shell, and an oval window was cut to access the manipulation space using curved scissors. Blunted forceps were then used to shift the chorioallantoic membrane and tear the amniotic membrane, which was used to shift the embryo's head toward the torn opening. A sharpened straight tungsten pin was then used to poke a hole through the

dorsal or ventral sclera of the embryo's right eye for retinal access. Approximately 2 microliters of a DNA mixture containing 10% Fast Green dye (Fast Green FCF, Thermo Fisher, Waltham, MA) for visibility was then injected between the vitreous body and retina via a capillary tube needle (half of a 1.0mm exterior, 0.75mm interior, 4" long thin-wall glass filament(A-M Systems, Inc., Sequim, WA) as pulled by a Narishige PC-10 capillary tube puller (Narishige Co. Ltd., Tokyo, Japan) at 62C) attached to a mouth pipette (A5177, Sigma-Aldrich, St. Louis, MO). Embryos were injected with one of several mixes: 0.75ug/uL pN2.1 (Clontech pEGFPN2 vector modified to contain a chick β-actin promoter for better expression in neurons) (EGFP-only controls); 0.9ug/uL pSUPER.neo+GFP (shRNA controls, OligoEngine); 0.75ug/uL pIRES2.1(Clontech pIRESN2 vector modified to contain a chick β-actin promoter) Ryk IRES EGFP and 1.25ug/uL pCDNA4B (Invitrogen, Carlsbad, CA) RykHA (Ryk overexpression); 0.75ug/uL pIRES2.1 EphB2 IRES EGFP and 1.25ug/ul pCDNA3 (Invitrogen, Carlsbad, CA) EphB2-Flag (EphB2 overexpression); 0.9ug/uL pSUPER.neo+GFP Ryk shRNA (Ryk shRNA, OligoEngine), or 1.0ug/uL pCIG2 RykDN IRES EGFP (Ryk dominant negative). After injection, the eye was electroporated at 21V using a BTX ECM830 Electro Square Porator (BTX Instrument Division (Harvard Apparatus), Holliston MA) with gold-plated electrodes (Model 512 in ovo L-shaped electrodes with 5mm gold tips, BTX, Holliston, MA). The chorioallantoic membrane was then readjusted to cover the embryo, and the window in the eggshell was sealed with another piece of packaging tape, after which the egg was returned to the incubator to continue developing.

At the appropriate age (E10-E14 for developmental progression studies, E11 for initiation studies, or E12-E15 for mediolateral choice studies), surviving electroporated

eggs were removed from the incubator for dissection and imaging. The electroporated eye and contralateral tectum were removed, and in some cases, the whole retina was dissected from the electroporated eye to ensure electroporation quality and chick health. After meninges were removed from a dissected tectum, it was placed electroporated axon-side down on a Superfrost glass slide and flattened slightly by pressing with a glass coverslip to decrease tectal curvature for more even imaging of the tectal surface.

Electroporated tecta were imaged using a Zeiss inverted confocal microscope (Zeiss LSM 510 (on an Axio Observer Z1 inverted microscope), Carl Zeiss Microimaging, LLC, Oberkochen, Germany). A tile scan of each tectum was taken to observe the quality, position, and length of electroporated axons in the tectum. Z-stacks of electroporated axons were taken along the length of axons for developmental progression studies and in regions containing interstitial branches for mediolateral direction choice and initiation studies. These images were taken at 3.75-micron intervals within the Z-stack, to a minimal tectal depth of 60 microns, with the tectal surface being defined as the first image in which the primary axons appeared in focus. Z-stack locations were selected by eye to tile regions containing the appropriate electroporated axons or branches.

Image Processing and Data Analysis

Gradient Western blot image preparation and quantification

Developed film of gradient Western blots was scanned and converted to 8-bit images, then measured for band area in ImageJ. Separate scans were used to ensure that only linear exposures for the loading control (α-tubulin) bands and the ligand (Wnt3 or

ephrinB1) bands were measured. The ligand bands were normalized to the loading control bands (to compensate for any unevenness of loading), then to the medial-most ligand band, setting that band as 100% signal. Three Western blots were used for each ligand and age (E10-E12); their normalized signal numbers were averaged per position (medial-most through lateral-most) to generate graphical data, with standard deviation as the calculated error. Statistical significance was calculated between ages and positions per ligand using an ANOVA with a Bonferroni post hoc test. Because gradient Western blots show comparative rather than absolute protein levels, the ligand conditions were not compared to each other.

Retinal explant image preparation and quantification

Z-stacks of cultured coverslips were converted to two-color (red for Ryk, green for EphBs) flattened projections using the Zeiss LSM Image Browser. Four images from a single well were selected for each of three experiments for each of the two conditions (Ryk-EphB1 and Ryk-EphB2). Axons ending in extended, open growth cones within each image were tallied for the presence of signals for Ryk, EphB, or both. Data for all images from a single experiment were added together, and these numbers were used to calculate percentages for each experiment. The experimental numbers were then averaged to determine the comparative percentages, with standard deviation as the calculated error. Significance was calculated for each condition using a χ^2 test.

Preparation and quantification of tectal images:

Preparation of images for morphological quantification

Tectal Z-stacks were converted into flattened black-and-white projections using LSM Image Browser, with the tectal surface (first image in the stack to be flattened) defined as the first image in which primary axons appeared to be in focus. For all studies involving measurement of primary axons, interstitial branches, and secondary branches, stacks of 8 images (26.25 microns at maximum depth) were employed. This both generally limited the axons and branches measured to those within the stratum opticum and decreased additional background and visibility issues which could be caused by including deeper arbors in the flattened projection. The projections from a given tectum were then pieced together in Adobe Photoshop CS4 (Adobe Systems Incorporated, San Jose, CA) using the Auto-Align: Reposition function, followed by readjustment by hand to ensure proper alignment of images. Quantification was performed on the complete combined images generated from these projections.

Quantification of primary axon length, branch length, %IB

For comparison of primary axon length between dorsally- and ventrally-electroporated populations of axons, complete combined tectal images were measured in ImageJ using the freehand measurement tool. Each primary axon was measured from its entry site, defined by a visible change in depth and angle of the primary axon as it enters the tectum, to its tip. Where necessary, a conversion factor from pixels to microns was determined by including a 200-micron scale bar in some images and measuring the scale bar during the measurement stage. Primary axon lengths for each tectum were averaged,

and the average of these per-tectal lengths was used to determine the average primary axon length for a given age and electroporation position. Unpaired Student's t-test was used to determine the p-value for dorsally- versus ventrally-electroporated populations at a given age, and standard error of the mean (SEM) was calculated to show error ranges.

Interstitial branches were defined as apparent branches over 5 microns in length (to distinguish branches from possible initiating membrane protrusions along the primary axon) located along the primary axon or perpendicular to the end of a primary axon, traveling no deeper than 26 microns into the tectal tissue (as limited by the projections prepared for quantification). Branches were measured, using the freehand tool in Image J, from their origin at the primary axon to the tip of the longest visible secondary branch. When necessary, as with primary axon measurements, a conversion factor was determined and employed as described above. During interstitial branch measurement, branch direction (medial or lateral, described in greater detail in a separate section below) and presence and number of secondary branches (all branches excepting the longest emerging from the interstitial branch itself) were also recorded. After conversion, average interstitial branch length was calculated for each tectum, and these averages were used to determine the average interstitial branch length for each age and position. Unpaired Student's t-test was used to determine the p-value for branch populations electroporated with various DNA mixtures or at different locations at a given age, with SEM calculated to show error ranges.

Percent interstitial branching was measured for developmental progression study tecta. Percent interstitial branching (or %IB) describes the percentage of primary axons in a given tectum that appear to have at least one interstitial branch of a length of 5

microns or greater. To determine this, the entire length of each primary axon in a tectum was inspected for the presence or absence of interstitial branches, and that presence or absence was recorded, generating a %IB for each tectum. These percentages were then averaged for a given population (dorsally- or ventrally-electroporated, by age), and unpaired Student's t-test was used to determine p-value between the two populations at a given age.

Quantification of branch direction choice ratio

Interstitial branch direction (medial or lateral) was recorded during the measurement of interstitial branch length. While branches were virtually never observed to completely change direction, for consistency, branch direction was defined as the mediolateral direction of the tip of the branch. Medial versus lateral direction was defined based on the eye electroporated and the method of imaging, and recorded in the image file during the imaging process; with the current version of the Zeiss-EMBL AIM software for the inverted Zeiss microscope and the tecta position used for imaging, medial is toward the right and lateral toward the left for all right-eye electroporations and reversed for (rare) left-eye electroporations in raw images. (All images were oriented with lateral as right for figures for consistency, unless labeled otherwise.)

To determine branch direction choice ratios, medial versus lateral-directed branch numbers were counted for each tectum. The larger of the two numbers was divided by the smaller, and 1 was subtracted to account for the inherent expected 1:1 medial:lateral ratio of branch direction choice in control populations; the ratio therefore describes number of branches above(lateral) or below (medial) balanced control populations.

Control (EGFP-only) populations should have a branch direction choice ratio of approximately 0, while a tectum having five medial branches per lateral branch (5:1 medial) would have a ratio of -4. The overall ratio for each condition and age was generated by averaging the ratios of the tecta of that population, and populations were compared by age and condition using unpaired Student's t-test.

Quantification of % secondary branching, branching index

Presence and number of secondary branches (branches emerging from interstitial branches, whether to form false early arbors or final, stable arbors) within the 26-micron depth of the approximate stratum opticum were recorded during measurement of interstitial branch length. Percent secondary branching describes the percentage of interstitial branches in a given tectum that appear to have at least one secondary branch. These percentages were calculated for each tectum, and the average of these percentages for a given population (by age and condition) used as the percentage of secondary branching for that population. Populations were compared using unpaired Student's t-test.

The branching index averages the numbers of branches displayed by interstitial branches that possess secondary branches, showing the degree to which further branches are formed in those interstitial branches inclined to secondary branching. Again, these numbers were calculated on a per-tectal basis, and the individual tectal numbers averaged to generate a branching index for a given type of electroporation and age, then compared using unpaired Student's t-test.

Preparation of depth-coded images

Tectal Z-stacks were converted into depth-coded images using LSM Image Browser, with the tectal surface (whose contents appear as dark blue) defined as the first image in which primary axons appeared to be in focus. For all studies involving the depth-based morphology of electroporated axons in the tectum, stacks of 17 images (60 microns at maximal depth, which appears as bright red) were employed. While some arbors traveled to depths greater than 60 microns in older tecta, the 60 micron limit provided a consistent point of comparison between populations, given that these older, deeper-targeting tecta could be visually compared by the degree of 60-micron (red) labeling present, rather than maximal depth. The depth-coded projections from a given tectum were then pieced together in Adobe Photoshop CS4 using the Auto-Align: Reposition function, followed by readjustment by hand to ensure proper alignment of images.

Chapter 2, in part, has been submitted for publication of the material. Richman, Alisha; Zou, Yimin. The dissertation author was the primary investigator and author of this material.

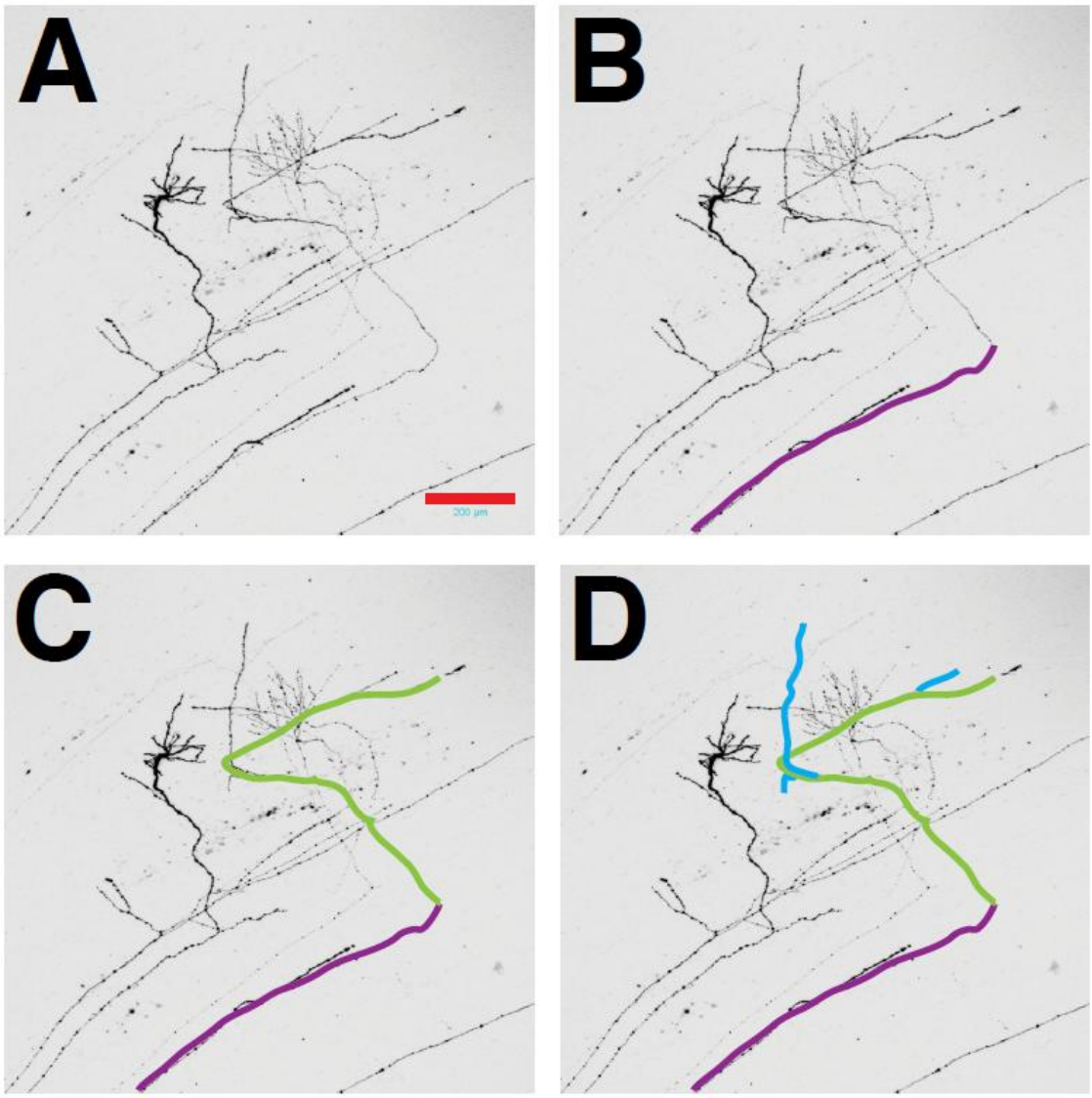

Figure 2.1. Quantifying interstitial branch direction, length, and secondary branching. (A) A region of an E14 ventrally-electroporated EGFP-only control tectum showing primary axons, interstitial branches and secondary branching. Red scale bar represents 200 microns. (B) First, identify the primary axon (purple). (C) Second, identify the interstitial branch (olive green) and measure its length from its perpendicular origin at the primary axon to the tip of its longest branch. This branch extends medially from the primary axon and is quantified as medial. (D) Count secondary branches (aqua) extending from the interstitial branch measured.

CHAPTER 3: RESULTS

Wnt3 gradient expands laterally, ephrinB1 gradient remains stable during mapping

While the presence of ephrinB1 (at E3-E14 in Braisted et al., 1997) and Wnt3 (at E10 in Schmitt et al., 2006) tectal gradients has been shown in the chick retinotectal system, a full temporal analysis has not been performed for Wnt3, and neither gradient has been subjected to quantitative analysis. For temporal analysis of expression, *in situ* hybridization (ISH) was performed with Wnt3 and ephrinB1 riboprobes in tecta at E10-E13, key ages framing the period of retinotectal mapping (Crossland et al, 1975; Thanos and Bonhoeffer 1983; Nakamura and O'Leary, 1989; Vanselow et al, 1989). This hybridization showed that between E10 and E13, the gradient expression of Wnt3 appeared to be limited to a laterally shifting region (indicated by small arrows), while the ephrinB1 gradient remains stable during this period (Figure 3.1A).

In situ hybridization indicates the mRNA expression of the tectal gradients within the ventricular epithelium; however, these gradient proteins must be trafficked from the ventricle to the tectal surface along radial glial cells in order to interact with incoming retinal axons (Braisted et al. 1997; Hindges et al, 2002; Schmitt et al., 2006). To characterize the surface protein expression of the two mediolateral gradients, Wnt3 and ephrinB1, during the period of mediolateral mapping, I used Western blotting with tectal position-specific lysates between E8 and E13. This indicated that the steepest part of Wnt3 protein gradient was initially limited to the medial tectum, and this front shifted from medial to lateral from E10 to E12 (Figure 3.1B-C). On the other hand, the ephrinB1 gradient remained constant during this period (Figure 3.1D-E). Wnt3 showed no

expression, and ephrinB1 low expression, at E8 and E9; while ephrinB1 expression remained at E13, Wnt3 expression surprisingly disappeared (data not shown). Superficial tectal tissue from five evenly spaced topographic positions along the medial-lateral axis was dissected from vibratome sections of tecta of appropriate ages, with samples from "position 1" being the most medial and those from "position 5" being the most lateral. Membrane fractions of these tectal tissues were then analyzed for the expression levels of Wnt3 and ephrinB1 using Western blots with Wnt3 and ephrinB1 antibodies. For quantification, Wnt3 or ephrinB1 bands were normalized to their respective α-tubulin loading controls, and then normalized to a percent pixel density with lane 1 (the medial-most tectal membranes) set at 100%. Overall, the results showed that Wnt3 gradient was much steeper and showed a lateral shift in its gradient front, while ephrinB1 gradient was both less steep and relatively stable (Figure 3.1B-E). This opened up the possibility that the intersection of these two gradients, based upon the lateral shift of the Wnt3 gradient, would move laterally over time, generating a series of laterally-shifting balance points for interstitial branches to target during retinotectal mapping.

Retinal ganglion cell axons develop in a medial-to-lateral temporal progression

Given the temporal component of gradient expression, I was interested in whether there was a corresponding directional progression of development in the retinotectal system. In order to investigate this, dorsal and ventral populations of retinal ganglion cells in age-matched chicks were electroporated with pN21 to express EGFP, and the developmental progression of the two sets was compared between E10 and E14.

To visualize the tecta along the entire length of the electroporated primary axons in the tecta, depth-coded images were generated from a series of 60-micron thick Z-stacks, where dark blue comprises the tectal surface (defined here as a point at which the primary axons are first in focus) while red represents the deepest arbors at 60 microns (see depth label in Figure 3.2J). These images were combined to show the developmental profile of these retinal axons. Directly comparing paired dorsal and ventral (lateral and medial tectal) images, it is apparent that at E10, retinal primary axons in the medial tectum outpace those in the lateral in tectum in extending posteriorly along the tectal surface (Figure 3.2A,F). While short interstitial branches begin to appear at E11 in both groups (Figure 3.2B,G), those in the medial tectum appear to be longer and more ramose until E13 (Figure 3.2C,D,H,I). By E14, both groups appear to have equally extended and developed interstitial branches (Figure 3.2E,J).

Several features of the developing retinal axons were quantified, including the length of primary axons and interstitial branches as well as the presence of interstitial branches on primary axons, to further clarify the developmental progression of these retinal axon populations. Quantification of the length of primary axons showed results similar to those observed in tectal images, with medial tectal axons being significantly longer than lateral axons at E10, after which the two populations were more similar in length (Figure 3.2K, Table 3.1). Medial tectal (ventrally-electroporated) retinal axons were quantified as significantly longer than lateral tectal populations from E11 through E13, with the two populations having similar length by E14 (Figure 3.2L, Table 3.1). The presence of interstitial branches on primary axons was also used as a metric for developmental progression, as primary axons must initiate and extend interstitial

branches in order to reach their ultimate mapping targets and form synapses with tectal cells. These percentages showed that medial axons were more likely to display interstitial branches than their lateral counterparts through E12, though the two were more evenly matched from E13 through the general saturation of the metric at E14 (Figure 3.2M, Table 3.1).

Ryk and EphBs localize to same retinal ganglion cells

Ryk, EphB2, and EphB3 are expressed in a high-ventral, low-dorsal gradient pattern in retinal ganglion cells (RGCs) in the ganglion cell layer of the retina during the development of the retinotectal map, while EphB1 is uniformly present in the ganglion cell layer (Schmitt et al., 2006; Holash and Pasquale, 1995; Kenny et al., 1995; Hinges et al., 2002). However, it was unclear whether Ryk and EphBs are expressed in the same or distinct subpopulations of RGCs. If these receptors were expressed in different populations of RGCs, they might separately guide retinal axons to their mapping locations based on a single gradient (possibly via biphasic activity (Hindges et al., 2002; McLaughlin et al., 2003b)), whereas if they were expressed in the same RGCs, two-gradient competition might occur. To examine these options, receptor expression was studied in retinal explants from embryonic day 6 (E6) chicks, in which the relevant receptors are expressed as RGCs extend their axons to exit the retina and travel toward the optic tectum.

In E6 retinal explants, only retinal ganglion cells extend their axons beyond the border of the explant and onto the laminin-coated coverslip. By performing immunohistochemistry (IHC) on these explants, it was shown that Ryk and EphB1, as

well as Ryk and EphB2, are localized to the same RGC axons and growth cones (Ryk and EphB1 $p< 0.05$, Ryk and EphB2 $p< 0.0032$, Figure 3.3A-C). The receptors displayed punctate expression, but Ryk and EphB punctae did not colocalize. Further, nearly all axons expressed both Ryk and EphB1 or EphB2, while exceedingly few expressed only Ryk, EphB1, or EphB2 (Figure 3.3C). Thus, Ryk and EphBs were present within the same axons and could be capable of inducing mapping competition within these axons.

EphB protein localization and activity in axons in the optic tectum has been well characterized (Holash and Pasquale 1995, Hindges et al., 2002; Mann et al, 2002), while Ryk localization has not. To observe the localization of Ryk in RGC axons engaged in retinotectal mapping, IHC was performed on tectal slices containing EGFP-electroporated retinal axons. Immunohistochemistry of Ryk in tectal slices showed that Ryk localized along electroporated axons and was limited to the outermost layer of the tectum, the stratum opticum (SO, Figure 2.4D for general laminar organization), suggesting that Ryk is involved in surface-limited activities such as mapping and possibly initial laminar invasion (Figure 3.4E-F).

Modulation of mapping receptor levels affects branch direction choice

Ryk and EphB2 expression in retinal ganglion cells depend on the dorsoventral position of the RGC soma within the retina, with more ventral RGCs expressing higher levels of these molecules than more dorsal populations (Holash and Pasquale, 1995; Kenny et al, 1995; Hindges et al, 2002; Schmitt et al, 2006). To observe whether mediolateral mapping guidance was directly dependent on receptor expression levels, I employed *in ovo* retinal electroporation at embryonic day 7 (E7) to modify receptor

expression levels and label modified cells. The electroporated chicks were then allowed to continue developing in order to observe labeled axons in the contralateral tectum at E12 through E15, the general period of mediolateral targeting and map formation (Nakamura and O'Leary, 1989; Yamagata and Sanes, 1995). Embryonic chicks electroporated with an EGFP-expressing control plasmid in dorsal RGCs showed consistent patterns of axon outgrowth in the tectum (Figure 3.4A-B). These axons and interstitial branches appeared healthy, with visible growth cones at the ends of the primary axons at E12 and E13 and easily distinguished interstitial branches throughout this period, with early arbors visible by E12 and more distinct arbors developing by E14 (Figure3.4A-B, also Figure 3.2A-J). The control axons displayed an approximate 1:1 ratio of lateral- to medial-directed interstitial branches (Figure 3.4M, Table 3.2).

Axons overexpressing EphB2 showed consistent interstitial branch modifications. Morphologically, these axons initially had interstitial branches which seemed relatively similar to those in the control tecta, although they appeared more likely to form further branches and had a noticeable tendency to generate ectopic interstitial branches posterior to the predicted termination zone (Figure 3.4C,M). By E14 and E15, this further branching trend easily distinguished EphB2 axons from controls, and some well-developed arbors could be identified. While EphB2-overexpressing axons initially showed a weak, nonsignificant trend in interstitial branch direction choice, by E13 a significant medial trend emerged, remaining significant through E15, the highest age studied (Figure 3.4M, Table 3.2).

Ryk overexpression induced more immediate differences in interstitial branch direction choice and morphology. Similar to EphB2-overexpressing axons, Ryk-

overexpressing axons were prone to forming ectopic interstitial branches posterior to the predicted termination zone at earlier ages, many of which remained through E15 (Figure 3.5D). Ryk-overexpressing interstitial branches displayed a consistently significant, increasing lateral direction choice trend from E12 through E15, beginning at 1.75 lateral branches per medial branch at E12 and increasing to 4.38 lateral branches per medial branch by E15 (Figure 3.4M, Table 3.2).

To confirm that altering mapping receptor levels controls branch direction choice, the downregulation of Ryk signaling and expression was induced, with the expectation of observing a medial shift in branch direction. To outcompete endogenous Ryk receptors and thus decrease Ryk signaling, a Ryk dominant negative construct lacking the intracellular domain (Schmitt et al., 2006) was electroporated into E7 dorsal chick retina. The resultant RGC axons, observed at E12 through E15, showed a consistent medial trend, which was significant at E12 but petered off with time, ranging between 1.34 and 1.66 medial branches per lateral branch (Figure 3.4F,M, Table 3.2). These branches appeared to be slightly shorter than those observed in controls and overexpression tecta, although they showed no noticeable differences in further branching or other morphological features (Figure 3.4F).

As the Ryk dominant negative construct outcompetes but does not necessarily decrease endogenous Ryk, we further tested the effects of decreasing Ryk receptor levels by employing a short hairpin RNA targeted to the Ryk intracellular juxtamembrane region. This Ryk shRNA construct was electroporated into E7 dorsal chick retina and was observed to induce a similar consistent medial shift to Ryk DN, initially significant at E13 but petering off with time (Figure 3.4E,M, Table 3.2), as well as a number of

specific changes to interstitial branches. First, primary axon growth and interstitial branching were delayed by approximately one day, such that these RGC axons entered the tectum at E11 and lacked stable interstitial branches prior to E13. Due to the lack of E12 interstitial branches, no data were collected for Ryk shRNA tecta at E12. Further, the branches observed at E13 appeared short and often gnarled (Figure 3.4E). This lack of elongation remained through E15, and it appeared that fewer of these interstitial branches produced further branches or formed distinctive arbors.

When electroporation was performed on ventral RGCs, which have much higher endogenous levels of Ryk, both Ryk overexpression and downregulation produced strongly significant effects on branch direction choice at E14, with Ryk showing a lateral choice trend while Ryk downregulation induced a medial trend, as with dorsal electroporations (Figure 3.4F-J,N, Table 3.3). In these ventral populations, Ryk downregulation showed no visible effect on branch initiation or outgrowth (Figure 3.4I-J).

Mapping receptor levels also affect the morphology of interstitial branches

Differences in branch length, shape, and arborization were readily observed during quantification of direction choice (Figure 3.5A-E). While several of these observed modifications were described above, quantification of elongation and further branching was used to clarify whether these effects were significant characteristics of modulation of Ryk and EphB2 levels.

To quantify branch length, each interstitial branch was measured freehand in ImageJ from its origin at the primary axon to the tip of its longest secondary branch (see

Figure 2.1 for example). These measurements indicated that while overexpression of Ryk and EphB2 had no apparent effect on overall branch length, downregulation of Ryk caused significant delays or decreases in interstitial branch outgrowth. Axons expressing the Ryk dominant negative construct showed significantly lesser interstitial branch length or outgrowth from E12 through E14, although they appeared to extend to control lengths by E15 (Figure 3.5F, Table 3.2). Interstitial branches of axons expressing Ryk shRNA were more strongly affected, with interstitial branching delayed until E13 and branch lengths through E15 significantly shorter than control lengths (Figure 3.5F, Table 3.2). This suggests that decreased Ryk levels, but not increased Ryk or EphB2 levels, affects branch development and outgrowth.

Arbor development was characterized by quantifying the presence and number of branches observed along each interstitial branch to a depth of 26 microns in Z-stack images. While the percentage of interstitial branches with secondary branches did not appear to be affected by modulation of mapping receptor levels (data not shown), the degree of secondary branching which occurred on interstitial branches displaying further branches was affected (Figure 3.5A-E,G, Table 3.2). The branching index describes the average number of branches displayed per interstitial branch displaying secondary branches; thus, a population in which each interstitial branch bifurcates but does not further elaborate in secondary branching would be 1, the minimal branching index possible. Using this metric, it appeared that at E14, EphB2 overexpression induced significantly more secondary branching than control populations; at E15, this also often produced more further branching, but with less apparent consistency than at E14 (Figure 3.5G, Table 3.2). Interestingly, interstitial branches expressing Ryk shRNA were

strongly affected at all ages studied, having significantly fewer branches than control populations from E13 through E15 (Figure 3.5G, Table 3.2).

Mediolateral direction choice decision is made close to branch initiation

Branch initiation occurs during E11 in both dorsal and ventral RGC populations, as shown earlier in this dissertation (Figure 3.2B,G,L, Table 3.1). To determine whether the branching decision was made close to the time of branch initiation, chicks dorsally electroporated with Ryk overexpression or EphB2 overexpression mixes were observed at E11, and the direction choices of their branches were quantified, with branches under five microns in length being excluded as unstable (Figure 3.6A-E). For both conditions, significant changes to mediolateral direction choice, as represented by the mediolateral ratio, were observed in the predicted directions (Figure 3.6E, Table 3.4).

Chapter 3, in part, has been submitted for publication of the material. Richman, Alisha; Zou, Yimin. The dissertation author was the primary investigator and author of this material.

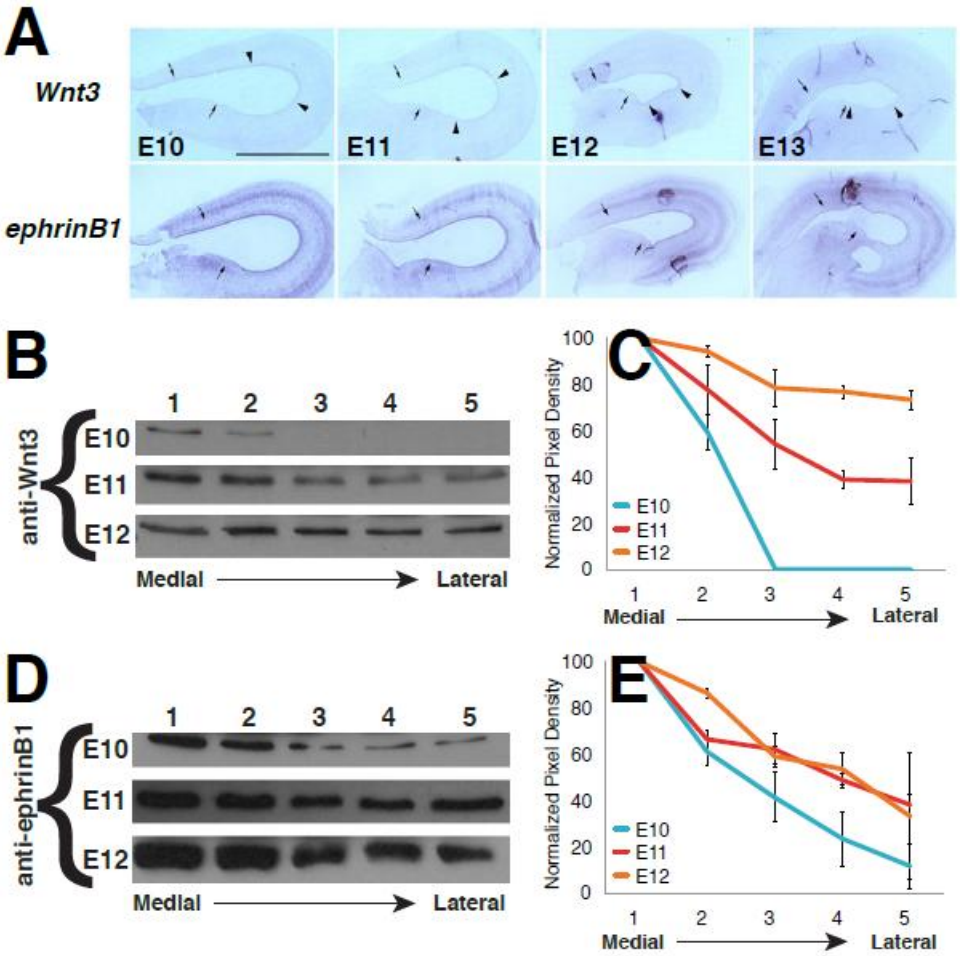

Figure 3.1. Wnt3 tectal gradient expands laterally during map development. (A) Expression of Wnt3 and ephrinB1 mRNA from E10 through E13 shows the shifting high-concentration region of Wnt3 expression (bold arrows). Small arrows show the region of Wnt3 and ephrinB1 expression. (B) Wnt3 expression in gradient Western blots at E10 through E12 indicates increasing lateral direction and intensity. (C) Relative intensity of Wnt3 bands, with the medial-most band set at 100%, shows that the Wnt3 gradient shifts laterally over time. (D) EphrinB1 expression in gradient Western blots at E10 through E12 appears relatively stable. (E) Relative intensity of ephrinB1 bands shows a consistent, shallower gradient. (F) Schematic of the moving gradient model of retinotectal mapping indicates that mapping occurs in a medial-to-lateral temporal sequence with the lateral shift of gradient mapping balance points.

Figure 3.2. The mediolateral map develops in a medial-to-lateral temporal sequence. (A-J) Representative images of time-matched pairs of dorsally- and ventrally-electroporated RGC populations in the tectum from E10 through E14 show temporal development differences. Tecta are oriented with medial (M) left and anterior (A) down (A), and are color coded by depth, with blue at the tectal surface and red at 60 μm depth (J). Scale bar: 500 μm (A). (K) Primary axon length measurements show that ventral RGC primary axons are first to enter and extend in the tectum. (L) Interstitial branch length measurements show that ventral RGCs initially extend their axons earlier than dorsal RGCs. (M) Percentages of primary axons with interstitial branches indicate that ventral RGC primary axons outpace dorsal populations in branch formation until E14. (K-M) Error bars represent ± s.e.m. *P*-values are shown with asterisks (* $p<0.05$, ** $p<0.005$, *** $p<0.0005$).

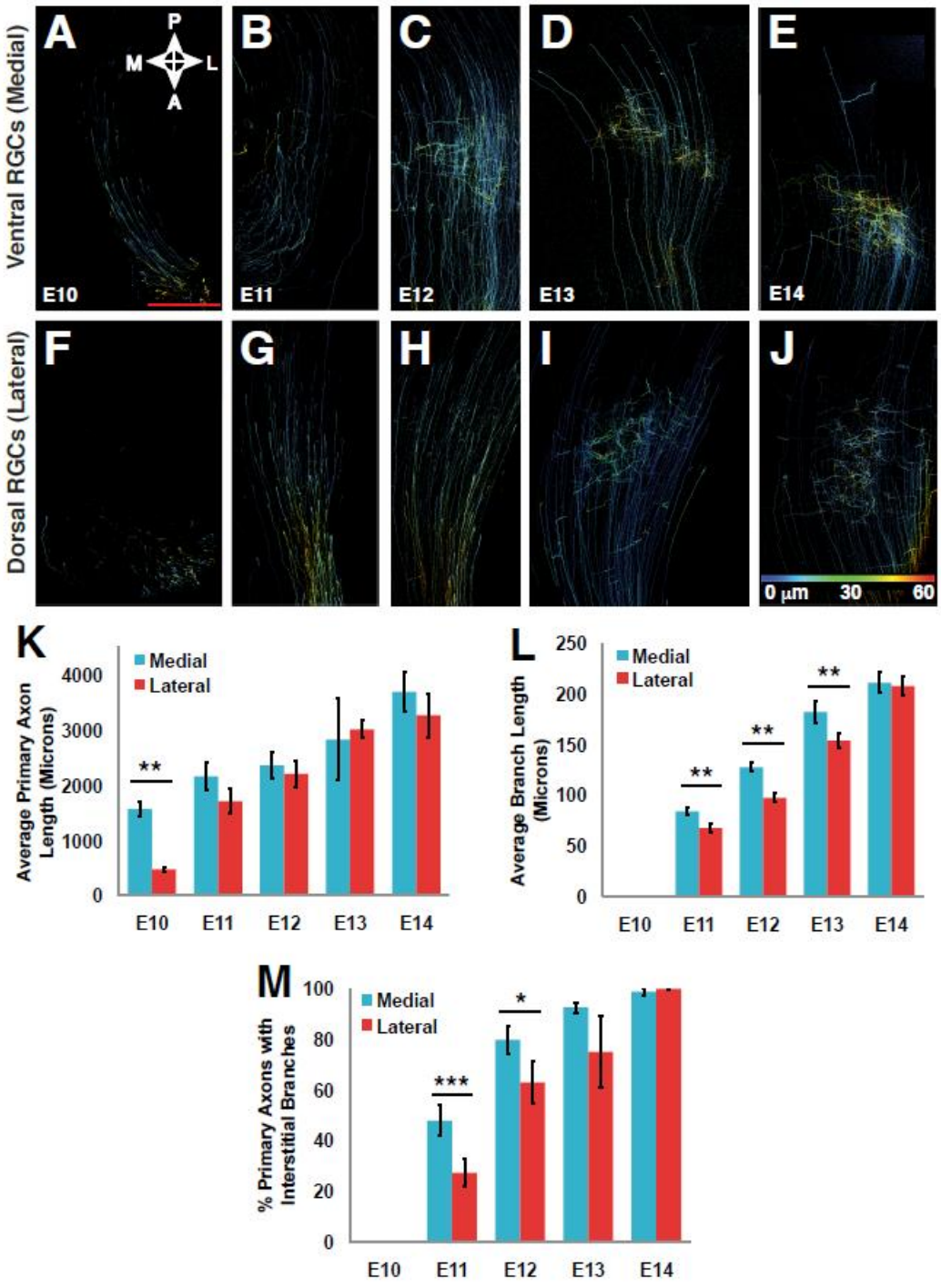
Ventral RGCs (Medial)
Dorsal RGCs (Lateral)
A
B
C
D
E
F
G
H
I
J
P
M
L
A
E10
E11
E12
E13
E14
0 µm
30
60
K
Average Primary Axon Length (Microns)
Medial
Lateral
4000
3000
2000
1000
0
**
E10
E11
E12
E13
E14
L
Average Branch Length (Microns)
250
200
150
100
50
0
**
**
**
M
% Primary Axons with Interstitial Branches
100
80
60
40
20
0
***
*

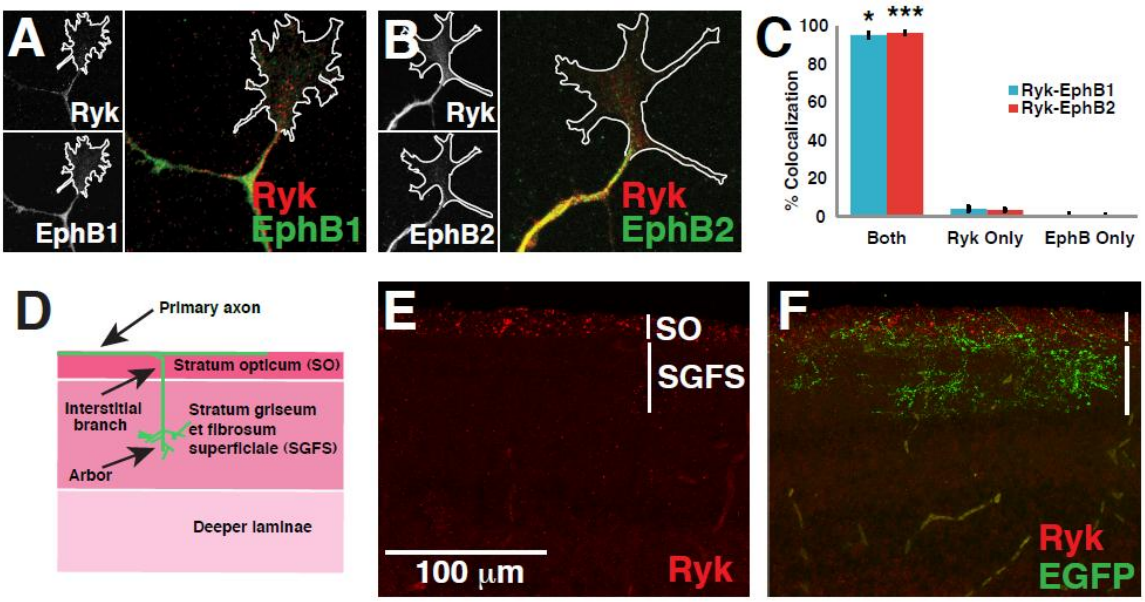

Figure 3.3. Ryk and EphB expression in retinal ganglion cells suggests their activities in the retinotectal system. (A-B) Ryk and EphB1 (A) and Ryk and EphB2 (B) in localize to the same branches and growth cones in E6 retinal explants cultured for 24 hours. (C) Quantification of Ryk-EphB localization confirms these receptors are located in the same RGCs. (D) A schematic of the tectum shows the stratrum opticum, in which mapping occurs; the SGFS, in which axons target specific sublaminae to elaborate their arbors and form synapses; and the deeper laminae into which RGC axons do not project. (E) Ryk expression appears in retinal axons the SO in E14 tectum. (F) Electroporated retinal axons travel through the SO, where Ryk expression remains, to synapse in the SGFS.

Figure 3.4. Ryk and EphB2 provide opposing guidance forces *in vivo* during retinotectal mapping. (A) Schematic of *in ovo* electroporation in dorsal retina shows the transit of axons from eye to tectum. (B-F) Representative E14 images of dorsal RGCs electroporated with EGFP only (B), Ryk overexpression (C), EphB2 overexpression (D), Ryk shRNA (E), or Ryk dominant negative construct (F), with medial-directed branches in magenta and lateral-directed branches in green show changes in branch direction choice. Images are oriented medial left, anterior down. Scale bars: 200 μm (B, C). (G) A schematic of *in ovo* electroporation in ventral retina shows targeting of the medial tectum. (H-K) Representative E14 images of ventral RGCs electroporated with EGFP only, (H) Ryk expression (I), Ryk shRNA (J), or Ryk dominant negative construct (K). A test of Ryk shRNA in Cos-7 cells co-transfected with a RykHA construct shows that Ryk shRNA decreases Ryk protein levels. GAPDH is shown as a loading control. (M-N) Mediolateral branch direction choice ratios for dorsal (M) and ventral (N) RGC populations show that receptor level modulation affects direction choice. Error bars represent ± s.e.m. *P*-values are shown with asterisks (* $p<0.05$, ** $p<0.05$, *** $p<0.0005$).

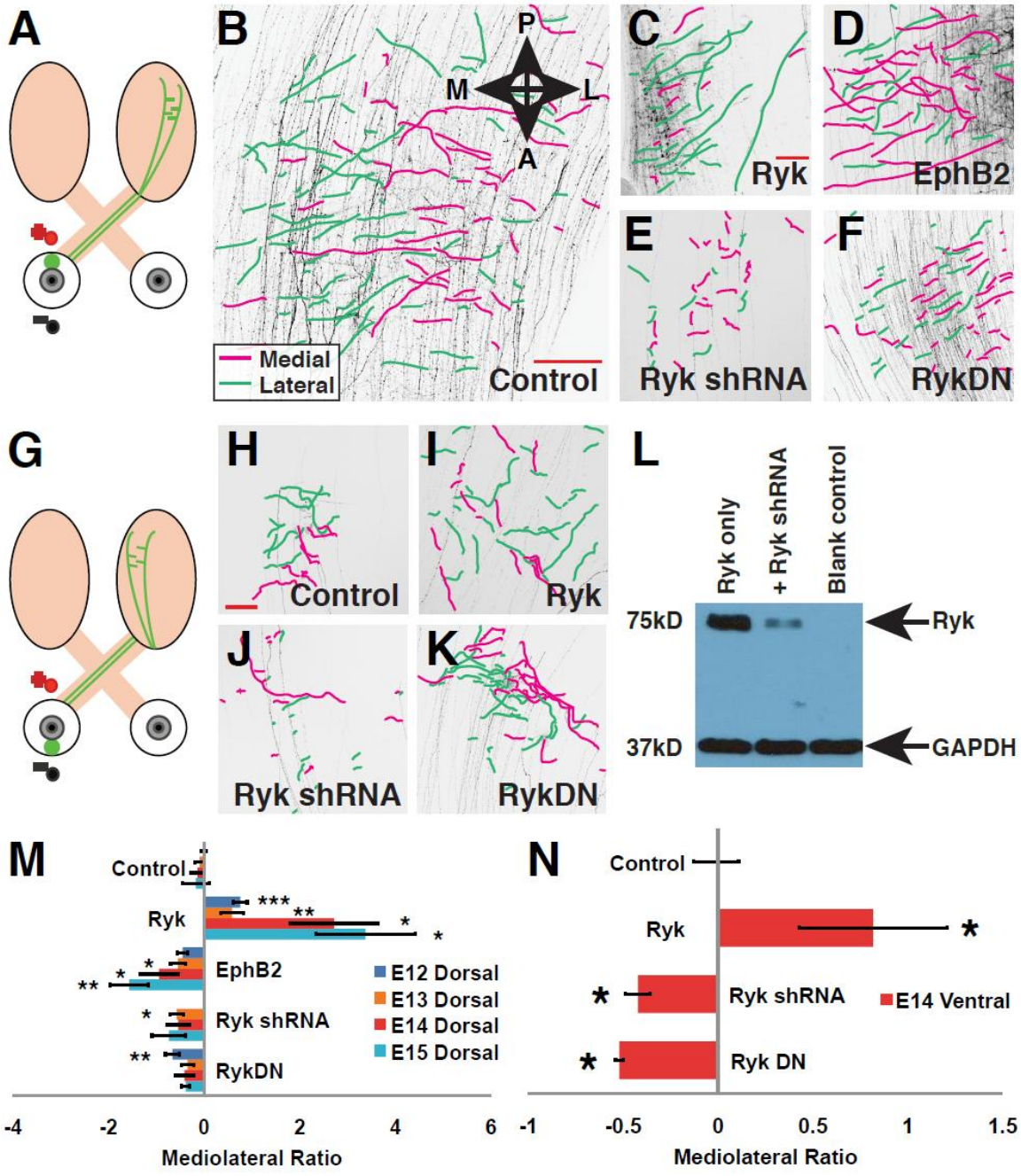
A
B
P
M
L
A
Medial
Lateral
Control
C
Ryk
D
EphB2
E
Ryk shRNA
F
RykDN
G
H
Control
I
Ryk
J
Ryk shRNA
K
RykDN
L
Ryk only
+ Ryk shRNA
Blank control
75kD
Ryk
37kD
GAPDH
M
Control
Ryk
EphB2
Ryk shRNA
RykDN
E12 Dorsal
E13 Dorsal
E14 Dorsal
E15 Dorsal
-4
-2
0
2
4
6
Mediolateral Ratio
N
Control
Ryk
Ryk shRNA
Ryk DN
E14 Ventral
-1
-0.5
0
0.5
1
1.5
Mediolateral Ratio

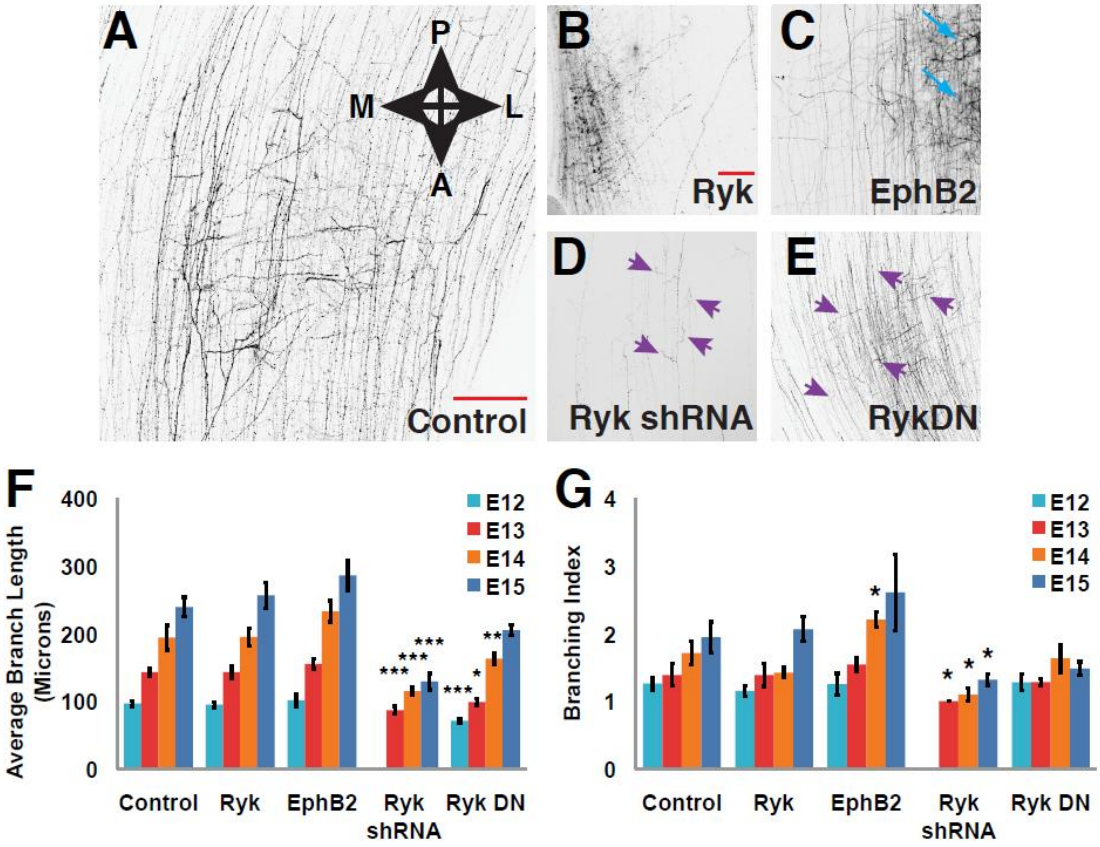

Figure 3.5. Ryk and EphB2 modulation affect interstitial branch morphology.
(A-E) Images from Figure 3.5 (B-F) without directional lines show common morphological effects observed in electroporated populations, including shortened interstitial branches (purple arrows) and increased arbor development (aqua arrows). (F) Quantification of interstitial branch length shows that decreased Ryk expression results in decreased branch outgrowth. (G) Quantification of a branching index indicates that in interstitial branches displaying further branching, EphB2 overexpression increases further branching at E14, while Ryk shRNA decreases or delays extensive further branching. (F-G) Error bars represent ± s.e.m. *P*-values are shown with asterisks (* $p<0.05$, ** $p<0.05$, *** $p<0.0005$).

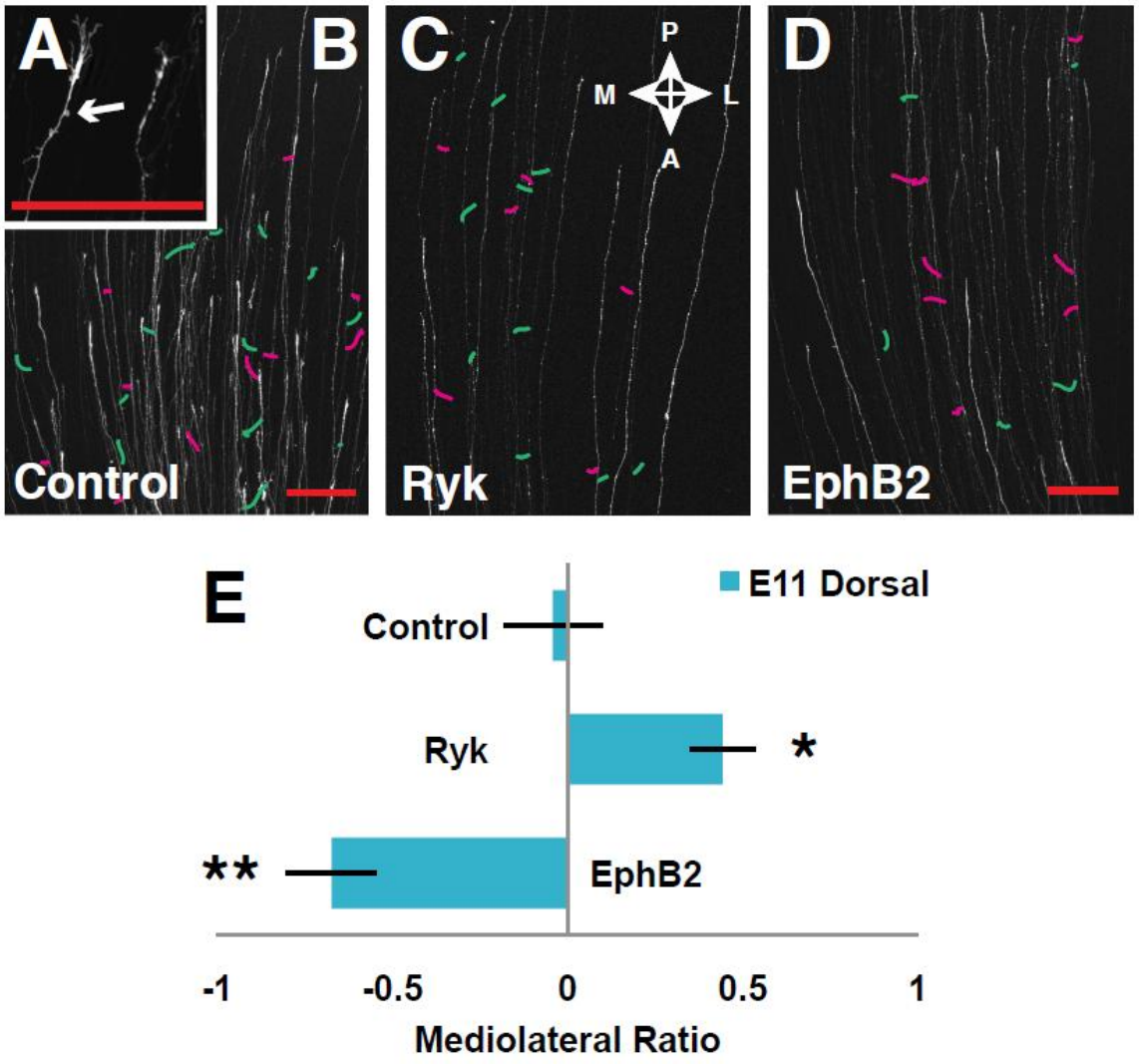

Figure 3.6. Mediolateral branch direction decision is made during branch initiation. (A) Interstitial branches form from small membrane protrusions along the primary axon (white arrow). A 5 μm minimum length was used to define interstitial branches versus protrusions. (B-D) Representative E11 images of EGFP-only (B), Ryk-overexpressing (C), and EphB2-overexpressing (D) electroporated dorsal RGC populations show differences in initiating branch direction choice. Medial-directed branches are labeled in magenta, lateral-directed branches in green. Images are oriented medial left, anterior down. Scale bars: 200 μm (A-E). (E) Mediolateral branch direction choice ratios at E11 indicate that mapping receptor levels affect branch direction early in branch development. Error bars represent ± s.e.m. *P*-values, determined using *t*-tests, are shown with asterisks (* $p<0.05$, ** $p<0.005$).

Table 3.1. Quantification of E10-E14 medial- and lateral-targeting RGC populations. Medial tectal-targeting (ventrally-electroporated) and lateral tectal-targeting (dorsally-electroporated) RGC axons were quantified for average primary axon length (PAL), average interstitial branch length (ABL), and percentage of primary axons displaying interstitial branches (%IB). Medial and lateral populations were then compared to determine whether there were significant differences in the development of dorsal versus ventral RGC populations.

Age, Orientation	N (tecta)	PAL (microns)	PAL p-value	ABL (microns)	ABL p-value	%IB	%IB P-value
E10 Medial	4	1561.395 ± 140.616	0.0026	NA	NA	0%	NA
E10 Lateral	4	471.323 ± 46.343		NA		0%	
E11 Medial	7	2157.866 ± 251.306	0.0618	83.687 ± 3.374	0.0048	47.82 ± 5.91%	0.0002
E11 Lateral	8	1703.619 ± 219.341		67.219 ± 4.294		27.15 ± 5.37%	
E12 Medial	5	2353.365 ± 240.744	0.7509	127.332 ± 4.311	0.0032	79.78 ± 5.55%	0.0276
E12 Lateral	5	2199.966 ± 233.180		97.247 ± 4.217		62.81 ± 8.30%	
E13 Medial	4	2819.966 ± 736.197	0.9336	181.849 ± 10.596	0.0010	92.52 ± 2.04%	0.2021
E13 Lateral	4	3005.25 ± 157.192		153.428 ± 7.127		75.03 ± 13.91%	
E14 Medial	4	3684.747 ± 360.070	0.8466	210.780 ± 10.150	0.0905	98.67 ± 1.33%	0.4807
E14 Lateral	4	3262.445 ± 396.747		207.535 ± 9.379		99.80 ± 0.20%	

Table 3.2. Quantification of dorsally-electroporated RGC axons expressing mapping receptor-modulating DNA constructs at E12-E15. Dorsal RGCs were electroporated with constructs designed modulate Ryk and EphB2 levels. Direction, branch length, and further branching of these axons were quantified to determine whether receptor levels affected mediolateral direction choice and/or retinal axon morphology.

Age, condition	N (tecta)	ML ratio	ML ratio p-value	ABL (microns)	ABL p-value	Branching index	BI p-value
E12 Control	9	-0.0121± 0.0509		96.492 ± 4.148		1.26 ± 0.0917	
E12 Ryk	5	0.755 ± 0.109	0.0001	94.712 ± 4.125	0.790	1.15 ± 0.0738	0.424
E12 EphB2	4	-0.451 ± 0.146	0.1388	101.248 ± 8.998	0.0836	1.25 ± 0.160	0.960
E12 Ryk shRNA	NA						
E12 Ryk DN	7	-0.663± 0.148	0.0004	71.093 ± 2.928	0.0001	1.28 ± 0.123	0.901
E13 Control	6	-0.0921 ± 0.0992		142.794 ± 5.109		1.39 ± 0.166	
E13 Ryk	5	0.583 ± 0.242	0.0326	142.636 ± 8.874	0.173	1.39 ± 0.168	0.997
E13 EphB2	5	-0.547 ± 0.155	0.0383	154.884 ± 7.126	0.411	1.54 ± 0.0971	0.452
E13 Ryk shRNA	4	-0.573 ± 0.136	0.0221	86.728 ± 5.811	0.0003	1.00 ± 0.00	0.0287
E13 Ryk DN	4	-0.348 ± 0.131	0.1556	98.580 ± 4.485	0.0123	1.28 ± 0.0497	0.605
E14 Control	6	-0.152 ± 0.140		193.813 ± 18.090		1.71 ± 0.173	
E14 Ryk	7	2.72 ± 0.922	0.0058	194.640 ± 12.599	0.303	1.42 ± 0.0754	0.132
E14 EphB2	6	-0.945 ± 0.401	0.0483	232.597 ± 15.552	0.506	2.20 ± 0.109	0.0364
E14 Ryk shRNA	4	-0.542 ± 0.226	0.1544	114.655 ± 6.382	0.0001	1.09 ± 0.0950	0.0272
E14 Ryk DN	4	-0.414 ± 0.199	0.3068	162.887 ± 8.243	0.0029	1.63 ± 0.204	0.7762
E15 Control	5	-0.174 ± 0.277		239.173 ± 14.226		1.94 ± 0.226	
E15 Ryk	6	3.38 ± 1.04	0.0148	256.342 ± 19.388	0.437	2.06 ± 0.181	0.688
E15 EphB2	5	-1.57 ± 0.400	0.0014	285.565 ± 21.500	0.0545	2.61 ± 0.562	0.306
E15 Ryk shRNA	4	-0.740 ± 0.352	0.0766	128.871 ± 11.993	0.0001	1.32 ± 0.0799	0.0406
E15 Ryk DN	5	-0.385 ± 0.0857	0.4880	204.760 ± 8.097	0.537	1.48 ± 0.101	0.0992

Table 3.3. Quantification of ventrally-electroporated RGC axons expressing Ryk-modulating DNA constructs at E14. Ventral RGCs were electroporated with constructs designed to overexpress or downregulate Ryk. Branch direction was then quantified to determine whether Ryk levels affected mediolateral direction choice in the interstitial branches of these axons.

Age, Conditions	N (tecta)	ML ratio	ML ratio p-value
E14 Control (ventral)	5	0.0625 ± 0.0686	
E14 Ryk (ventral)	4	0.8846 ± 0.3912	0.0246
E14 Ryk shRNA (ventral)	4	-0.4952 ± 0.0659	0.0003
E14 Ryk DN (ventral)	4	-0.5176 ± 0.0200	0.0001

Table 3.4. Quantification of dorsally-electroporated RGC populations expressing receptor overexpression constructs at E11. Dorsal RGCs were electroporated with constructs designed to overexpress Ryk or EphB2. Branch direction was then quantified at E11 to determine whether overexpression of these mapping receptors affected mediolateral branch direction choice during or soon after branch initiation.

Age, Conditions	N (tecta)	ML ratio	ML ratio p-value
E11 Control	7	-0.0417 ± 0.1363	
E11 Ryk	7	0.4426 ± 0.08847	0.0107
E11 EphB2	7	-0.6735 ± 0.1237	0.0030

CHAPTER 4: DISCUSSION AND CONCLUSIONS

This dissertation proposes that a Moving Gradient Model of retinotopic mapping organizes the topographic map along the mediolateral axis in the chick retinotectal system by creating a series of laterally-shifting balance points at the intersection of a laterally-expanding Wnt3 gradient in combination with a stable ephrinB1 gradient. At each balance point, primary axons which are lateral of the balance point extend interstitial branches that are attracted medially up the ephrinB1 gradient toward the balance point, while axons medial of the balance point have their interstitial branches repulsed laterally down the Wnt3 gradient toward the balance point, as controlled by the opposing mapping forces of laterally repulsive Wnt3-Ryk signaling and medially attractive ephrinB1-EphB signaling. These events are temporally limited by the medial-to-lateral progression of retinal axon development and interstitial branching during the period of Wnt3 gradient expansion, such that initiating branches respond to a very limited range of shifting balance points, generating a centralized termination zone for each responsive grouping of primary axons and interstitial branches as balance points advance laterally. This combination of events creates an accurately defined mediolateral retinotopic map during chick development.

Interaction of moving and stable gradients forms mediolateral mapping targets

Understanding the characteristics and interactions of the mediolateral gradients during development provides insights into Gierer's dual gradient model (Gierer, 1981; Gierer, 1983; Gierer, 1987) and clarifies the specific roles of these two gradients during

map development. Extensive study of the ephrinB1 gradient in chick has shown that ephrinB1 mRNA appears in a high-medial, low-lateral gradient in the ventricular epithelium as early as E3 and remains stable while increasing in mRNA expression overall through E14, at which point the ventricular epithelium is not longer retained and ephrinB1 expression is no longer observed (Braisted et al., 1997). The differential gradient is created via differences in mRNA expression within the ventricular epithelial cells, with medial cells transcribing more ephrinB1 mRNA than more lateral cells; the ephrinB1 protein is then trafficked to the tectal surface, where retinal axons invade and form the map, via radial glial cells, as demonstrated by EphB2-Fc binding (Braisted et al., 1997). The Wnt3 gradient, however, has been minimally characterized; a high-medial, low-lateral mRNA gradient has been reported at E10 (Schmitt et al., 2006).

Here, the Wnt3 gradient is further characterized, and surface protein expression is described in greater detail. *In situ* hybridization of Wnt3 between E10 and E13 in chick tectum showed the presence of Wnt3 mRNA in the ventricular epithelium in a high-medial, low-lateral gradient, with the high expression front of the Wnt3 gradient traveling laterally around the ventricular epithelium during this period. This both confirmed the presence of Wnt3 throughout the period of map development as well as provided new questions about the presence of gradient proteins at the tectal surface. By performing Western blots on lysates derived from five equal medial-to-lateral regions of a thin strip of tectal surface, I demonstrated both the expression and the relative levels of actual proteins in the area of the tectum in which mapping occurs; a smaller demonstration of this concept, with three regions, was previously shown for Wnt3 at E10 (Schmitt et al., 2006). Tectal surface gradient Western blots showed that, as suggested by ISH, the Wnt3

gradient appeared at the medial end of the tectal surface at E10, extended across the tectal surface by E11, increased in relative lateral expression levels by E12, and ceased to appear by E13, showing both the lateral extension and lateral expansion of the Wnt3 gradient during mapping. While Schmitt and colleagues showed weak lateral expression at E10 in their tectal gradient Western blots, this may have been due to a minor difference in the timing of chick development, as tectal surface gradient Western blots performed at E10.5 in my hands also showed signs of weak lateral Wnt3 expression (data not shown). This technique also confirms the stability of the ephrinB1 gradient at the tectal surface during this period, while suggesting that ephrinB1 protein levels may increase, as indicated in studied by Braisted and colleagues (Braisted et al., 1997). Unlike previous studies, which focused on mRNA expression at the ventricular epithelium or receptor binding to indirectly describe protein localization, these studies provide information about protein levels at the tectal surface, describing the conditions that retinal axons encounter during mapping, as well as creating a comparative medial-to-lateral view of surface gradients.

This new knowledge of the Wnt3 and ephrinB1 gradients at the tectal surface also begins to answer questions about the observed gradient organization in the mediolateral axis and how the two gradients operate *in vivo* in map formation. Both Wnt3 and ephrinB1 are expressed in high-medial, low-lateral gradients, such that their highest expression and lowest expression are localized to the same areas, rather than being in opposing alignments, such that their highest and lowest expression levels would be on opposing ends of the mediolateral axis. This does permit competition of forces, as Wnt3-Ryk signaling directs branches laterally away from high medial Wnt3 concentrations and

ephrinB1-EphB signaling directs branches medially toward high medial ephrinB1 concentrations. However, the strengths of these forces in earlier, non-moving models of the system would appear to be medially and laterally balanced at each point, making it unclear how accurate mapping positions were formed.

A moving Wnt3 gradient corresponding with a stable ephrinB1 gradient changes the entire perception of these concerns. First, if the Wnt3 and ephrinB1 gradients are of differing steepness, there is no longer a similar balance of gradients across the tectal surface at each point, providing confusion about determining specific mapping positions. Instead, the relative positions and steepnesses of the two gradients create clearly defined situations in which a specific balance point exists, such that branches lateral of the point are attracted medially and those medial of the balance point are repulsed laterally, meeting at the balance point. The gradients in this situation are thus no longer the same, balancing equally at all points, despite a similar overall orientation (high medial, low lateral). Second, the expansion of the Wnt3 gradient generates a series of balance points traveling laterally across the tectal surface. If the Wnt3 and ephrinB1 gradients differed in steepness alone, assuming relative rather than absolute responses to gradient molecule signaling, then rather than collecting entirely to one end or the other of the map as described under relative conditions with a single gradient, all branches would target the single balance point between the two gradients. However, because the Wnt3 gradient expands laterally, it generates a series of balance points moving across the tectal surface. This allows groupings of branches to target certain balance points, causing branches to generate a series of centralized (to each set of primary axons) termination zones rather than a single termination at either end or the center of the map. Furthermore, the

combination of differing gradient steepnesses and gradient movement is necessary to target branches appropriately. Without differences in gradient steepness, it remains unclear how branches are balanced to one point preferentially over a similarly balanced point. Without Wnt3 gradient motion, only one balance point is generated where the two gradients are balanced, such that all branches would gather to this single point rather than being distributed across the map. An additional third factor, the limited temporal responsiveness of branches to specific balance points, is also required to prevent all branches from ultimately targeting the later edge of the map, following the moving balance point to its ultimate resting point; this concept will be further discussed later in this section.

The Moving Gradient Model explains several aspects of map development while not excluding a number of additional, possibly complementary concepts. While both the movement and differing steepness of the two gradients allows for mapping along the entire surface of the map, this does not change the fact that both Wnt3 and ephrinB1 expression levels are weakest at the lateral edge of the map, nor that it is currently difficult to fully clarify how the interaction of the moving and stable gradients operates at the medial edge of the map. One possibility at these edges is that biphasic responses to these gradients provide additional mapping information. For example, high levels of ectopic ephrinB1 were shown to cause chick interstitial branch repulsion *in vivo* (McLaughlin et al., 2003b); perhaps this would provide additional repulsion from the medial edge prior to Wnt3 expression, allowing for the formation of termination zones close to the medial edge. Similarly, low concentrations of Wnt3 induce mild axon outgrowth *in vitro*, possibly due to attractive signaling via Frizzleds (Schmitt et al.,

2006); this might add another level of medial attractive force at the lateral edge of the map, combining with the ephrinB1-EphB force to balance against the lateralmost movements of the Wnt3 gradient's Wnt3-Ryk repulsion. In addition to these forces, it is also possible that non-graded guidance molecules, additional gradients, and countergradients, using molecules such as ephrinB2, ephrinB3, Wnt4, or Wnt5a, could also provide additional signaling feedback within this system. While some work has been done with ephrinB retinal countergradients in mouse (Thakar and Henkemeyer, 2010), further study is needed to determine the roles of these molecules and gradients in topographic map formation. More crucially, the Moving Gradient Model itself requires further testing to clarify its activities. Affecting gradient movement timing via differently aged tectal transplant studies (attempted unsuccessfully for these studies, data not shown) or by stopping gradient movement or flattening the gradient by as yet unidentified mechanisms would advance the study of this model greatly.

Mediolateral development and its integration into retinotectal map formation

Preordering of retinal inputs to the tectum has been observed, to varying degrees, across most animal models, from fish to rodents. In the chick retinotectal system, aspects of both the temporal development and spatial alignment of retinal ganglion cells are preserved in the ordering of their axons within the optic nerve, with the dorsoventral retina axis retaining strong preordering to the tectum (DeLong and Coulombre, 1965; Goldberg, 1974; Crossland et al., 1974; Rager and Rager, 1978; Rager and von Oeynhausen, 1979; Rager, 1980; Thanos and Bonhoeffer, 1983). While this developmental preordering has been studied in some detail to determine the entry, pacing,

and organizational principles of the retinal axons within the optic nerve and along the tectal surface, no studies have attempted to connect specific aspects of axonal preordering and chemoaffinity in warm-blooded animals, beyond basic observations of positional shift indicating that both methods are involved in map formation. (Several studies, discussed previously, were done in fish and frogs, which employ direct targeting of topographic positions along both axes simultaneously; in these systems, preordering, despite being observed during development, appears to be irrelevant to map formation.)

The current studies use electroporation of dorsal and ventral RGC populations to compare the timing of developmental events in retinal axons along the mediolateral tectal axis. I demonstrated that ventral RGCs, which target the medial tectum, have axons which enter the tectum earlier, extend across the tectum earlier, sprout longer interstitial branches, and are more likely to generate interstitial branches earlier than their dorsal counterparts, suggesting a medial-to lateral progression of retinal axon development. As branch initiation in these retinal populations occurs during E11 (and possibly late E10), the branches would be able to temporally coordinate with the lateral expansion of the Wnt3 gradient between E10 and E12. The timing of these two sets of events would therefore enable initiating and early developing branches to be present during the period in which the laterally moving balance points cross the tectal surface, allowing mediolateral positions to be determined.

Some processes that appear to be generated by preordering may actually correspond to both preordering and chemoresponsive activities or to chemoresponsive activities alone. In chick, primary axons travel anteroposteriorly then sprout interstitial branches in a permissive axonal segment located at the appropriate AP target. Disturbing

the localization of interstitial branching by disrupting aspects of anteroposterior mapping, as in several multi-ephrinA knockout mice and EphA7 knockout mice, results in both AP and ML guidance defects (Feldheim et al., 2000; Rashid et al., 2005; Pfeiffenberger et al., 2006; Cang et al., 2008). If primary axons activate branching by crossing over appropriate hotspots at certain times, then both the timing of outgrowth and the localization and appropriate targeting of branch-permissive gradient regions along the AP axis would be responsible for generating interstitial branches at temporally and spatially appropriate locations. Additionally, the AP axis of the chick optic nerve is not strongly preordered, and primary axons appear to enter based on the temporal development of RGCs, showing delays as they reach the tectum and begin to process gradient cues (DeLong and Coulombre, 1965; Goldberg, 1974; Thanos and Bonhoeffer, 1983; Nakamura and O'Leary, 1989). Under these conditions, is possible that while the preodering of axons within the optic nerve determines the initial placement of axons, allowing them to properly target and develop (Fujisawa et al., 1984), the temporal progression of their development after tectal entry is mostly defined by axonal responses to AP and later ML gradients. While there are indications that axons manage to grow within the superior colliculus regardless of AP gradient disruptions in mouse, additional studies are needed to determine the situation in chick (Feldheim et al., 2000; Brown et al., 2000; Hindges et al., 2002; Feldheim et al., 2004; Rashid et al., 2005; Plas et al., 2008). On the other hand, reaching the permissive branching region along the AP axis may simply be a holding point, and once interstitial branching is initiated, it becomes easier for axons to reach later developmental milestones. The fact that most parameters in this dissertation showed one to two days of delay between the ventral and dorsal RGC

populations while interstitial branches are initiated in both at approximately the same time fails to clarify this situation, as the delay in dorsal RGC branch outgrowth, for example, could be due to either some aspect of the initial delay in primary axon extension or due to a weaker initial outgrowth/guidance response due to lower endogenous levels of Wnt3-Ryk and ephrinB1-EphB signaling in those axon populations.

Another developmental factor is that the tectal laminae develop in an anterolateral-to-posteromedial direction, opposing that of the retinal axons (LaVail and Cowan, 1971a; Crossland et al., 1975; Scicolone et al., 1995; Hilbig et al., 1998; Fujiwara et al., 2000). Due to this developmental progression, medial tectal laminae are thinner, more closely spaced, and less developed than their lateral counterparts. This difference in laminar thickness may explain the deeper and more detailed arbors of the ventral as opposed to dorsal RGCs observed in the current studies. Under these conditions, ventral RGCs would be able to travel into deeper laminae earlier in development because these laminae are less thick in the medial tectum than in the lateral tectum, such that as appropriate laminae migrate and specify identifying cues, these axons are already present in appropriate locations and thus more readily innervate them.

Further study is required to better delineate the interface between axonal preordering and map formation. While attempts have been made to affect developmental timing by transplanting younger or older eyes or tecta into differently aged hosts, these experiments have not been successful. Still, it is possible that others could successfully use such studies to affect both the timing of RGC arrival and gradient movement within this system. The use of partial tectal ablation may also help in these studies if performed consistently, as both timing and placement of axons would be affected by the removal or

regions of the tectal surface; however, in this situation, additional gradient studies on both axes would need to be performed to confirm the status and stability of the molecular situation in the modified tectum.

Ryk-EphB competition and mediolateral branch direction choice

In these studies, I have shown that Ryk provides a lateral-directed mapping force that competes against the medial-directed guidance of EphBs within the same retinal interstitial branches. The upregulation of Ryk via overexpression and downregulation of Ryk via shRNA and dominant negative constructs, along with previous studies on gradient expression and retinal axon response, is sufficient to confirm Ryk as a mediolateral mapping gradient according to the Luo and Flanagan criteria (Luo and Flanagan, 2007). However, the interaction of Ryk and EphBs within the retinal axon itself is unclear. Ryk and EphBs may signal separately within the growth cone, with additional pathways or aspects of cytoarchitecture determining whether the branch will travel medially or laterally. On the other hand, Ryk and EphBs may participate in more direct signaling competition. Biochemical studies indicate that EphB2 and EphB3, standard receptor tyrosine kinases, are capable of phosphorylating Ryk, an RTK which does not undergo autophosphorylation due to an atypical kinase domain (Halford et al., 2000; Trivier and Ganesan, 2002). In addition, Ryk deficient mice display a phenotype similar to EphB2/B3 double knockout mice, with improper formation of the cleft palate and other aspects of craniofacial development, suggesting that they may operate along the same pathways (Halford et al., 2000). Unfortunately, Ryk knockout mice tend to die perinatally, so studies on map formation in mice, which mostly occurs in the first

postnatal week, cannot be performed until conditional Ryk mice are generated. Another possibility is that Wnt3 and ephrinB1 signaling might compete downstream at Disheveled, a common mediator of several Wnt signaling pathways, as Dvl-EphB2 binding has been shown to be involved in repulsive EphB signaling in *Xenopus* and an EphB2-Daam1-Dvl2 complex is involved in convergent extension in zebrafish (Tanaka et al., 2003; Kida et al., 2007). Further biochemical studies, preferably in RGCs, are necessary to delineate whether and where signaling crosstalk between Ryk and EphBs occurs.

Modulating Ryk levels showed several interesting direction choice phenotypes over time. Downregulation of Ryk resulted in a fairly constant, slightly medial effect on mediolateral choice, while Ryk overexpression caused a consistently increasing lateral trend in direction choice; similarly, EphB2 overexpression showed a strong and increasing trend in medial choice. During the time of this increase, furthermore, branches were never observed to change direction, suggesting that inappropriately targeted branches are pruned back, rather than changing in direction choice. Thus, the increase in ratio is not the result of changes toward the preferred direction but rather the result of the removal of branches which selected the non-preferred direction. The increasing direction choice ratios seen in Ryk and EphB2 overexpressing interstitial branches, coupled with the lack of direction choice changes, suggests that the branch choice decision is made in early development, as no branches change their decision later in extension. However, this could be examined by performing retinal electroporation with receptor modulation constructs after branch initiation (E11 in the populations studied). Additionally, the mediolateral choice decision and the balance of receptor expression determine which

branches are “correctly” oriented, given that in unmodified retinal axons, branches appear to be pruned equally, while in receptor-overexpressing axons, branches in the direction counterindicated by the dominant guidance force are removed.

Why, then is an increase in the mediolateral choice ratio not observed under Ryk downregulation conditions? One possibility is that the presence of Ryk, even in low amounts, is sufficient to prevent branches from being pruned. Similarly, while the Ryk shRNA and dominant negative constructs affect Ryk levels in different ways, neither removes more than the majority of Ryk (or Ryk signaling). Compared to the higher ratios generated by strong overexpression, it may be that the Ryk downregulation constructs affect Ryk levels enough to drive and maintain changes in the initial choice of branch direction but does not shift the ratio enough to strongly affect the later pruning decisions, leaving the ratio relatively consistent across map formation. A third possibility is that overexpression drives a signaling pathway that causes certain branches to be preferentially selected and that Ryk downregulation, retaining more endogenous signaling levels, fails to activate this pathway or this level of signaling. Studies with either multiple Ryk shRNAs targeting different parts of the receptor or possibly the combination of Ryk shRNA and dominant negative Ryk could further decrease Ryk levels, which may result in stronger effects on medial direction choice (or not, given Ryk downregulation’s effect on branch outgrowth). Another option might be to generate Ryk deletion constructs to determine which Ryk domains are required for direction choice specifically, in order to possibly generate direction choice changes without affecting outgrowth; given that for Ryk-Wnt5a signaling, repulsion and outgrowth are controlled

by different signaling pathways, this could be a feasible way to tease apart portions of this question (Li et al., 2009).

Ryk affects branch development, while EphB2 affects arbor formation

While overexpression of Ryk does not affect branch outgrowth, downregulation of Ryk through the shRNA construct and through a dominant negative Ryk both resulted in decreases or delays in interstitial branch elongation, with the Ryk shRNA construct causing two-day delays in branch initiation and decreases or delays in the further branching of interstitial branches as well. Given that, unlike many other repulsive receptors, Ryk provides repulsion coupled with axon outgrowth, these results are unsurprising (Li et al., 2009; Hutchins et al., 2011). Decreases in Ryk expression and signaling likely affected branch outgrowth directly, producing the results observed. The fact that the Ryk shRNA had a stronger effect on branch development than the dominant negative could be due to several factors. First, the presence of higher levels of endogenous Ryk in the dominant negative branches may have prevented some of the stronger phenotypes, despite it making up a small percentage of the Ryk present in the axon. Second, the continued presence of the Ryk extracellular and transmembrane domains in the dominant negative Ryk construct may have been less disruptive to outgrowth signaling than the lack of Ryk overall. This could be tested by creating Ryk deletion constructs deficient in the domains necessary for outgrowth-related signaling. These constructs would still contain the extracellular and transmembrane domains, such that comparing the truncated region of the dominant negative and the deleted region of the outgrowth-deficient Ryk should clarify this issue. Third, the Ryk shRNA may have

had a stronger early effect; thus, the more extreme phenotype may simply be due to Ryk shRNA-expressing axons and branches being developmentally delayed from early on, such that the outgrowth and secondary branching phenotypes reflect delayed development rather than specific effects of Ryk downregulation. Performing a post-branch initiation electroporation of Ryk shRNA and dominant negative constructs would therefore place the two on more equal footing, which might better distinguish the degree of the outgrowth effect between the two.

EphB2 overexpression results in an increase in secondary branching at later stages, while Ryk shRNA expression results in decreases or delays in secondary branching. EphB-ephrinB signaling has previously been shown to play a role in retinal synapse formation and stabilization in *Xenopus* (Lim et al., 2008), so it is possible that this could also be in play in chick as well, in line with the increase in branching. Based on these results, further study of the roles of ephrinB forward and reverse signaling on the development of arbors in chick may be warranted.

Timing of the mediolateral direction choice implicates initiating interstitial branches

Observation of electroporated axons at E11, soon after branch initiation, showed that mediolateral direction choice had already been affected by receptor level modulation. Furthermore, later observations indicated that branches never changed direction after the initial choice. These data indicate that the branch direction decision is made during or soon after branch initiation, at a point in time when the initiating branches would be specifically able to respond to the laterally-moving balance point generated by the intersection of the moving Wnt3 gradient and stable ephrinB1 gradient.

However, studies on post-E11 axons suggest that this interpretation is incomplete. In comparing the developmental progression of dorsal and ventral RGC axons in the tectum, I observed that over time, the percentage of primary axons with interstitial branches increases, to the point where all primary axons display at least one interstitial branch by E14. This clearly shows that many branches must be initiated after E11, when the first visible initiating branches are observed. Yet measures of mediolateral direction choice for branches in older tecta indicate that these branches make the appropriately biased direction decisions. In the context of the Moving Gradient Model, the conditions to which later branches are exposed are different to those in previous hours or days, so how can this be reconciled? One possibility is that later-initiating branches might be influenced by the direction choices of other branches on the same or nearby primary axons, selecting their direction based not on the original gradient conditions but rather on the earlier decisions of their peers in response to those gradients. This might work in a manner similar to axon-axon competition, where crosstalk between branches, rather than axons, places the branches appropriately in both space and direction.

However, an additional oddity in light of this concept is that Ryk shRNA-expressing branches, which aren't initiated until E13, still show direction choice bias. These branches have clearly missed both the appropriately timed balance point and the expression of the Wnt3 gradient, which disappears during E13, and cannot depend on the activity of earlier formed branches on other axons to determine their branch direction bias, as they are biased but the earlier initiating branches on other axons are not. However, given that the primary axon has extended and is present during the moving gradient period, the branching region may become preferentially primed to generate

branches in one direction or the other by the ambient conditions when it first reaches an area suitable to permit branch formation. The observation of stretches of the primary axon that produce groupings of multiple branches oriented in the same direction could indicate this initial preference, and the pre-branching priming of a branch initiation-eligible region would explain the Ryk shRNA result (while also suggesting that Ryk shRNA does specifically cause, among other things, a delay in branch initiation as well as outgrowth).

Further studies with additional electroporation ages both before and after E7 may further inform the initiation question, as different RGC populations are initiated between E3 and E9 and send their retinal axons to the tectum as mildly variable times. Performing receptor modulation electroporations on these populations and coupling these experiments with limited DiI labeling in the region may also be able to show whether later branches can be influenced by earlier branches, causing the branches of unelectroporated axons to show directional bias in accord with those on the electroporated axons.

CONCLUSIONS

This dissertation examines a Moving Gradient Model of mediolateral retinotopic mapping. In the Moving Gradient Model, the intersection of similarly oriented gradients of differing steepness and opposing guidance forces provides a series of balance points through the lateral movement of one gradient while the second remains stable. This moving intersection of gradient forces, or balance point, coordinates with the medial-to-

lateral progression of retinal axon development, such that only a spatially limited population of initiating interstitial branches is able to respond to any given balance point within a specified period of time. The opposition of the forces of the two gradients at this time determines the direction choice of each branch, with branches of axons medial to the balance point being repelled laterally while those of axons lateral to the balance point are attracted medially. This generates a series of appropriately targeted termination zones across the mediolateral axis.

To demonstrate the existence of the Moving Gradient Model, I have confirmed multiple attributes of the system. First, using tectal surface gradient Western blots, I have shown that the Wnt3 gradient extends and then expands laterally while the ephrinB1 gradient remains stable, making it capable of generating a laterally-moving balance point. Second, I have electroporated dorsal and ventral RGC populations to show that ventral RGCs, targeting the lateral tectum extend primary axons, generate interstitial branches, and extend their interstitial branches earlier than their dorsal counterparts, indicating a medial-to-lateral progression of retinotectal projection development. Third, I showed that Ryk and EphBs were present in the same retinal ganglion cells, then used receptor constructs to increase and decrease Ryk signaling and increase EphB2 signaling in retinal axons. This resulted in a predicted direction choice bias in interstitial branching, with Ryk-overexpressing branches tending laterally and Ryk-downregulated and EphB2-overexpressing branches tending medially, indicating that these receptors are capable of providing opposing guidance forces within the same branches, such that they could respond to the laterally-shifting balance points in the expected manner. Last, changes in branch direction choice were observed soon after branch initiation, indicating that the

direction choice decision was made close to this time in development. Given that branches are never observed to change mediolateral direction during elongation, this suggests that the branch direction choice decision is made during initiation and never adjusted afterward, such that the lateral movement of the balance point would not cause such branches to continue to track laterally as the balance point continued laterally.

This Moving Gradient Model integrates aspects of both the chemoaffinity hypothesis and the preordering of retinal inputs, two of the major aspects of axon behavior previously shown to be involved in retinotopic mapping. (Other aspects not specifically covered in this model include neural activity and axon-axon competition, although the latter may be suggested by the behavior of later branches in this model.) As a model, the Moving Gradient Model builds on Gierer's dual gradient model, which showed mathematically that two relative signaling gradients of opposing force were necessary to define specific mapping positions on a topographic axis, as a singular relative gradient would drive all axons to one of the edges of the map. This is the first full *in vivo* demonstration of the behavior of the dual gradient model, as branches as directed to specific topographic positions by the opposing forces of Ryk-directed lateral repulsion and EphB-directed medial attraction. This model also clarifies how two opposing gradients of similar orientation can define specific topographic targets; for this, both differing steepness and the movement of one gradient are necessary in order to distinguish the relative activities of the two gradients on either side of the balance point as well as to generate balance point targets across the entire mediolateral axis. Using this model, if it also possible to demonstrate how a series of centrally-meeting termination

zones is generated across the axis, a point of consternation among retinotectal systems researchers and modelers.

Further studies are needed both to confirm the Moving Gradient Model and to better understand many aspects of the mediolateral axial mapping observed in this dissertation. Modifications of gradient steepness and timing are important to observe responses to affecting the balance and positions of the two gradients in this system. Wnt3 modulation is also needed in order to fulfill the Luo and Flanagan criteria, bringing the Ryk-Wnt3 gradients in line with other fully acknowledged topographic mapping gradients. Additional electroporation studies should be used to observe the behaviors of non-E7-electroporated RGCs in order to confirm the universality of the model across the entire retina, as well as to better observe the specific responses of different populations of initiating axons. Studying the possibilities for signaling competition between Ryk and EphBs would provide greater comprehension of how the mediolateral choice decision is made, as well as why and how it is specified to a limited time period close to branch initiation. Additionally, looking at the role of ephrinA-EphA and BDNF-TrkB in permitting the accurate AP localization of initiating branches may shed further light on how the appropriate timing of branches is achieved.

Overall, this model informs several aspects of topographic map formation which have not previously been fully delineated. The model studies the intersection of developmental, temporal, and chemoresponsive elements of topographic mapping, which are relevant across systems and species. Thus, the Moving Gradient Model provides a new way of thinking about topographic mapping that is widely applicable in neural development.

Chapter 4, in part, has been submitted for publication of the material. Richman, Alisha; Zou, Yimin. The dissertation author was the primary investigator and author of this material.

SECTION II: Wnts and Frizzleds in Laminar Termination

INTRODUCTION

The nervous system is comprised of a series of precisely wired neural circuits. These series of consistently ordered connections between neurons allow information to be passed concisely and accurately between various parts of the body and brain in order to process, interpret, and respond to internal and external stimuli. During development, neurons extend their axons to identify and form specific synaptic connections with the processes of other neurons, using specific molecular cues and patterns of activity to locate appropriate targets and develop stable communications with the dendrites, axons, or cell bodies therein. Determining how these synaptic targets are located and selected for synapse formation is necessary to understand the formation of the nervous system.

Within the brain, neural circuits are employed to process and interpret a wide variety of information across many modalities. These neurons receive sensory inputs from the body and sensory organs, then combine and enhance relevant aspects of the information received until wide scale comprehension of senses from balance to touch to vision is possible. While we experience this sensory information in a seemingly holistic manner, these experiences are defined by the appropriate combinations of neurons, targeting and providing information to the correct neurons within given circuits. Thus, by understanding the proper composition and development of neural circuits, it is possible to gain further insight on how we perceive the outside world.

The visual system is the best studied of all sensory modalities at present. Within this system, information derived from the receipt of visible light by the photoreceptors is processed through a series of bipolar, horizontal, amacrine, and finally retinal ganglion cells within the eye. Each retinal ganglion cell then sends out a single axon, the retinotectal projection, along the optic nerve to make appropriate connections within the brain. The information processed at such locations, including the superior colliculus, lateral geniculate nucleus, and primary visual cortex in humans and mice, is then sent to additional processing stations within the brain until the salient details have been defined.

The chick retinotectal projection provides a simpler way to study the crucial connection between eye and brain. While in mice and humans, retinal ganglion cells send their axons to multiple sites within both the ipsilateral and contralateral brain hemispheres, many of them with unclear cytoarchitectural qualities, chick retinal ganglion cells specifically target the contralateral optic tecta, where they form synapses in anatomically distinct tectal laminae. In order to reach the appropriate tectal location for synapse formation in chick, these retinal axons exit the eye, travel along the optic nerve to the contralateral tectum, send primary axons anteroposteriorly across the tectal surface, and initiate interstitial branches at topographically appropriate AP locations; the interstitial branches then locate topographically appropriate mediolateral targets, at which point they invade the tectal surface and select specific laminae in which to develop their arbors and form synapses with tectal cells.

While molecular cues for many of the steps involved in appropriately targeting chick retinotectal projections have been studied, the specific cues needed to target these axons to appropriate retinorecipient laminae are almost entirely unknown. In this portion

of the dissertation, I explore Wnts and their Frizzled receptors as possible guidance cues for this process, focusing on a series of techniques to isolate limited populations of retinal ganglion cells on which the effects of Wnt-Frizzled guidance can be tested.

CHAPTER 5: BACKGROUND

The development of the chick eye and its neurons has been a subject of intense study for many decades, from initial anatomical work beginning in the late 1800s forward to the present day, as discussed in part in the chapter on the history of retinotopic mapping studies. During this time, the development and morphology of retinal axon arbors within the tectum have been thoroughly described, but the methods by which specific laminae or tectal neurons are selected for termination and synapse formation remain almost entirely unknown. Only within the past twenty years, particularly within the past decade, has the study of possible molecular mechanisms of laminar termination across subtypes and groupings of retinal axons become possible.

On the development of tectal laminae

While the specific mechanisms of targeting RGCs to retinorecipient laminae have only become feasible for study in recent years, anatomical studies on the development of the chick have had a long, fruitful history. A number of German and Italian anatomists were the first to study the tectal laminae, with Stieda and Schulgen describing 13 tectal laminae, while Bellonci instead classified 11 laminae in the chick optic tectum (Stieda, 1868; Schulgin, 1881; Bellonci, 1888). Santiago Ramón y Cajal further and more accurately characterized the tectal laminae and sublaminae in chick, labeling fifteen laminae from the pial surface inward to the ventricle, with the stratum opticum as 1 and the deepest laminae at 15, a system which is still sometimes used today (Ramón y Cajal , 1889; Ramón y Cajal, 1911). The current major tectal laminar labeling system, which I

employ in this dissertation, separates the tectum into 6 strata (the stratum opticum, SGFS, SGC, SAC, SGP, and SFP, from outside to inside), with the SGFS separated into ten sublaminae lettered from A through J (Huber and Crosby, 1933).

The tectal laminae develop in a prescribed sequence. First, a group of cells in the deepest tectum are specified into the SGC, SGP, and SFP (LaVail and Cowan, 1971b). Next, a group of cells migrates toward the outer tectum between E5 and E8 to begin developing into the SO and SGFS A-G; of specific interest in this dissertation, SGFS-A/B, C, D, and G are present at E12, with SGFS-E and F appearing and SGFS-A separating from SGFS-B by E16 (LaVail and Cowan, 1971b; Yamagata et al., 1995). The final series of cells to migrate travels between these two populations to become SGFS H-J (LaVail and Cowan, 1971b). This sequence proceeds throughout the tectum in a graded direction, with ventral anterolateral tectum development as much as two days advanced over the dorsal posteromedial tectum, both in terms of laminar specification and laminar thickness (Cowan et al., 1968; LaVail and Cowan, 1971a). Several molecules have been noted to play roles in the formation, arrangement, and density control of laminae, including multiple cadherins and Sema3F (Inoue and Sanes, 1997; Miskevich et al., 1998; Gänzler-Odenthal and Redies, 1998; Watanabe and Nakamura, 2008), while transcription factors such as Brn3a and Pax6 are involved in specifying subtypes of tectal neurons (Fedtsova et al., 2008).

On the targeting of retinal axons to tectal laminae

Chick retinal ganglion cell axons project to a series of appropriate targets in the optic tectum in a consistent order and manner which can be observed regardless of

individual or subtype differences between RGCs. Specifically, these axons exit the eye, travel along the optic nerve, cross the optic chiasm, and continue to the contralateral optic tectum, where they extend primary axons anteroposteriorly along the tectal surface and send out interstitial branches mediolaterally to map to appropriate positions, as described in the first part of this dissertation. These interstitial branches then invade the tectal laminae to select appropriate laminar and cellular targets for arbor formation and synapse stabilization.

A number of groups attempted to clarify the nature of these latter events through the observation of labeled populations of small, spatially limited groupings of retinal ganglion cells. In 1989, the O'Leary lab used the lipophilic anterograde tracer DiI to label small groups of retinal cells in the peripheral temporal chick retina, observing the development of the retinal projections in the optic tectum from the vantage point of the tectal surface (Nakamura and O'Leary, 1989). These retinal axons sent out a number of interstitial branches, many of which bifurcated or formed secondary branches to develop into shallow, incorrectly placed arbors which were removed by approximately E14 (Nakamura and O'Leary, 1989). The remaining, appropriate arbors then continued to stabilize, reaching their mature locations and general appearance by E16, though pruning continued beyond this period (Nakamura and O'Leary, 1989).

The general features of these developing arbors, as well as the laminae they targeted, had been well characterized by the time of Nakamura and O'Leary's study (LaVail and Cowan, 1971a; Kelly and Cowan, 1972; Acheson et al., 1980; Thanos and Bonhoeffer, 1987). Earlier groups, such as the Cowan lab, used a combination of direct and indirect techniques to comprehend the relationship between retinal axons and the

laminae they innervated. Comparing the labeled laminae of tecta which received or failed to receive retinal inputs, the Cowan lab observed a distinct thinning of a number of plexiform laminae, most notably within the SGFS sublaminae, including SGFS-A, SGFS-E, SGFS-H, and SGFS-I; they hypothesized that besides those laminae directly receiving input, deeper laminae were affected because their projections into the shallower tectal laminae did not receive retinal connections (Kelly and Cowan, 1972). They later applied radiographic labeling of RGCs to observe the time points at which retinal axons reached specific tectal laminae, identifying the increasing thicknesses of specific laminae as well as noting the higher presence of labeling in specific laminae as the retinal axons developed and refined their arbors (Crossland et al., 1975).

Specific targeting of tectal laminae by retinal axons was directly observed and categorized in the 1990s, with Yamagata and Sanes observing sections containing DiI-labeled RGCs in order to demonstrate that the retinal axons stabilize their arbors in SGFS-B, -D, and -F (Yamagata and Sanes, 1995a). Targeting to SGFS-C had earlier been implied by observations of increasing retinal axon presence in the region (LaVail and Cowan, 1971a; Kelly and Cowan, 1972) but was not directly visualized until later molecular markers were identified (Yamagata et al., 2006). Furthermore, retinal axons were only rarely observed to travel into or beyond SGFS-G, likely due to the presence of a strong repulsive cue, as observed via tectal slice co-culture with retinal explants (LaVail and Cowan, 1971a; Yamagata and Sanes, 1995a). Thus, during the development of retinotectal projections, axons send out multiple interstitial branches which form a series of false arbors; while inappropriate branches and arbors are being pruned, the single

appropriate interstitial branch proceeds to further expand its arbor within the deeper tectal laminae, targeting SGFS-B, -C, -D, or -F and stabilized by E16.

On the identifying the characteristics of RGC subsets in chick and mouse

While retinal ganglion cell axons exhibit the same general patterns of outgrowth and targeting during development, individual RGCs display different axonal and dendritic morphology, target different combinations of retinal and tectal sublaminae, express different molecular markers, and show different patterns of activity. However, the spontaneous retinal activity waves that occur during retinal axon targeting and laminar selection affect aspects of anteroposterior mapping and retinal laminar targeting but do not appear to play a role in tectal laminar targeting (Inoue and Sanes, 1997; Wong, 1999; Nevin et al., 2008; Dhande et al., 2011). Thus, only the first three categories of these characteristics are useful in distinguishing retinal ganglion cell subsets with the goal of discerning the nature of their specific laminar targeting selections.

Dendritic morphology and the retinal laminar targets of the dendrites have long been used to categorize specific retinal ganglion cell subtypes in both chick and mouse, as the features of the RGC soma and dendritic field relate to the numbers and types of connections they form with other retinal cells. A number of studies have used dendritic morphology as a method of avian RGC sorting, regardless of whether Golgi staining, Nissl, or other methods were applied (Ramón y Cajal, 1892; Binggeli & Paule, 1969; Ehrlich, 1981; Wathey & Pettigrew, 1989; Thanos et al., 1992). For example, in a recent study, Naito and Chen employed a combination of Lucifer Yellow injections and DiI labeling to categorize RGCs into four major groupings with two minor subgroupings

based specifically upon the size of the soma, the extent of the dendritic field, and the degree of dendritic branching (Naito and Chen, 2004). Mammalian retinal cells have been similarly studied and characterized, with mouse RGCs being commonly sorted into 22 separate subtypes, which have then been grouped by various combinations of characteristics (Rockhill et al., 2002; Sun et al., 2002; Badea and Nathans, 2004; Kong et al., 2005; Völgyi et al., 2005; Coombs et al., 2006; Völgyi et al., 2009).

While these techniques identify the distinguishing characteristics of the retinal ganglion cells within the retina, they frequently neglect to combine these observations with the resultant laminar targeting of the retinal axons within the tectum from a purely morphological standpoint. Additionally, two papers published this year using transgenic and viral labeling techniques in mouse have begun to reconnect somal and axonal characteristics in individual retinal ganglion cells. The Crair lab employed a Lox/Cre system to label single RGCs in the mouse retina by using large concentrations of two constructs, one containing a Lox-STOP cassette followed by RFP and the other containing Cre; by injecting high concentrations of the RFP construct with 10,000-fold lower concentrations of the Cre construct, labeled cells were limited to only those which received both constructs (Dhande et al., 2011). While the Crair lab used this primarily to study the specific roles of activity in retinal projection development, comparing wild-type mice with AChRβ2 knockout mice (which lack early spontaneous cholinergic activity waves in the retina), a similar system could be used to characterize individual RGCs or to target specific subpopulations. In the Sanes lab, CreER mice were bred to RGC subtype-labeling mice, then treated with low concentrations of tamoxifen to activate YFP labeling in limited, randomly positioned populations of RGCs; by using knowledge about

topographic mapping and retinal soma position, it was possible to distinguish and separately characterize the few YFP-positive RGCs across the entire retina in a single animal (Hong et al., 2011). Similarly, use of a Cre-containing virus was applied in various Lox-STOP-XFP lines to activate labeling in small populations of RGC for similar studies (Hong et al., 2011). Interestingly, in connecting dendritic and axonal morphology in this study, it appeared that retinal ganglion cells showing persistent morphological characteristics do not necessary show homogenous axonal characteristics (Hong et al., 2011), further confirming that other characterization techniques are necessary to comprehend laminar targeting.

Using molecular markers to define retinal subtypes, while not as clear cut in providing direct connections between protein expression and eventual RGC function, has the benefit of generating a consistent method for labeling these subtypes for studies on RGC function. In chick, for example, early characterization of cholinergic receptor subunits led to the characterization of a population of AChRβ2-positive RGCs (Britto et al., 1992a; Britto et al., 1992b; Yamagata and Sanes, 1995b). These retinal ganglion cells, localized to the ganglion cell layer as well misplaced to the inner nuclear layer, showed marker expression by E8 and consistently targeted SGFS-F by the time of its appearance at E16, displaying antibody labeling in both the soma and the tectal arbor without labeling any obfuscating retinal or tectal structures (Yamagata and Sanes, 1995b; Yamagata et al., 2006). Numerous other RGC subtype and tectal laminar markers have been identified over the years, from neuropeptides to neurotransmitter receptor subunits to cell adhesion molecules to axon guidance receptors (Yamagata and Sanes, 1995b; Miskevich et al., 1998; Wöhrn et al., 1998; Yamagata et al., 2006). These markers may

also play a role in laminar targeting, given that several of them show ligand-receptor-like pairing, such as substance P-positive RGCs targeting SP-receptor-rich SGFS-B or Cad7-positive RGCs targeting the Cad7-rich SGCS-C (Yamagata et al., 2006).

An additional, somewhat similar avenue of inquiry has arisen with the use of transgenic mouse lines labeling specific subpopulations of RGCs based on marker expression. Andrew Huberman has characterized two GFP-labeling lines: a DRD4-GFP line labeling a subset of On-Off direction-selective RGCs that target the upper half of the superior colliculus (the uSGS) and a CB2-GFP line labeling a subset of tOFF-αRGCs that target the lower half of the superior colliculus (the lSGS) (Huberman et al., 2008; Huberman et al., 2009). The Sanes lab has also characterized multiple subset labeling lines, many of them targeted to different regions of the Thy-1 promoter (Kim et al., 2008; Kim et al., 2010; Hong et al., 2011). These mice both permit the characterization of dendritic and axonal morphology of RGC subsets as well as provide a tool for future RGC subset studies, serving as a background on which retinal or tectal laminar targeting molecules could be tested.

On the search for axonal and dendritic laminar targeting cues

While the search for tectal laminar targeting cues is still in its infancy, several groups have begun to successfully identify appropriate cues for the targeting of RGC dendrites to specific sublaminae within the inner plexiform layer (IPL) of the retina. Within the IPL, these dendrites are able to generate synapses with amacrine cells in order to receive incoming information from within the retina. RGC dendrites target to one of five (or ten, halving each of those five) perceived sublaminae within the IPL; these

targets appear to be RGC subtype-specific, to some degree, and individual retinal ganglion cells tend to target only one or a few of these sublaminae to form their synapses. In chick, DSCAMs and Sidekicks appear to control aspects of retinal laminar targeting, with hemophilic interactions between specific Sidekicks, DSCAM and DSCAM, or DSCAM-l and DSCAM-l determining the layer in which connections are formed (Yamagata and Sanes, 2008; Yamagata and Sanes 2010). In mouse, semaphorin-plexin signaling appears to guide appropriate retinal laminar targeting; Sema6A and PlexinA4 were shown to be expressed in complimentary regions of the inner plexiform layer of the mouse retina, and knockout lines for Sema6A, PlexinA4, or the double knockout line for both showed RGC dendritic targeting errors in several marker-labeled populations of RGCs (Matsuoka et al., 2011). Unfortunately, thus far universal guidance molecules for retinal laminar targeting have not been identified, as mammalian DSCAMs appear to regular dendritic arbor spacing rather than laminar targeting (Fuerst et al., 2009; Huberman, 2009).

Identification of tectal laminar targeting molecules is likely not far behind. Beyond the use of subset-labeling transgenic mouse lines, other groups have been applying axon guidance techniques to explore laminar targeting possibilities. In chick, Nel has been identified as a possible repulsive molecule responsible for preventing axons from passing into and through SGFS-G into the deeper, non-retinorecipient laminae. Initial evidence showed that Nel mRNA and protein localized to the future SGFS-G, SGC, and SGP from E10 onward, Nel bound to retinal axons both *in vitro* and *in vivo*, and chick retinal axons were repelled by Nel in culture (Jiang et al., 2009). Hopefully future studies will be able to identify cues for retinorecipient laminae.

In this section of the dissertation, I consider Wnts and Frizzleds as possible molecular guidance cues for tectal laminar targeting. Wnts have increasingly been shown to act as guidance molecules, both attractive and repellant, for axons in the developing nervous system, directing targeting choices in commissural axons in the spinal cord (Lyuksyutova et al., 2003), axons crossing the corpus callosum (Keeble et al., 2006; Hutchens et al., 2011), and axons of several different populations of monoamingeric neurons in the midbrain and brainstem (Fenstermaker et al., 2010; Blakely et al., 2011). In the chick retinotectal system, *in situ* hybridization shows that several Wnts are localized to tectal laminae, while numerous Frizzled are expressed in large subsets of retinal ganglion cells during the period of map formation and laminar targeting. *In ovo* retinal electroporation and antibodies for subset labeling were used to test the chick system for *in vivo* tectal laminar targeting studies. These mechanisms have been used in initial tests to explore the effects of Frizzled overexpression on tectal laminar targeting, moving toward identifying a possible candidate for specific laminar targeting.

CHAPTER 6: MATERIALS AND METHODS

Maintenance of embryonic chicks

Fertilized White Leghorn chicken eggs were obtained from McIntyre Poultry & Fertile Eggs (Lakeside, CA). Eggs were stored at 4C for up to 7 days prior to initiating further development. To initiate development, eggs were placed in a humidified 37C hatching incubator (1550 Hatcher, GQF, Savannah, GA) with the long axis of the egg facing upward; the day on which eggs were placed into the incubator is considered embryonic day 0 (E0). Once the eggs reached E3 or E4, a syringe (3 mL Luer-lock syringe, BD Biosciences, Franklin Lakes, NJ) bearing an 18-gauge needle (BD 305196 18-gauge x 1½ inch needle, BD Biosciences, Franklin Lakes, NJ) was inserted into the wider end of each egg to remove approximately 4 milliliters of albumen (egg white) from the lower part of the egg; this resulted in the contents of the egg sinking slightly toward the bottom of the egg, generating an upper air space useful for access during later manipulations. Eggs were then returned to the incubator to continue developing until the appropriate age for experimentation.

Fixation and preparation of tissues for *in situ* hybridization

For *in situ* hybridization, whole chick right eyes and left tecta were dissected from live embryos at E10, E12, E14, and E16 in chilled 1x PBS using lightly blunted forceps. Excess epithelial tissue was removed from the sclera surface of the chick eyes, and the temporal side of each eye was ripped slightly to allow for better fluid access. Similarly, meninges and remaining skull and epithelial tissue were removed from the dissected

tecta. After this, retinas and tecta were transferred to pre-chilled 4C 4% paraformaldehyde (PFA) in DEPC-treated water in a 15-milliliter conical tube (VWR International, West Chester, PA) and kept at 4C overnight for fixation. After the resultant solution was allowed to sit open overnight in a fume hood to ensure complete diffusion and autoclaved, paraformaldehyde was added to the appropriate concentration, heated to 65C to ensure complete dissolution, and then chilled to 4C for experimental use.) After overnight fixation, the paraformaldehyde was removed from the fixed retinas and tecta. The tissues were rinsed once with 1x PBS to remove any remaining PFA residue, then transferred into 30% sucrose in 1x PBS and kept at 4C until the tissue was observed to reach the density of the sucrose solution, sinking to the bottom of the conical. At this point, half of the sucrose solution was removed and replaced with OCT medium (Tissue-Tek OCT Compound, Ted Pella, Inc., Redding, CA). The new solution was mixed by vortexing (Vortex Genie 2, Scientific Industries, Bohemia, NY) and tilting the tube back and forth to obtain an even consistency, then the tissue-containing conical was returned to 4C for a minimum of two hours (to a maximum of overnight) to equilibrate to the solution. After this, the tissue was embedded in OCT in small cryostat molds (22mm x 22mm square molds, Electron Microscopy Services (EMS), Hatfield, PA). Eyes were oriented with the lens toward the bottom of the mold and the dorsal retina oriented toward the orientation protrusions; tecta were oriented with the ventral (ventricular) side toward the bottom of the mold and the posterior end toward the protrusions. Molds were then placed in crushed dry ice with 100% ethanol for quick, even freezing and stored at -80C.

In situ hybridization of chick retinal and tectal tissues

Tissues were sectioned at a thickness of 20 microns using a cryostat (Leica 3050 S cryostat, Leica Microsystems, Wetzlar, Germany). Retinal tissue blocks were oriented to create sections with dorsal upward, ventral downward, and the cornea visible to either the left or right; only sections in which the cornea was clearly visible were used. Tectal tissue blocks were oriented such that the medial, lateral, and dorsal (opposite ventricular opening) sides of the tectum were present and the ventricular opening and the nucleus mesencephalicus lateralis, pars dorsalis (or MLd, an auditory nucleus located in the deeper tectal laminae on the lateral side of the tectum) could be observed; only sections in which the ventricular opening could be observed, with the addition of a few immediately before or after the opening, were used. Tissue sections were mounted directly onto Superfrost Plus slides (Fisherbrand Superfrost Plus slides, Thermo Fisher Scientific, Waltham, MA) after sectioning and allowed to air dry for at least 20 minutes prior to beginning the *in situ* hybridization process. For the appropriate direct comparison of gradient strength and position, retinas or tecta of each age (E8-E16) were mounted on the same slides, with 3-5 sections of each age per slide to ensure redundancy in case of tissue damage or loss.

The first day of the *in situ* hybridization(ISH) process involves preparing the tissue for the riboprobe hybridization and starting the hybridization proper. After drying the tissue-covered slides, the slides were placed in 4%PFA in 1x PBS treated with DEPC (DEPC-PBS) for ten minutes at room temperature, then washed in 1x PBS-DEPC three times, three minutes per wash. To minimize non-specific hybridization, the slides were then placed in a freshly made acetylation solution for 10 minutes, after which the slides

were again washed in 1x PBS-DEPC three times, five minutes per wash. To acclimate the slides for hybridization, they were then placed into a 20x saline sodium citrate (SSC) buffer treated with DEPC for fifteen minutes, after which excess fluid was wiped from the backs of the slides using a Kimwipe. The slides were then placed into a pre-warmed (to 58C) hybridization chamber humidified using a 4x SSC/ 50% formamide solution on whatman paper (GE Healthcare, Little Chalfont, UK). Six-hundred microliters of pre-warmed hybridization buffer were added to each slide, and the chamber was placed in a 58C hybridization oven for pre-hybridization. During this time, riboprobes were prepared by mixing 1.2 microliters of the relevant 400ng/mL riboprobe stock with 1.2 microliters of 0.1 mM EDTA per slide, then denaturing the probe mixture at 80C for five minutes. After this, 300 microliters of hybridization buffer per slide was added to the mixture. At this point, the hybridization buffer was removed from the slides and the probe solution was added to the appropriate slide (at 300 microliters per slide), after which each slide was covered with a HybriSlip (247459, Research Products International, Mt. Prospect, IL) to ensure an even distribution of probe across the slide surface and prevent prove solution from leaking off the slide. The slides were returned to the hybridization chamber and thence to the hybridization oven at 58C for 40 hours in order to allow the probes to hybridize with mRNA in the tissue sections.

The second day of the ISH process (the third day overall) involves the removal of nonspecifically-bound riboprobes and the addition of probe-targeting antibodies. After hybridization, the Hybrislips and probe solution were removed from the slides, and the slides were placed in pre-heated 0.2x SSC (without DEPC) at 65C for two incubations of 90 minutes each in order to detach non-specifically bound probes. The slides were then

washed in room temperature 0.2x SSC for 10 minutes, after which they were transferred to B1 solution (0.1M Tris (pH 7.5), 0.15M NaCl) for five minutes. During this time, B2 solution (B1 plus 1% blocking solution (a 1:10 dilution of 10% Boehringer Mannheim blocking reagent power (11 096 176 001, Roche Diagnostics GmbH, Mannheim, Germany) in pH 7.5 maleic acid buffer)) with anti-digoxygenin-AP (alkaline phosphatase) (1:5000, 11 093 274 910, Roche Applied Science, Mannheim, Germany) was generated. B1 was removed from the slides, which were then covered in B2 (1 milliliter per slide) and transferred to a 4C cold room overnight.

The third day of the ISH process (the fourth day overall) involves the development and processing of the slides to reveal mRNA expression patterns. After the overnight incubation in anti-digoxygenin-AP antibodies, the slides were washed five times, ten minutes per wash in B1 at room temperature. The slides were then transferred to B3 (0.1M Tris (pH 9.5), 0.1M NaCl, 50mM $MgCl_2$) for five minutes to begin activating the alkaline phosphatase, during which time the colorimetric developing solution was generated (20 microliters of NBT/BCIP (11 681 451 001, Roche Applied Science, Mannheim, Germany) in 980 microliters of B3 per slide). The slides were then removed from the B3 and placed in an aluminum foil-covered slide box, at which time the NBT/BCIP developing solution was added. Slides were monitored every 15 to 30 minutes for visibility of a purple NBT/BCIP precipitate. One the colorimetric reaction was considered to be sufficiently dark for clear visualization, slides were transferred to 1x TE for 10 minutes, then rinsed in water and allowed to dry in a dark, room temperature location overnight. Slides were mounted using Poly-Mount (#08381, Polysciences, Inc., Warrington, PA) and 22mm x 50mm glass coverslips.

In some experiments, to remove nonspecific precipitate, an ethanol-xylene dehydration series was used prior to mounting. For this dehydration series, slides were placed into 30% ethanol, then 50% ethanol, 75% ethanol, 95% ethanol, and 100% ethanol for up to 2 minutes each, then transferred to xylene for two washes of up to one minute each. Slides were monitored during this process to prevent excessive signal removal.

Probes employed for *in situ* hybridization

Most probes were generated from bacterial stocks created by previous members of the Zou lab. All probes were constructed from 200-900bp regions of the relevant genes and, in some cases, their 3' UTRs, cloned into a pCRII-TOPO vector (Invitrogen, Carlsbad, CA). Probes were tagged with digoxygenin during transcription for labeling during *in situ* hybridization.

***In ovo* retinal electroporation**

On E7, eggs were checked for the survival, health, and location of their embryos by placing them up to a brightly shining gooseneck lamp, a procedure known as candling. Eggs were selected for electroporation if the interior membranes appeared continuous and the chorioallantoic membrane showed bright red blood vessels and had detached from the egg surface, generating an appropriate manipulation space for the electroporation.

To access the embryo, a piece of clear heavy-duty packaging tape (Scotch 3500 High-Performance Packaging Tape, 3M Company, Preston, MN) was smoothed onto the egg shell, and an oval window was cut to access the manipulation space using curved scissors. Blunted forceps were then used to shift the chorioallantoic membrane and tear

the amniotic membrane, which was used to shift the embryo's head toward the torn opening. A sharpened straight tungsten pin was then used to poke a hole through the dorsal or ventral sclera of the embryo's right eye for retinal access. Approximately 2 microliters of a DNA mixture containing 10% Fast Green dye (Fast Green FCF, Thermo Fisher, Waltham, MA) for visibility was then injected between the vitreous body and retina via a capillary tube needle (half of a 1.0mm exterior, 0.75mm interior, 4" long thin-wall glass filament (A-M Systems, Inc., Sequim, WA) as pulled by a Narishige PC-10 capillary tube puller (Narishige Co. Ltd., Tokyo, Japan) at 62C) attached to a mouth pipette (A5177, Sigma-Aldrich, St. Louis, MO). Embryos were injected with one of two mixes: 0.75 ug/uL pN2.1 (Clontech pEGFPN2 vector modified to contain a chick β-actin promoter for better expression in neurons) (EGFP-only controls) or 1.0 ug/uL Frizzled1 in pIRES2.1 (Clontech pIRESN2 vector modified to contain a chick β-actin promoter) (Fz1 overexpression). After injection, the eye was electroporated at 21V using a BTX ECM830 Electro Square Porator (BTX Instrument Division (Harvard Apparatus), Holliston MA) with gold-plated electrodes (Model 512 *in ovo* L-shaped electrodes with 5mm gold tips, BTX, Holliston, MA). The chorioallantoic membrane was then readjusted to cover the embryo, and the window in the eggshell was sealed with another piece of packaging tape, after which the egg was returned to the incubator to continue developing.

At the appropriate age (generally E16 for these studies, though several were studied at other ages between E14 and E17, inclusive), surviving electroporated eggs were removed from the incubator for dissection and imaging. The electroporated eye and contralateral tectum were removed. After meninges were removed from a dissected

tectum, it was placed electroporated axon-side down on a Superfrost glass slide and flattened slightly by pressing with a glass coverslip to decrease tectal curvature for more even imaging of the tectal surface.

Electroporated tecta were imaged using a Zeiss inverted confocal microscope (Zeiss LSM 510 (on an Axio Observer Z1 inverted microscope), Carl Zeiss Microimaging, LLC, Oberkochen, Germany). A tile scan of each tectum was taken to observe the quality, position, and length of electroporated axons in the tectum. Z-stacks of electroporated axons were taken along the length of axons for developmental progression studies and in regions containing interstitial branches for mediolateral direction choice and initiation studies. These images were taken at 3.75-micron intervals within the Z-stack, to a minimal tectal depth of 60 microns, with the tectal surface being defined as the first image in which the primary axons appeared in focus. Z-stack locations were selected by eye to tile regions containing the appropriate electroporated axons or branches.

For later immunohistochemistry, whole retinas were dissected from the electroporated eyes and fixed in individual eppendorf tubes containing 4C 4% PFA in 1xPBS for two hours. Electroporated, imaged tecta were carefully detached from imaging slides and preserved in the manner described above for ISH tissue samples.

Immunohistochemistry of whole mount retinas

After their 2-hour fixation in room temperature 4%PFA in 1x PBS, retinas were individually washed three times, ten minutes per wash with 1x PBS at room temperature on a Nutator (BD Clay Adams Nutator, BD Biosciences, Franklin Lakes, NJ). The

Nutator ensured that fluids completely washed over the retinal surface. After washing, retinas were blocked in a 0.3% Triton X-100, 0.5% serum in 1xPBS solution for one hour at room temperature, then incubated at 4C overnight on a Nutator in primary antibody solution (0.5% Triton X-100, 0.5% serum, 1:1000 mouse anti-GFP (A11120, Invitrogen, Carlsbad, CA), and 1:200 rat anti-chick AChRβ2 (mAb270, DSHB, Iowa City, IA (Whiting et al., 1987) in 1x PBS, 1 milliliter per tube).

The retinas were then washed three times, twenty minutes each, with 1x PBS on a Nutator, after which the eppendorf tubes were covered with aluminum foil. The retinas were then incubated in a secondary antibody solution (0.3% Triton X-100, 0.5% serum, 1:1000 goat anti-mouse Alexa488 (A10680, Invitrogen, Carlsbad, CA), and 1:1000 goat anti-rat Alexa555 (A21434, Invitrogen, Carlsbad, CA) in 1x PBS, 1 milliliter per tube) at room temperature for 2 hours on a Nutator. In some samples, 1:20,000 DAPI was added to the tubes for the last ten minutes of the incubation period.

After this, all retinas were washed three times, twenty minutes each, in 1x PBS in their foil-covered eppendorf tubes. Each retina was carefully removed from its tube and placed onto a Superfrost slide, then manipulated with dull-edged forceps under a dissection scope to lay out and flatten the retina, placing the ganglion cell layer upward for better imaging. The retina was then mounted with Fluoromount-G (SouthernBiotech, Birmingham, AL) and a glass coverslip and allowed to stabilize for an hour in a dark drawer, after which the coverslip was sealed with clear nailpolish.

Whole mount retinal IHC slides were imaged using a Zeiss inverted confocal microscope.

Preparation and immunohistochemistry of retinal and tectal sections

Electroporated tecta prepared for immunohistochemistry were sectioned at 40-micron intervals on a Leica cryostat. Sections were generated coronally with regard to the internal planes of the tectum, such that the mediolateral and dorsoventral planes could be fully observed. Sections from each entire tectum were placed sequentially onto Superfrost Plus slides to ensure that the entire electroporated region could be analyzed. A single E16 tectum under these conditions usually requires 4-5 slides.

Similarly, whole chick eyes prepared as described previously for *in situ* hybridization were sectioned at 20-micron intervals on a Leica cryostat. These sections focused on a central region of the eye, such that each section included at minimum the iris, although most included both lens and iris, and some also included the pectin and optic nerve. Several sections were included on each slide in order to visualize the normal distribution of AChRβ2-positive cells in standard retinal sections.

Slides were allowed to dry in a dark drawer for an additional thirty minutes after sectioning was completed, then rehydrated in 1x PBS for 15 minutes. Slides were blocked in a 0.5% Triton X-100, 1% serum in 1x PBS solution for one hour, then stored in a 4C cold room overnight to incubate in a primary antibody solution (0.5% Triton X-100, 1% serum, 1:1000 mouse anti-GFP (A11120, Invitrogen, Carlsbad, CA), and 1:200 rat anti-chick AChRβ2 (mAb270, DSHB, Iowa City, IA (Whiting et al., 1987)) in 1x PBS, 0.75 milliliters per slide).

After incubation, slides were washed four times, fifteen minutes each wash, in 1x PBS on a shaker (Barnstead Lab-line lab rotator, Thermo Fisher Scientific, Waltham, MA) at room temperature. Slides were then placed into a dark slide box for secondary

antibody incubation (4 hours at room temperature in a 0.5% Triton X-100, 0.5% serum, 1:1000 goat anti-mouse Alexa488 (A10680, Invitrogen, Carlsbad, CA), and 1:1000 goat anti-rat Alexa555 (A21434, Invitrogen, Carlsbad, CA) in 1x PBS, 0.75 milliliters per slide). During the last 15 minutes of incubation, 100 microliters of 1:20,000 DAPI was added to each slide. After this, all slides were again washed four times, fifteen minutes per wash. Excess fluid was removed and slides were mounted with Fluoromount-G and coverslipped. Tectal slides were imaged using a Zeiss inverted confocal microscope.

Image Processing and Data Analysis

Processing of tectal Z-stack images (Depth coding)

Tectal Z-stacks were converted into depth-coded images using LSM Image Browser, with the tectal surface (axons in/on which appear as dark blue) defined as the first image in which primary axons appeared to be in focus. For all studies involving the depth-based morphology of electroporated axons in the tectum, stacks of 22 images (82.5 microns at maximal depth, which appears as bright red) were employed. While some arbors traveled to depths greater than 82.5 microns, the 82.5 micron limit provided a consistent point of comparison between populations, as well as allowing for greater clarity of morphology. For images comprised of multiple Z-stacks, depth-coded projections from a given tectal region were pieced together in Adobe Photoshop CS4 using the Auto-Align: Reposition function, followed by readjustment by hand to ensure proper alignment of images.

For some experiments, tectal Z-stacks were converted into flattened black-and-white projections using LSM Image Browser, with the tectal surface (first image in the

stack to be flattened) defined as the first image in which primary axons appeared to be in focus. These images were used to look directly at morphological details without depth information.

Processing of Z-stack images from retinal and tectal IHC slides

Subsets of Z-stack images taken from whole mount retina IHC were defined based upon the first and last images in the series in which any portion of the ganglion cell layer (as determined by the presence of electroporated RGCs) appeared in focus. These stacks were then used to create multi-color projections, with electroporated RGCs in green and AChRβ2+ cells (which are limited to the ganglion cell and the innermost edge of the inner nuclear layer (Yamagata and Sanes, 1995b)) in red.

Subsets of Z-stack images taken from 40-micron tectal sections were defined based upon the first and last images in the series in which retinal axons appeared to be in focus. These stacks were used to create multi-color projections, with electroporated retinal axons in green, AChRβ2+ cells and projections in red, and DAPI-labeled nuclei in blue.

Identification of relevant RGCs in whole mount retina

AChRβ2+ RGCs were identified based on morphological and IHC characteristics. First, RGCs were identified by the presence of the primary axon, defined as a long neurite traveling beyond the site of electroporation; observation of serial slices in a retinal Z-stack in LSM Image Viewer was used to confirm the soma source of each identified primary axon. The presence or absence of AChRβ2 antibody labeling (in fluorescent red)

around the RGC soma determined whether the RGC was AChRβ2-positive or -negative. After identification, AChRβ2+ RGCs were compared to determine shared features of dendritic morphology.

Identification of targeted laminae in tectal sections

In chick tectum, laminae can be easily identified based upon the apparent cell density (as labeled by DAPI), thickness, and location within the section (Ramón y Cajal, 1911; La Vail and Cowan, 1971; Hunt and Brecha, 1984; Yamagata and Sanes, 1995a; Yamagata et al., 1995; Karten et al., 1997). Retinal axonal arbors observed to be contained within a single lamina, as observed via expression of EGFP, were considered to be targeted to that lamina; those that were not could not be considered to be definitively targeted to a lamina. General qualities of laminar targeting could also be observed, such as failure of any labeled axons to reach SGFS-G, or a tendency of axons to cross SGFS-G.

CHAPTER 7: RESULTS

Expression of Wnts and Frizzleds in the developing retinotectal system

Wnt3 has been shown to act in the formation of the retinotopic map (Schmitt et al., 2006; current dissertation), and other Wnts and Wnt receptors have been shown to serve as axon guidance cues in many regions of the developing nervous system (Sanchez-Camacho et al., 2005; Wang et al., 2002; Yoshikawa et al., 2003; Lyuksyutova et al., 2003; see Chapter 5 for additional commentary and references). I used *in situ* hybridization to study whether Wnts and Frizzleds, the seven-transmembrane G-protein coupled receptors which act as their main signaling receptors, displayed expression patterns suggestive of possible roles in tectal laminar targeting. Because sequences were available for fifteen Wnts (out of the eighteen now believed to be expressed in chick (Fokina and Frolona, 2006)), these fifteen were tested. These Wnts were Wnt1, Wnt2, Wnt2b, Wnt3, Wnt3a, Wnt4, Wnt5a, Wnt5b, Wnt6, Wnt7a, Wnt7b, Wnt8b, Wnt8c, Wnt9a, Wnt10a, and Wnt11. Wnt9b, Wnt10b, and Wnt16 were not tested due to lack of sequence information at the time of probe construction.

Of the 15 Wnts tested, only five showed tectal expression during E10, E12, E14, or E16: Wnt3, Wnt4, Wnt5a, Wnt7a, and Wnt7b. The expression pattern of Wnt3 has been described previously, both in publication and in more detail in this dissertation, with Wnt3 mRNA expression appearing in the ventricular epithelium by E9 and disappearing by about E14 (Figure 3.1A, Schmitt et al., 2006). The four previously undescribed Wnts (Wnt4, 5a, 71, and 7b) all displayed somewhat different expression patterns between E10 and E16. Wnt4 expression appeared at E10 in a vague band toward the outer tectal

laminae. This pattern became more stable and increasingly strongly localized to cell bodies in SGFS-C from E12 through E16 (Figure 6.1A). Wnt5a showed bands of expression in SGFS-G, SGFS-I, and the ventricular epithelium during this period. This expression was not consistently localized to the tectal cell bodies in SGFS-G and SGFS-I, but appeared to be associated with at minimum a population of cell bodies in these laminae. Expression in the ventricular epithelium appeared to be higher medially than laterally, much like the ephrinB1 gradient, and remained stable in gradient expression from E10 through E14, weakening as the ventricular epithelium was removed at E16 (Figure 6.1B). Expression of Wnt7a appeared in SGFS-G and the ventricular epithelium. Expression in the ventricular epithelium, which appeared mildly stronger medially than laterally, was much stronger than that in SGFS-G, which appeared around E14. Weak labeling in SGFS-G appeared through E16 (Figure 6.1C). Wnt7b expression localized to SGFS-I during this period (Figure 6.1D).

All ten Frizzleds (Fz1-10) were tested for expression in the chick retina at E10, E12, E14, and E16. Of these ten Frizzleds, six were clearly expressed in retinal ganglion cells during this time period: Fz1, Fz2, Fz5, Fz7, Fz8, and Fz9 (Figure 6.2). Frizzled4, Fz6, and Fz10 were not expressed, while Fz3 showed some expression in the inner nuclear layer (INL) of the retina but not in the ganglion cell layer (where RGCs are located).

Ganglion cell layer expression during some or all of these time periods has been previously described for all six of the aforementioned Frizzleds. Fuhrmann and colleagues observed the expression of all ten Frizzleds in the developing chick retina, looking at Hamburger Hamilton embryonic chick stages including HH 29 (approximately

E6), HH 42 (E16), and occasionally HH 35 (late E8), but not at any intervening stages (Hamburger and Hamilton, 1951 (1992); Fuhrmann et al., 2003). At E16, as I also observed, this group notes that Fz1, Fz2, Fz7, Fz8, and Fz9 are present in the ganglion cell layer, among other locations (Fuhrmann et al., 2003). While this group did not observe Frizzled5 expression after HH29, weak Frizzled5 expression in the ganglion cell layer at E10 has previously been reported (Fuhrmann et al., 2003; Schmitt et al., 2006).

In situ hybridization of Frizzled in chick eye sections showed differing degrees of labeling in the ganglion cells layer for the various Frizzled between E10 and E16. Frizzled1 and Fz2 showed strong ganglion cell layer labeling through the entire period and appeared to label most or all retinal ganglion cells, while Fz5 appeared somewhat weakly in a majority of retinal ganglion cells at E10 and showed virtually no expression by E16 (Figure 6.2 A-C). Frizzled7, Fz8, and Fz9 showed fairly strong RGC labeling during this period, but appeared to label large subsets of retinal ganglion cells rather than all retinal ganglion cells, as some RGCs lacking expression of these Frizzleds can be clearly identified in retinal slice ISH slides and images (Figure 6.2 D-F). None of these Frizzleds show graded expression along the dorsoventral retinal axis, unlike Ryk (Schmitt et al., 2006); all appear to be evenly expressed or distributed to RGCs within the ganglion cell layer (Figure 6.2).

Use of retinal electroporation to study laminar termination and arbor morphology

Studies on the morphology of retinal ganglion cells date back to Ramón y Cajal, but the specific study of the morphology of individual RGCs and targeted RGC populations has not become a priority until recent years. To observe the laminar

termination and morphology of small, spatially targeted populations of retinal ganglion cells, EGFP-expressing constructs were electroporated into the retinas of E7 embryonic chicks. The chicks were allowed to age until E14-E17, at which point the whole retinas were dissected and preserved for IHC while the whole tecta were imaged then preserved for additional IHC. In these electroporated chick populations, survival after E15 was minimal. It also appeared that, even in well-labeled chicks, the number of surviving labeled RGCs decreased with age, so few electroporated chicks older than E15 were successfully imaged for data collection purposes. While the brightness of the EGFP label appeared weaker with time in some electroporated chicks, it is likely that much of the apparent signal weakness was due to the increasing thickness of the tectal tissue during development. Under these conditions, axons traveling to appropriate laminae would appear dimmer due to the greater scattering of signal as it reflected through these thicker laminae to reach the tectal surface and the observer.

In order to observe the morphology and targeting of retinal arbors, both confocal imaging of whole-mounted freshly dissected tecta and immunohistochemistry on sections of preserved tecta were employed. After dissection, tile scans of the tectal surface were used to visualize the spread of the labeled termination zone and the general shape and spacing of arbors. After this, Z-stacks of the entire termination zone were used to generate depth-coded images, with blue at the tectal surface and red at a depth of 60 or more microns (Figure 6.3A-B, E-F, K-L). Surface tile scans combined with confocal imaging were sufficient to clearly distinguish the approximate size and spacing of these arbors, as well as to observe gross morphological differences in arbor shape; when combined with images of the respective whole-mounted retina, it was possible to

consider similarities in RGC spacing with those seen in the arbors, but not to directly connect any specific RGC soma in the retina with its axonal arbor in the tectum (Figure 6.3A-B, E-F, K-L).

However, while differences in arbor depth could sometimes be observed, identifying the specific laminae targeted by retinal arbors via depth coding proved ineffective. Both variations in tectal thickness with age and position, as well as minor depth adjustments caused by the slight flattening of the tecta prior to imaging to minimize tectal curvature effects and the multi-laminar and weakly pruned structure of pre-E18 arbors, made distinguishing differences in laminar targeting via Z-stacks uncertain. To clarify this laminar targeting, preserved, imaged tecta were sectioned at 40 microns to collect thick regions containing portions of whole arbors; sections thicker than 40 microns showed decreases in the effectiveness of both staining and stable tissue attachment, making the 40 micron thickness optimal. Tectal sections were labeled with DAPI to distinguish between tectal laminae, which have readily apparent differences in cell density that have been well characterized. The tecta were also labeled with GFP antibodies to maintain and strengthen the electroporated axon labels as well as, in some cases, laminar labels such as AChRβ2, which labels a diffuse region surface-ward of SGFS-G prior to E15, then settles toward SGFS-F during E15 and E16 (Yamagata and Sanes, 1995b; Yamagata et al., 2006). Tectal sectioning, IHC, and DAPI labeling permitted the laminae targeted by retinal axons to be clearly determined; these methods also exposed additional details of the developing arbors, such as differences in fiber thickness between arbors and better visualization of the deepest tips of arbors, which were not apparent during confocal imaging of the whole tectum (Figure 6.3C-D,G-H).

The spacing of these arbors, as well as their general shape, allowed some arbors in tectal sections to be paired with their confocal images (Figure 6.3I-L). This suggests that while confocal imaging may not be sufficient to pair an RGC soma to its arbor, if molecular markers are used to label the whole mount retina and the sectioned tectum, then the sectioned labeled arbors (which can be paired to confocal arbors) would be sufficient to determine the original labeled RGC soma in the retina for additional morphological and targeting studies.

The first of these targeting studies has already been initiated. An overexpression construct for Fz1, which appears to be ubiquitously expressed in RGCs during mapping and laminar targeting (Figure 6.2A, Fuhrmann et al., 2003), was electroporated into dorsal chick retina at E7 to observe effects on retinotectal projection development and targeting. However, the construct appears highly toxic thus far, as no chicks overexpressing Fz1 have survived past E12 at present. Several E12 Fz1-overexpressing tecta were collected for observation; these tecta appear developmentally delayed and show minimal interstitial branching (Figure 6.4A,C). Several E12 tecta overexpressing Fz7 have also been collected thus far; these appear fairly normal (Figure 6.4B,D).

AChRβ2-positive RGCs as a subset population for study

The mAB270 antibody, a rat monoclonal antibody targeting the chick nicotinic acetylcholine receptor subunit β2, has previously been used to characterize a population of retinal ganglion cells which are evenly distributed throughout the ganglion cell layer of the chick retina as well as occasionally misplaced to the inner nuclear layer (Yamagata and Sanes 1995b; Yamagata et al., 2006). Their dendrites appear to target retinal internal

plexiform layer sublayers 3, 4, and 5 (using the five-sublayer system of IPL labeling), while their axons initially appear diffusely in the general retinorecipient tectal regions at E12 and are specifically sequestered to SGFS-F as it stabilizes around E16 (Yamagata and Sanes, 1995b; Yamagata et al., 2006).

This antibody was used to further characterize the AChRβ2-positive subpopulation of RGCs in order to test them as a possible useful RGC subset for tectal laminar targeting studies. Results from the immunostaining of retinal and tectal slices between E12 and E17 appeared strongly similar to those reported by the Sanes lab. Retinal sections showed clear labeling in the cell bodies and some dendrites of retinal ganglion cells located in the ganglion cell layer, as well as displaced RGCs localized to the inner edge of the inner nuclear layer (Figure 6.5A-D, red fluorescent label). Tectal sections showed vague labeling between the tectal surface and SGFS-G prior to E15, with the signal being compressed toward SGFS-G during E15 and stabilizing to SGFS-F by E16 (Figure 6.5E).

Whole mounted retinas from electroporated chicks were also labeled for AChRβ2 in order to identify whether RGCs from this subpopulation had been electroporated. While the immunostaining proved fairly effective, very few AChRβ2-positive RGCs were labeled; in six test retinas ranging between E14 and E16, only two total AChRβ2-positive EGFP-electroporated RGCs were labeled, out of a total of 134 EGFP-electroporated RGCs identified (Figure 6.5F-H). To estimate whether this degree of co-labeling (2/134, or approximately 1.5% of the total population of retinal ganglion cells) reflected the actual distribution of AChRβ2-positive RGCs in the retina, I quantified the number of AChRβ2-positive and –negative retinal ganglion cells observed in the

ganglion cell layer of IHC-labeled retinal sections. Retinal sections, rather than whole mounted retinas, were used due to the ability to use DAPI staining to distinguish cell bodies in the retinal sections, allowing AChRβ2-negative RGCs to be clearly distinguished, based on laminar position, from non-RGC retinal calls. Using this method on sections from four E14 retinas, 11.2±2.87% of all cells in the ganglion cell layer were considered AChRβ2-positive. Thus, electroporation of AChRβ2-positive RGCs was lower than expected.

A second population of RGCs characterized by substance P and known to target SGFS-B were also tested (Yamagata and Sanes, 1995b; Yamagata et al., 2006). Because of the apparent clarity of the labeling, as well as the shallower laminar target, these RGCs were considered likely to be more effective for laminar termination studies than AChRβ2-positive RGCs. However, two antibodies reported to label substance P in chick, one from AbD Serotec and the other from Abcam (O'Donnell and Puri, 2010, labeling chick cloacal cells), failed to distinguish substance P-positive RGCs from other RGCs, instead labeling the central regions of virtually all retinal ganglion cells, as well as a number of cells in the inner nuclear layer and pigment epithelium (green fluorescent label in Figure 6.5A,C). Thus, the substance P antibodies used did not provide a sufficiently specific label for an SGFS-B-targeting population of RGCs, instead labeling multiple cell types.

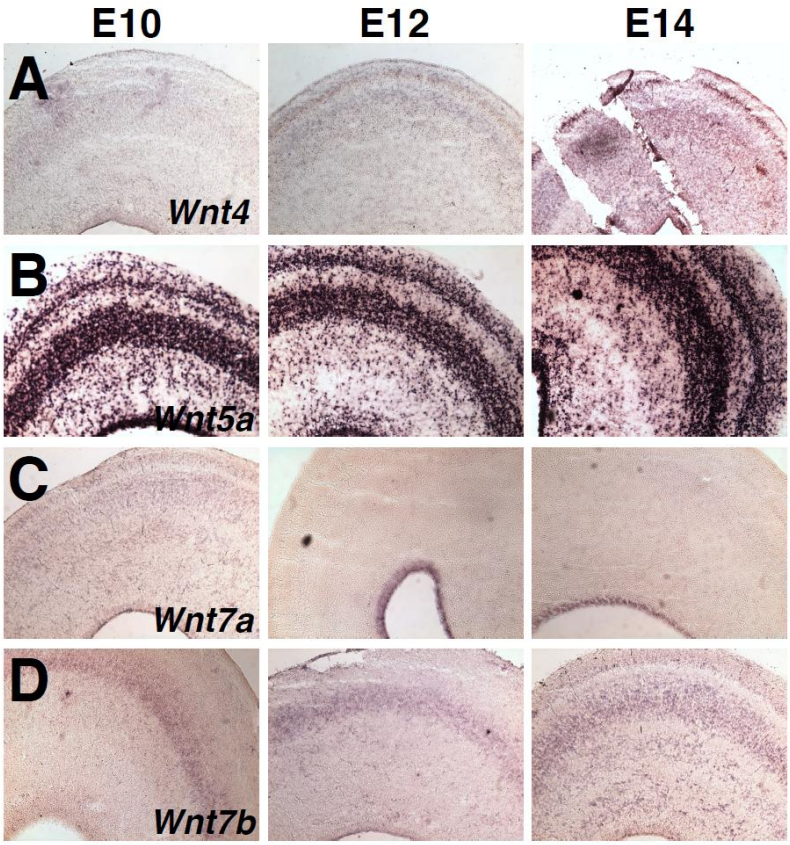

Figure 7.1. Expression of Wnts in tectal laminae. (A) Wnt4 appears in a vague band of expression at E10, becoming a clear label for cell bodies in SGFS-C by E12. (B) Wnt5a expression localizes to SGFS-G, SGFS-I, and the ventricular epithelium. (C) Wnt7a localizes to SGFS-G and the ventricular epithelium, while (D) Wnt7b localizes to SGFS-G and SGFS-I.

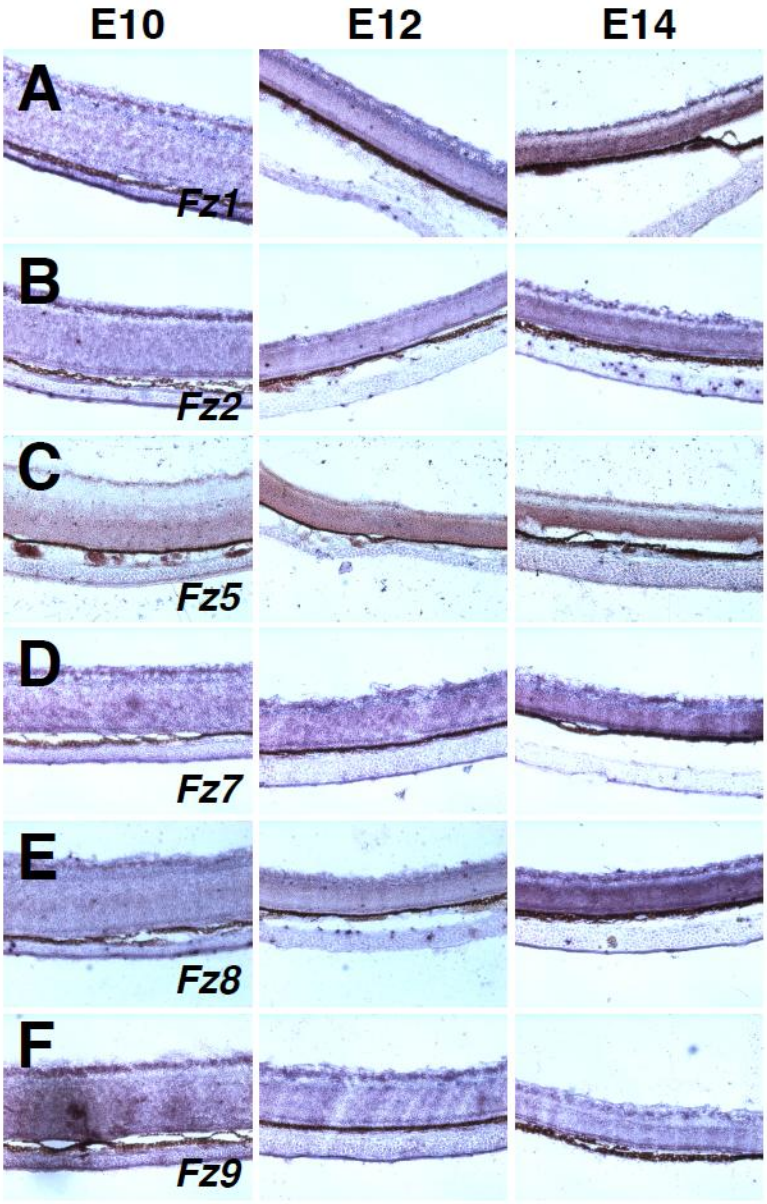

Figure 7.2. Frizzleds are expressed in subsets of retinal ganglion cells. (A) Frizzled1 and (B) Frizzled2 are ubiquitously expressed by RGCs in the ganglion cell layer between E10 and E14. (C) Frizzled5 is expressed in the ganglion cell layer, but its expression decreases over time. (D) Frizzled7, (E) Frizzled8, and (F) Frizzled9 are expressed in large subsets of RGCs in the ganglion cell layer.

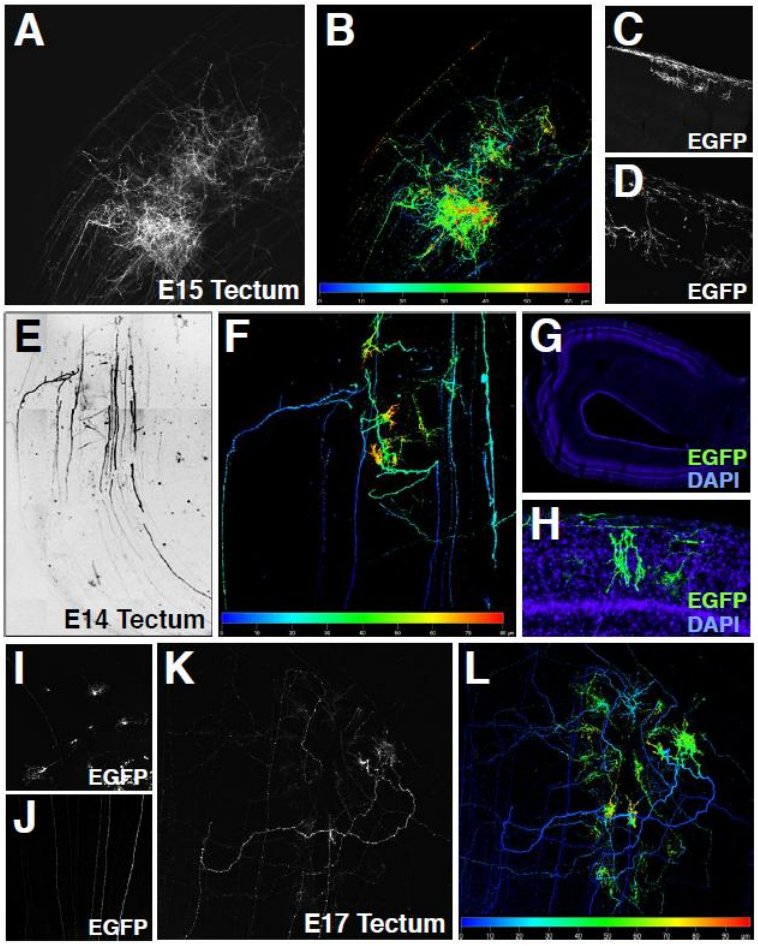

Figure 7.3. Labeling retinal axons to identify their laminar targets. (A) A flat projection and (B) depth-coded image (surface (blue) at 0 µm, maximum depth (red) at 65 µm) of an EGFP-electroporated E15 tectum. (C) 10x and (D) 20x images of a 40 µm thick section of the tectum shown in (A) and (B), with IHC enhancement of the EGFP label to show the morphology of the arbors. (E) Tile scan of the tectal surface and (F) depth-coded image (blue 0 µm, red 80 µm) of the termination zone of an EGFP-electroporated E14 tectum. (G) Tile scan and (H) flat projection of a section of a 40 µm thick section labeled with DAPI (blue) to distinguish the tectal laminae. Electroporated axons, shown in green, correspond to the two arbors developing in the center of the images shown in (E) and (F), one with thicker and one with thinner fibers. (I) Cell bodies and (J) axons of electroporated RGCs in an E17 whole mount tectum. (K) Flat projection and (L) depth-coded image of the tectum receiving axons from the retina shown in (I) and (J), with distinct spacing, shape, and depth of arbors.

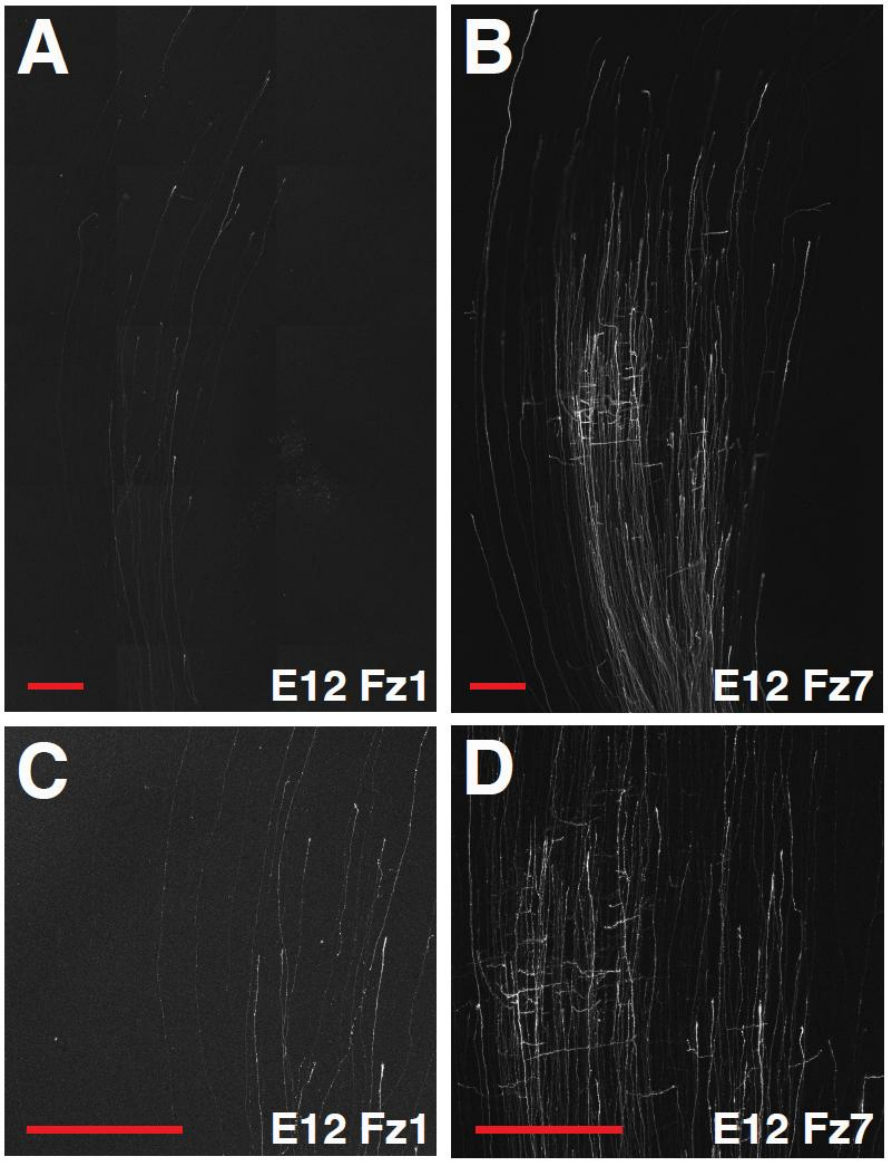

Figure 7.4. Overexpression of Frizzled1 and Frizzled7 in tectum. (A) Frizzled1 overexpression in RGCs, shown as a tile scan of an electroporated E12 tectum, appears to cause developmental delays and later embryonic death. (B) Tile scan of Frizzled7-overexpressing retinal axons shows normal development at E12. Flat projections of images from the predicted termination zones of these (C) Frizzled1-overexpressing and (D) Frizzled7-overexpressing retinal axons shows distinct differences in the degree of interstitial branching, with Frizzled1-overexpressing axons being developmentally delayed. (A-D) Red scale bar = 200 microns; Anterior is down, lateral is right.

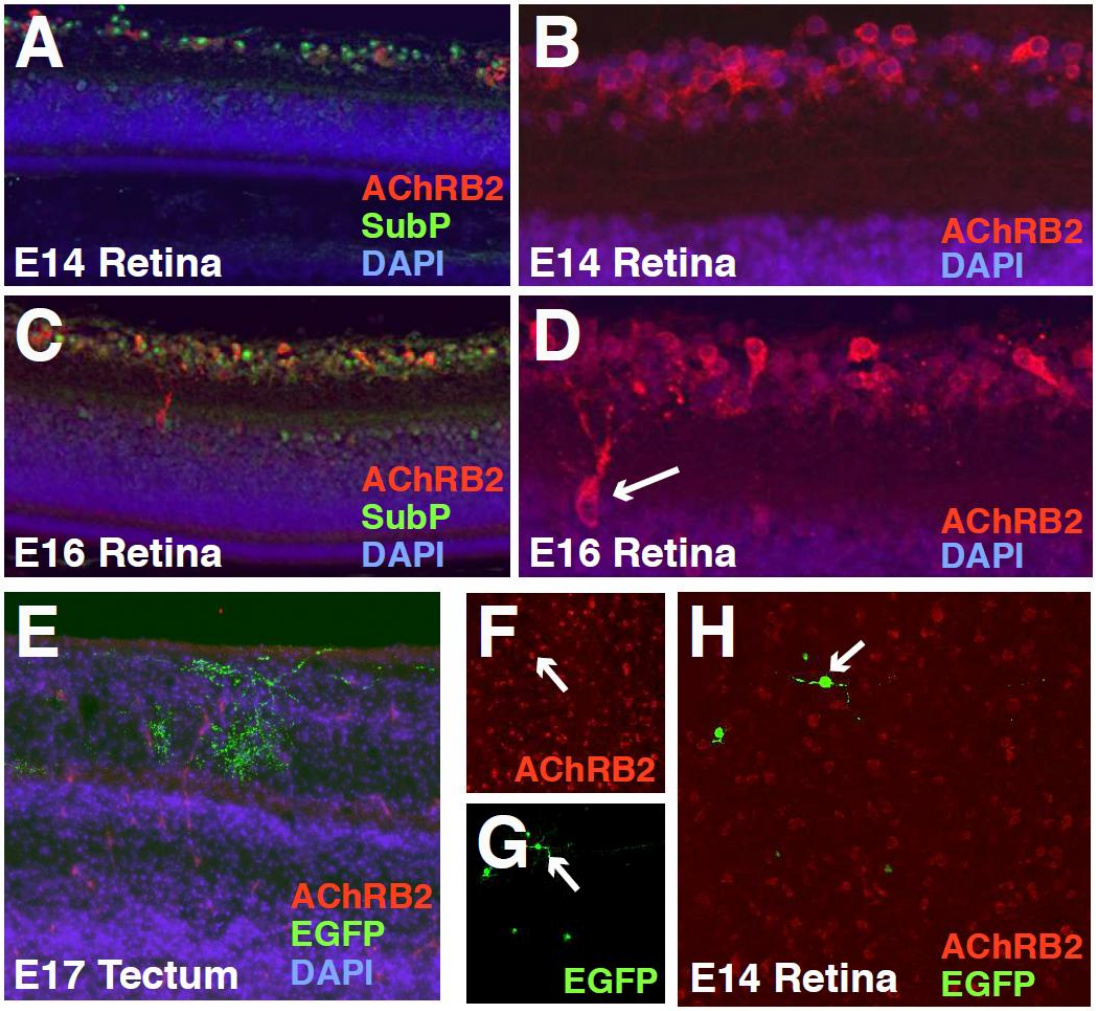

Figure 7.5. Labeling RGC subpopulations in the chick retina. (A,B) E14 and (E16) retinal sections labeled with mAb270 (red), DAPI (blue), and substance P antibodies (green in (A) and (C)) distinguish the AChRβ2-positive RGCs localized to the ganglion cell layer (top) and displaced to the inner nuclear layer (white arrow in D), but do not distinguish the substance P-positive RGC population. (E) AChRβ2-positive retinal axons target SGFS-F in this image of an EGFP-electroporated (green axons) E17 tectal section. DAPI (blue) distinguishes the tectal laminae. (F-H) However, very few electroporated RGCs (green, G and H) are labeled by mAb270 (red, F and H) in whole mount electroporated retinas; (F-H) white arrow labels AChRβ2-positive EGFP-electroporated neuron.

CHAPTER 8: DISCUSSION AND CONCLUSIONS

Wnt and Frizzled expression patterns suggest roles in development and targeting

Several Wnts were expressed in different tectal laminae during the period of map formation and laminar targeting, making it possible that these Wnts play a role or roles in axon guidance during mapping (likelyWnt5a and/or Wnt7a, given their ventricular epithelial localization similar to Wnt3) or tectal invasion (possibly Wnt4 as an attractive force, though Wnt5a, Wnt7a, and/or Wnt7b could also do so). Of the Wnts characterized, only Wnt4 showed expression in a retinorecipient lamina, SGFS-C. It is therefore possible that Wnt4 may serve as a guidance cue to target certain retinal axons to SGFS-C or as an attractive cue to direct axons into the general area of SGFS-C to respond to additional guidance cues. Wnt4 may also, however, serve a function necessary to specify or maintain the identity of SGFS-C, as Wnt4 expression appears around the time that SGFS-C tectal neurons have completely migrated to the approximate final location of SGFS-C and remains active through E16, when the tectal laminae are in the last stages of their stabilization. Ectopic expression studies using the *in ovo* electroporation or viral expression of Wnt4 in the shallow tectal laminae, combined with DiI labeling of RGC targeted to the overexpression region, could distinguish whether Wnt4 attracts retinal axons toward its lamina. Similarly, either ISH with Cad7 probes or IHC with Cad7 antibodies after Wnt4 overexpression could determine whether SGFS-C specification is affected, while DAPI staining would indicate whether the tectal architecture was affected. A final role for Wnts, particularly those in SGFS-G, may be either to repel axons, preventing them from passing into or through SGFS-G (Yamagata and Sanes, 1995b), or

they may serve to attract axons into the retinorecipient laminae, where they then encounter additional short-range cues to attract or repel them to specific laminae. Studying retinal axon response to the identified Wnts *in vitro* using Wnt-coated coverslips, Wnt-enriched media, or axon turning assays may assist in identifying whether these Wnts play attractive or repellant roles in the tectum.

Another possible consideration is that Wnts can serve as diffusible ligands. Thus, while Wnt mRNA for Wnt5a, Wnt7a, and Wnt7b may appear in SGFS-G and/or SGFS-I, their proteins may diffuse or be trafficked to the retinorecipient laminae. Immunostaining for specific Wnts would clarify this issue. Additionally, if possible, assays using the cysteine-rich Wnt-binding domains for the relevant Frizzleds may show where Frizzled binding occurs in the tectum, indicating the type of role that Wnt-Frizzled signaling plays in the tectum as well as which Wnts are likely to be involved in these activities.

One apparent anomaly in the Wnt *in situ* hybridization results involves the expression pattern of Wnt8b. While these studies indicate that Wnt8b is not expressed in the chick optic tectum between E10 and E16, a study by Medina lab using whole mount chick embryo ISH showed Wnt8b expression in the optic tectum at both E8 and E10 in one of the deeper tectal laminae (Garda et al., 2002). This study also indicated that Wnt7b showed ventricular epithelial gradient expression at E10 in addition to its SGFS laminar expression (Garda et al., 2002). This suggests that the mRNA epitope for the Wnt8b probe should be checked; if the Zou lab probe and the Medina lab probe are targeted to different regions of the Wnt8b mRNA, it is possible that there is some type of Wnt8b variant in chick. The Wnt7b labeling, on the other hand, may be more visible

using thicker tectal sections or by repeating the Medina lab's whole mount ISH studies; these may enhance weaker ventricular epithelial labeling.

Six Frizzleds were expressed in most or all RGCs in the retina during the period studied. Because several of these Frizzleds are ubiquitously expressed, it is unclear how these Frizzleds might act in retinal axon targeting activities. Looking solely at their wide and frequently ubiquitous expression, these Frizzleds may be involved in an activity performed by all retinal ganglion cells, such as the decision to invade the tectal laminae in order to locate appropriate laminar targets or repulsion from SGFS-G to remain within the retinorecipient laminae. On the other hand, because some Frizzled are expressed in large subsets, it is possible that combinations of Frizzleds may perform different functions in laminar targeting, including targeting retinal axons to the Wnt4-positive cell bodies in SGFS-F. Additionally, it is known that FrzB, SFRP1, and SFRP2 are expressed in RGCs, and SFRP1 affect aspects of retinal axon guidance and outgrowth *in vitro* (Ladher et al., 2000; Rodriguez et al., 2005). Thus, ubiquitous Frizzled expression may be modified by the presence of SFRPs to determine guidance activities for retinal axons.

In ovo retinal electroporation as a method to study laminar targeting of RGCs

Using *in ovo* retinal electroporation of EGFP to label spatially limited populations of RGCs, it was possible to observe laminar targeting of retinal axons, differing thickness of retinal fibers, the full extent and detail of retinal dendritic arbors, and the spatial morphology and overlay of axonal arbors. While previous studies focused on dendritic or axonal characteristics or on the characteristics of neurons labeled with specific molecular markers, this method, much like the single neuron labeling method employed by the Crair

lab in mice (Dhande et al., 2011), could be used to bring further clarity to the characteristics of individual chick RGCs during development.

As a method for labeling RGCs, *in ovo* retinal electroporation has its benefits, drawbacks, and limits. It is effective for labeling cells in a limited spatial region and cannot purposely or accidentally spread beyond the electroporated region, so it is generally more specific than DiI; similarly it does not tend to label all cells within a region, only a portion of those cells, making it easier to identify the morphology and activities of individual axons. Furthermore, the cells it labels are apparently random within the electroporated region; when one seeks to label RGCs, this is sufficient, but when one wishes to label neurons from a specific subpopulation, such as AChRβ2-positive RGCs, it may be less efficient than other methods. Despite the random quality of the label, it can still be combined with other methods, such as IHC or tagging for electron microscopy (Sebestény et al., 2002), providing it with flexibility given sufficient concentration of the electroporation labeling solution.

Among the greatest drawbacks is that electroporation decreases chick embryo survival at higher stages, making it difficult to study later developmental events while using this method, and it may have minor effects on developmental timing. Furthermore, when using expression constructs containing effector genes, the cell is affected starting 12-24 hours after the time of electroporation. To observe specific effects of changes in gene expression on later developmental events without affecting earlier events, it would be best to electroporate perhaps two days before those events. However, because chick survival tends to show a significant decrease if retinal electroporation is performed after E8, electroporation generally must occur by E7 in order to retain enough post-

electroporation survivors for further study. Thus, in gene expression studies using *in ovo* electroporation, if, for example, overexpression of Frizzled shifts topographic map targets, it would be more difficult to discern whether Frizzled expression levels affect tectal laminar targeting or other post-mapping events.

Combining *in ovo* retinal electroporation with tectal sectioning and immunohistochemistry provides several additional advantages within the system. It allows for the identification of laminar targets as well as for the visualization of effects on tectal cytoarchitecture, neither of which can be clearly ascertained from confocal images alone. It also allows for the sharp visualization of the deepest portions of the retinal arbors as well as capturing finer details of arbor morphology which may be minimized by reflected light within the whole tectum during confocal imaging. It can also be used with molecular markers, in conjunction with immunohistochemistry on retinal sections or whole mount retina, to pair a retinal soma with its axonal arbor in the tectum. These additional steps can thus improve the understanding of the morphology of individual arbors as well as visualize effects on laminar targeting and characterization of retinal subsets.

With regard to using *in ovo* electroporation to study the effects of Frizzled on tectal laminar targeting of retinal axons, there are several concerns and possibilities. First, the extremely low survival of chicks electroporated with a Frizzled1 overexpression construct is unusual and would normally suggest contamination of either the incubator (in which case survival across the board would be much lower) or of the electroporation DNA mix (which would cause survival issues in most or all chicks electroporated with the contaminated mix). However, because the purification of new DNA did not improve

survival, it may be necessary to look in more detail into how this construct is affecting the chick. Another concern, similar to that regarding EphBs in this system, is that RNAi is unlikely to be effective due to the redundancy of Frizzleds in RGCs. While EphB2 has a dominant negative construct demonstrated to affect a large percentage of EphB activity despite redundant EphBs, it is unclear whether such a construct exists for and would be effective for Frizzleds. Still, despite these concerns, if Frizzled activity or the activity of certain Frizzleds is specifically limited to post-mapping events, then, assuming Frizzled overexpression does not bleed into mapping activity, it should still be possible to observe the effects on post-mapping events.

AChRβ2 as a marker for RGCs involved in laminar targeting

While AChRβ2 proved effective at labeling RGC cell bodies in the retina, it may not be the most effective marker for the current laminar termination studies. Because mAb270 labels axons diffusely, these axons appear as a vague expression pool in the tectum until E16, when the axons finally target SGFS-F. Because the labeling is vaguely spread throughout the retinorecipient region, it would not be possible to discern early errors in laminar invasion or arbor forming behavior prior to SGFS-F targeting. Additionally, because this targeting cannot occur until late E15 at the earliest, to study this RGC subset requires the survival of a significant number of E16 electroporated chicks; given that some Frizzled constructs appear to affect survival and E16 post-electroporation survival is not inherently high, AChRβ2-positive RGCs may be counteradvised in this study.

On the other hand, if substance P antibodies improved sufficiently to label the appropriate subset, these concerns would be almost entirely mitigated; substance P labeling appears punctately along axon fibers, allowing them to be distinguished from each other, and these fibers target SGFS-B, which is close to the tectal surface and thus available for access from as early as E12 (although the layer does not fully separate from SGFS-A until E16) (Yamagata and Sanes, 1995a; Yamagata and Sanes, 1995b). A similar option would be to use somatostatin I antibodies, as somatostatin I-positive RGCs also target SGFS-B; however, as the appearance of the retinal axons in the tectum is not noted, it may still show some of the difficulties associated with AChRβ2-positive RGCs (Yamagata et al., 2006).

Still, labeling AChRβ2-positive RGCs may provide additional information about the targeting behaviors of these neurons. The dendritic morphology of these neurons in chick has not been described in detail, nor have the retinal laminar targets been confirmed, although somatostatin II-positive cells, which show over 90% overlap with AChRβ2-positive RGCs, target to IPL sublayers 3-5 (Yamagata et al., 2006). It is possible that further studies might indicate that AChRβ2-positive RGCs targeting different IPL sublayers have distinct differences in morphology, such that this RGC subset shares a molecular marker but covers several different types of dendritic morphology.

CONCLUSIONS

In this section of the dissertation, I showed that multiple Wnts and Frizzleds are expressed in the retinotectal system during topographic mapping and laminar targeting,

and that the effects of Frizzled overexpression on laminar targeting could theoretically be observed in great detail using a combination of confocal imaging of whole tecta, sectioning and immunohistochemistry of retinal and tectal sections, and RGC subset marker labeling of whole mount retinas and tectal sections. In future studies, the effects of Frizzled expression on retinal axon development will be observed in chick as well as in mouse, using a combination of GFP subset-labeling mouse lines crossed to Frizzled knockout mouse lines. These studies may indicate whether Wnt-Frizzled signaling plays a role in topographic mapping, invasion, laminar attracting, laminar targeting, SGFS-G repulsion, arbor stabilization, or other aspects of retinal axon development, as well as whether and which Frizzleds respond to which Wnts to affect these activities.

REFERENCES

Acheson DW, Kemplay SK, Webster KE. Quantitative analysis of optic terminal profile distribution within the pigeon optic tectum. Neuroscience 5, 1067-84 (1980).

Alfano G, Conte I, Caramico T, Avellino R, Arnò B, Pizzo MT, Tanimoto N, Beck SC, Huber G, Dollé P, Seeliger MW, Banfi S. Vax2 regulates retinoic acid distribution and cone opsin expression in the vertebrate eye. Development 138, 261-71 (2011).

Arora HL, Sperry RW. Optic nerve regeneration after surgical cross-union of medial and lateral optic tracts. Am Zool 2, 389 (1962).

Arora HL. Effect of forcing a regenerative optic nerve bundle toward a foreign region of the optic tectum in fishes. Anat Rec 145, 202 (1963).

Attardi D, Sperry RW. Preferential selection of central pathways by regenerating optic fibres. Exptl. Neurol 7, 46-64 (1963).

Badea TC, Nathans J. Quantitative analysis of neuronal morphologies in the mouse retina visualized by using a genetically directed reporter. J Comp Neurol 480, 331-351 (2004).

Barbera AJ, Marchase RB, Roth S. Adhesive recognition and retinotectal specificity. PNAS 70, 2482-6 (1973).

Bellonci. Ueber die centrale Endigung des Opticus bei Vertebraten. Zeitschrift für wissenschaftliche Zoologie 47 (1888).

Binggeli RL, Paule WJ. The pigeon retina: Quantitative aspects of the optic nerve and ganglion cell layer. J Comp Neurol 137, 1-18 (1969).

Birgbauer E, Cowan CA, Sretavan DW, Henkemeyer M. Kinase independent function of EphB receptors in retinal axon pathfinding to the optic disc from dorsal but not ventral retina. Development 127, 1231-41 (2000).

Blakely BD, Bye CR, Fernando CV, Horne MK, Macheda ML, Stacker SA, Arenas E, Parish CL. Wnt5a regulates midbrain dopaminergic axon growth and guidance. PLoS One 6, e18373 (2011).

Bonhoeffer F, Huf J. Recognition of cell types by axonal growth cones *in vitro*. Nature, 288, 162-4 (1980).

Bonhoeffer F, Huf J. *In vitro* experiments on axon guidance demonstrating an anterior-posterior gradient on the tectum. EMBO 1, 427-31 (1982).

Braisted JE, McLaughlin T, Wang HU, Friedman GC, Anderson DJ, O'Leary DD. Graded and lamina-specific distributions of ligands of EphB receptor tyrosine kinases in the developing retinotectal system. Dev Biol 191, 14-28 (1997).

Britto LRG, Keyser KT, Lindstrom JM, Karten HJ. Immunohistochemical localization of nicotinic acetylcholine receptor subunits in the mesencephalon and diencephalon of the chick (*Gallus gallus*). J Comp Neurol 317, 325-40 (1992a).

Britto LRG, Hamassaki-Britto DE, Ferro ES, Keyser KT, Karten HJ, Lindstrom JM. Neurons of the chick brain and retina expressing both a-bungarotoxin-sensitive and a-bungarotoxin-insensitive nicotinic acetylcholine receptors: an immunohistochemical analysis. Brain Res 590, 193-200 (1992b).

Brown A, Yates PA, Burrola P, Ortuño D, Vaidya A, Jessell TM, Pfaff SL, O'Leary DD, Lemke G. Topographic mapping from the retina to the midbrain is controlled by relative but not absolute levels of EphA receptor signaling. Cell 102, 77-88 (2000).

Brunet I, Weinl C, Piper M, Trembleau A, Volovitch M, Harris W, Prochiantz A, Holt C. The transcription factor Engrailed-2 guides retinal axons. Nature 438, 94-8 (2005).

Bunt SM, Horder TJ, Martin KAC. Evidence that optic fibers regenerating across the goldfish tectum may be assigned termination sites on a "first come, first served" basis. J Physiol (Lond) 276, 45-6 (1978).

Bunt SM. Retinotopic and temporal organization of the optic nerve and tracts in the adult goldfish. J Comp Neurol 206, 209-26 (1982).

Bunt SM, Lund, RD. Optic fiber arrangements in the visual pathways of Long-Evans hooded rats. Soc Neurosci Abstr 8, 451 (1982).

Bunt SM, Lund RD, Land PW. Prenatal development of the optic projection in albino and hooded rats. Dev Brain Research 6, 149-68 (1983).

Bunt SM, Horder TJ. Evidence for an orderly arrangement of optic axons within the optic nerves of the major non-mammalian vertebrate classes. J Comp Neurol 213, 94-114 (1983).

Campbell DS, Regan AG, Lopez JS, Tannahill D, Harris WA, Holt CE. Semaphorin 3A elicits stage-dependent collapse, turning, and branching in Xenopus retinal growth cones. J Neurosci 21, 8538-47 (2001).

Cang J, Wang L, Stryker MP, Feldheim DA. Roles of ephrin-As and structured activity in the development of functional maps in the superior colliculus. J Neurosci 28, 11015-23 (2008).

Chandrasekaran AR, Plas DT, Gonzalez E, Crair MC. Evidence for an instructive role of retinal activity in retinotopic map refinement in the superior colliculus of the mouse. J Neurosci 25, 6929–38 (2005).

Cheng HJ, Flanagan JG. Identification and cloning of ELF-1, a developmentally expressed ligand for the Mek4 and Sek receptor tyrosine kinases. Cell 79, 157-68 (1994).

Cheng HJ, Nakamoto M, Bergemann AD, Flanagan JG. Complementary gradients in expression and binding of ELF-1 and Mek4 in development of the topographic retinotectal projection map. Cell 82, 371-81 (1995).

Cohen-Cory S, Fraser SE. Effects of brain-derived neurotrophic factor on optic axon branching and remodelling in vivo. Nature 378, 192-6 (1995).

Connor RJ, Menzel P, Pasquale EB. Expression and tyrosine phosphorylation of Eph receptors suggest multiple mechanisms in patterning of the visual system. Dev Biol 193, 21-35 (1998).

Coombs J, Van Der List D, Wang G-Y, Chalupa LM. Morphological properties of mouse retinal ganglion cells. Neuroscience 140, 123-36 (2006).

Cowan WM, Martin AH, Wenger E. Mitotic patterns in the optic tectum of the chick during normal development and after early removal of the optic vesicle. J Exp Zool 169, 71-92 (1968).

Cox EC, Miller B, Bonhoeffer F. Axonal guidance in the chick visual system: posterior tectal membranes induce collapse of growth cones from the temporal retina. Neuron 4, 31-7 (1990).

Crossland WJ, Cowan WM, Rogers LA, Kelly JP. The specification of the retinotectal projection in the chick. J Comp Neurol 155, 127-64 (1974).

Crossland WJ, Cowan WM, Rogers LA. Studies on the development of the chick optic tectum. IV. An autoradiographic study of the development of retino-tectal connections. Brain Res 91, 1-23 (1975).

DeLong GR, Coulombre AJ. Development of the retinotectal connections studied by retinal grafts onto the optic tectum in chick embryos. Devel Biol 13, 351-63 (1965).

DeLong GR, Coulombre AJ. The specificity of retinotectal connections studied by retinal grafts onto the optic tectum in chick embryos. Devel Biol 16, 513-31 (1967).

Demyanenko GP, Maness PF. The L1 cell adhesion molecule is essential for topographic mapping of retinal axons. J Neurosci 23, 530-8 (2003).

Detwiler SR. On the hyperplasia of nerve centers resulting from excessive peripheral loading. PNAS 6 (1920).

Dhande OS, Hua EW, Guh E, Yeh J, Bhatt S, Zhang Y, Ruthazer ES, Feller MB, Crair MC. Development of single retinofugal axon arbors in normal and β2 knock-out mice. J Neurosci 31, 3384-99 (2011).

Drescher U, Kremoser C, Handwerker C, Löschinger J, Noda M, Bonhoeffer F. *In vitro* guidance of retinal ganglion cell axons by RAGS, a 25 kDa tectal protein related to ligands for Eph receptor tyrosine kinases. Cell 82, 359-70 (1995).

Easter S, Rusoff A, Kirsh P. The growth and organization of the optic nerve and tract in juvenile and adult goldfish. J Neurosci 1, 793-811 (1981).

Ehrlich D. Regional specialization of the chick retina as revealed by the size and density of neurons in the ganglion cell layer. J Comp Neurol 195, 643-57 (1981).

Fawcett J. How axons grown down the Xenopus optic nerve. J Embryol Exp Morphol 65, 219-33 (1981).

Fedtsova N, Quina LA, Wang S, Turner EE. Regulation of the development of tectal neurons and their projections by transcription factors Brn3a and Pax7. Dev Biol 316, 6-20 (2008).

Feldheim DA, Vanderhaeghen P, Hansen MJ, Frisén J, Lu Q, Barbacid M, Flanagan JG. Topographic guidance labels in a sensory projection to the forebrain. Neuron 21, 1303-13 (1998).

Feldheim DA, Kim YI, Bergemann AD, Frisen J, Barbacid M, Flanagan JG. Genetic analysis of ephrin-A2 and ephrin-A5 shows their requirement in multiple aspects of retinocollicular mapping. Neuron 25, 563-74 (2000).

Feldheim DA, Nakamoto M, Osterfield M, Gale NW, DeChiara TM, Rohatgi R, Yancopoulos GD, Flanagan JG. Loss-of-function analysis of EphA receptors in retinotectal mapping. J Neurosci 24, 2542-50 (2004).

Feldheim DA, O'Leary DDM. Visual map development: Bidirectional signaling, bifunctional guidance molecules, and competition. CSH Perspect Biol 2, 1-20 (2011).

Fenstermaker AG, Prasad AA, Bechara A, Adolfs Y, Tissir F, Goffinet A, Zou Y, Pasterkamp RJ. Wnt/planar cell polarity signaling controls the anterior-posterior organization of monoaminergic axons in the brainstem. J Neurosci 30, 16053-64 (2010).

Fokina VM, Frolina EI. Expression patterns of Wnt genes during development of an anterior part of the chicken eye. Devel Dyn 235, 496-505 (2006).

Friedman GC, O'Leary DDM. Retroviral misexpression of engrailed genes in the chick optic tectum perturbs the topographic targeting of retinal axons. J Neurosci 16, 5498–509 (1996).

Frisén J, Yates PA, McLaughlin T, Friedman GC, O'Leary DD, Barbacid M. Ephrin-A5 (AL-1/RAGS) is essential for proper retinal axon guidance and topographic mapping in the mammalian visual system. Neuron 20, 235-43 (1998).

Fuerst PG, Bruce F, Tian M, Wei W, Elstrott J, Feller MB, Erskine L, Singer JH, Burgess RW. DSCAM and DSCAML1 function in self-avoidance in multiple cell types in the developing mouse retina. Neuron 64, 484-97 (2009).

Fuhrmann S, Stark MR, Heller S. Expression of Frizzled genes in the developing chick eye. Gene Expr Patterns 3, 659-62 (2003).

Fujisawa H, Thanos S, Schwarz U. Mechanisms in the developmental of retinotectal projections in the chick embryo studied by surgical deflection of the retinal pathway. Devel Biol 102, 356-67 (1984).

Fujisawa H. Axonal growth in developing and regenerating amphibian retinotectal projection. Prog Brain Res 71, 75–88 (1987).

Fujiwara A, Ohozone Y, Naito J. The developmental study on lamination of the optic tectum in relation to the retinotectal projection in chicks and chick embryos. J Vet Med Sci 62, 511-6 (2000).

Gale NW, Holland SJ, Valenzuela DM, Flenniken A, Pan L, Ryan TE, Henkemeyer M, Strebhardt K, Hirai H, Wilkinson DG, Pawson T, Davis S, Yancopoulos GD. Eph receptors and ligands comprise two major specificity subclasses and are reciprocally compartmentalized during embryogenesis. Neuron 17, 9–19 (1996).

Gänzler-Odenthal SII, Redies C. Blocking N-cadherin function disrupts the epithelial structure of differentiating neural tissue in the embryonic chicken brain. J Neurosci 18, 5415-25 (1998).

Garda AL, Puelles L, Rubenstein JL, Medina L. Expression patterns of Wnt8b and Wnt7b in the chicken embryonic brain suggest a correlation with forebrain patterning centers and morphogenesis. Neuroscience 113, 698-98 (2002).

Gardner CA, Darnell DK, Poole SJ, Ordahl CP, Barald KF. Expression of an engrailed-like gene during development of the early embryonic chick nervous system. J Neurosci Res 27, 426-37 (1988).

Gaze, RM. Regeneration of the optic nerve in *Xenopus laevis*. Quart J Exp Physiol 44, 290-308 (1959).

Gaze RM, Jacobson M, Székely G. The retino-tectal projection in Xenopus with compound eyes. J Physiol 165, 484-499 (1963).

Gaze RM, Jacobson M, Székely G. On the formation of connexions by compound eyes in Xenopus. J Physiol 176, 409-17 (1965).

Gaze RM, Sharma SC. Axial differences in the reinnervation of the goldfish optic tectum by regenerating optic nerve fibers. Exp Brain Res 10, 171-81 (1970).

Gaze RM, Keating MJ, Chung S-H. The evolution of the retinotectal map during development in Xenopus. Proc. R. Soc B 185, 301-30 (1974).

Gaze RM, Straznicky K. Regeneration of optic nerve fibres from a compound eye to both tecta in Xenopus: Evidence relating to the state of specification of the eye and tectum. J Embryol Exp Morphol 60, 125-40 (1980).

Gierer A. Development of projections between areas of the nervous system. Biol Cybern 42, 69-78 (1981).

Gierer A. Model for the retino-tectal projection. Proc R Soc Lond B Biol Sci 218, 77-93 (1983).

Gierer A. Directional cues for growing axons forming the retinotectal projection. Development 101, 479-89 (1987).

Goldberg S. Studies on the mechanics of development of the visual pathways in the chick embryo. Devel Biol 36, 24-42 (1974).

Golz S, Mühleisen T, Schulte D, Mey J. Regulation of RALDH-1, RALDH-3 and CYP26A1 by transcription factors cVax/Vax2 and Tbx5 in the embryonic chick retina. Int J Dev Neurosci 26, 435-35 (2008).

Gosse NJ, Nevin LM, Baier H. Retinotopic order in the absence of axon competition. Nature 452, 892-5 (2008).

Gottlieb DI, Arington C. Patterns of adhesive specificity in the developing central nervous system of chick. Dev Biol 71, 260-73 (1979).

Halfter W, Claviez M, Schwarz U. Preferential adhesion of tectal membranes to anterior embryonic chick retina neurites. Nature 292, 67-70 (1981).

Halford MM, Armes J, Buchert M, Meskenaite V, Grail D, Hibbs ML, Wilks AF, Farlie PG, Newgreen DF, Hovens CM, Stacker SA. Ryk-deficient mice exhibit craniofacial defects associated with perturbed EphB receptor crosstalk. Nat Genetics 25, 414-8 (2000).

Hamburger V, Hamilton HL. A series of normal stages in the development of the chick embryo. J Morph 88, 49-92 (1951). (Reprinted in: Dev Dyn 195, 231-72 (1992).)

Hansen MJ, Dallal GE, Flanagan JG. Retinal axon response to ephrin-as shows a graded, concentration dependent transition from growth promotion to inhibition. Neuron 42, 717–730 (2004).

Harris WA. The transplantation of eyes to genetically eyeless salamanders: Visual projections and somatosensory interactions. J Neurosci 2, 339-53 (1982).

Harris WA. Axonal pathfinding in the absence of normal pathways and impulse activity. J Neurosci 4, 1153-62 (1984).

Harris WA, Holt CE, Bonhoeffer F. Retinal axons with and without their somata, growing to and arborizing in the tectum of Xenopus embryos: a time-lapse video study of single fibres in vivo. Development 101, 123–133 (1987).

Harris WA, Holt CE. From tags to RAGS: Chemoaffinity finally has receptors and ligands. Neuron 15, 241-4 (1995).

Harrison RG. Some unexpected results of the heteroplastie transplantation of limbs. PNAS 10 (1924).

Harrison RG. Heteroplastic transplantations of the eye in *Amblystoma.* Proc. Amer. Soc. Zool., Anat. Ree. 31 (1925).

Harrison RG. Correlation in the development and growth of the eyestudied by means of heteroplastic transplantation. Arch. f. Entwinech., Bd. 120 (1929).

Henkemeyer M, Orioli D, Henderson JT, Saxton TM, Roder J, Pawson T, Klein R. Nuk controls pathfinding of commissural axons in the mammalian central nervous system. Cell 86, 35-46 (1996).

Herrick CJ. The amphibian forebrain. III. The optic tracts and centers of Amblystoma and the frog. J Comp Neurol 30 (1925).

Hindges R, McLaughlin T, Genoud N, Henkemeyer M, O'Leary DD. EphB forward signaling controls directional branch extension and arborization required for dorsal/ventral retinotopic mapping. Neuron 35, 475-87 (2002).

Hilbig H, Roth G, Brylla E, Robiné KP. Cytoarchitecture of the stratum opticum in Japanese quail. Neuroscience 86, 663-78 (1998).

Holash JA, Pasquale EB. Polarized expression of the receptor-protein tyrosine kinase Cek5 in the developing avian visual system. Dev Biol 172, 683-93 (1995).

Holash JA, Soans C, Chong L, Shao H, Dixit VM, Pasquale EB. Reciprocal expression of the Eph receptor Cek5 and its ligand(s) in the early retina. Dev Biol 182, 256-69 (1997).

Holt CE, Harris WA. Order in the initial retinotectal map in Xenopus: a new technique for labelling growing nerve fibers. Nature 301, 150-2 (1983).

Holt CE. Does timing of axon outgrowth influence initial retinotectal topography in *Xenopus*? J Neurosci 4, 1130-52 (1984).

Hong YK, Kim IJ, Sanes JR. Stereotyped axonal arbors of retinal ganglion cell subsets in the mouse superior colliculus. J Comp Neurol 519, 1691-711 (2011).

Hoopfer ED, McLaughlin T, Watts RJ, Schuldiner O, O'Leary DD, Luo L. Wlds protection distinguishes axon degeneration following injury from naturally occurring developmental pruning. Neuron 50, 819-21 (2006).

Horder TJ, Martin KAC. Morphogenetics as an alternative to chemospecificity in the formation of nerve connections. Cell-cell Recognition Soc for Exp Biol Symp 32, 275-358 (1978).

Huber GC, Crosby EC. A phylogenetic consideration of the optic tectum. PNAS 19, 15-22 (1933).

Huberman AD, Manu M, Koch SM, Susman MW, Lutz AB, Ullian EM, Baccus SA, Barres BA. Architecture and activity-mediated refinement of axonal projections from a mosaic of genetically identified retinal ganglion cells. Neuron 59, 425-38 (2008).

Huberman AD, Wei W, Elstrott J, Stafford BK, Feller MB, Barres BA. Genetic identification of an On-Off direction-selective retinal ganglion cell subtype reveals a layer-specific subcortical map of posterior motion. Neuron 62, 327-34 (2009).

Huberman AD. Mammalian DSCAMs: they won't help you find a partner, but they'll guarantee you some personal space. Neuron 64, 441-3 (2009).

Hunt SP, Brecha NC. The avian optic tectum: a synthesis of morphology and biochemistry. In: H Vanegas, Editor, Comparative Neurology of the Optic Tectum, Plenum Press, New York 619-48 (1984).

Hutchins BI, Li L, Kalil K. Wnt/calcium signaling mediates axon growth and guidance in the developing corpus callosum. Dev Neurobiol 71, 269-83 (2011).

Ichijo H, Fujita S, Matsuno T, Nakamura H. Rotation of the tectal primordium reveals plasticity of target recognition in retinotectal projection. Development 110, 331-42 (1990).

Inoue A, Sanes JR. Lamina-specific connectivity in the brain: regulation by N-cadherin, neurotrophins, and glycoconjugates. Science 276, 1428-31 (1997).

Itasaki N, Ichijo H, Hama C, Matsuno T, Nakamura H. Establishment of rostrocaudal polarity in tectal primordium: engrailed expression and subsequent tectal polarity. Development 773, 1133-44 (1991).

Itasaki N, Nakamura H. Rostrocaudal polarity in the tectum in birds: correlation of *en* gradient and topographic order in retinotectal projection. Neuron 8, 787-98 (1992).

Jacobson M, Gaze RM. Selection of appropriate tectal connections by regenerating optic nerve fibres in adult goldfish. Exp Neurol 13, 418-430 (1965).

Jiang Y, Obama H, Kuan SL, Nakamura R, Nakamoto C, Ouyang Z, Nakamoto M. *In vitro* guidance of retinal axons by a tectal lamina-specific glycoprotein Nel. Mol Cell Neurosci 41, 113-9 (2009).

Johns P. Growth of the adult goldfish eye III: Source of new retinal cells. J Comp Neurol 176, 343-58 (1977).

Kaprielian Z, Patterson PH. The molecular basis of retinotectal topography. BioEssays 16, 1-11(1994).

Karten HJ, Cox K, Mpodozis J. Two distinct populations of tectal neurons have unique connections within the retinotectorotundal pathway of the pigeon (*Columba livia*), J Comp Neurol 387, 449-65 (1997).

Keeble TR, Halford MM, Seaman C, Kee N, Macheda M, Anderson RB, Stacker SA, Cooper HM. The Wnt receptor Ryk is required for Wnt5a-mediated axon guidance on the contralateral side of the corpus callosum. J Neurosci 26, 5840-8 (2006).

Kelly JP, Cowan WM. Studies on the development of the chick optic tectum. III. Effects of early eye removal. Brain Res 42, 263-88 (1972).

Kenny D, Bronner-Fraser M, Marcelle C. The receptor tyrosine kinase QEK5 mRNA is expressed in a gradient within the neural retina and the tectum. Dev Biol 172, 708-16 (1995).

Kida YS, Sato T, Miyasaka KY, Suto A, Ogura T. Daam1 regulates the endocytosis of EphB during the convergent extension of the zebrafish notochord. PNAS 104, 6708-13 (2007).

Kim IJ, Zhang Y, Yamagata M, Meister M, Sanes JR. Molecular identification of a retinal cell type that responds to upward motion. Nature 452, 478-82 (2008).

Kim IJ, Zhang Y, Meister M, Sanes JR. Laminar restriction of retinal ganglion cell dendrites and axons: subtype-specific developmental patterns revealed with transgenic markers. J Neurosci 30, 1452-62 (2010).

King, H. D. Experimental studies on the eye of the frog embryo. Arch. Ent. Mech. 19: 85-107 (1905).

Kong J-H, Fish DR, Rockhill RL, Masland RH. Diversity of ganglion cells in the mouse retina: unsupervised morphological classification and its limits. J Comp Neurol 489, 293-310 (2005).

Ladher RK, Church VL, Allen S, Robson L, Abdelfattah A, Brown NA, Hattersley G, Rosen V, Luyten FP, Dale L, Francis-West PH. Cloning and expression of the Wnt antagonists Sfrp-2 and Frzb during chick development. Dev Biol 218, 183-98 (2000).

LaVail JH, Cowan WM. The development of the chick optic tectum. I. Normal morphology and cytoarchitectonic development. Brain Res 28, 391-419 (1971a).

LaVail JH, Cowan WM. The development of the chick optic tectum. II. Autoradiographic studies. Brain Res 28, 421-441 (1971b).

Lee SM, Danielian PS, Fritzsch B, McMahon AP. Evidence that FGF8 signaling from the midbrain-hindbrain junction regulates growth and polarity in the developing midbrain. Development 124, 959-69 (1997).

Levine RL, Jacobson M. Deployment of optic nerve fibers is determined by positional markers in the frog's tectum. Exp Neurol, 527-38 (1974).

Lewis, WI. Experimental Studies on the development of the eye in Amphibia. I. On the origin of the lens, *Rana palustris.* Amer. J. Anat. 8 (1904).

Li L, Hutchins BI, Kalil K. Wnt5a induces simultaneous cortical axon outgrowth and repulsive axon guidance through distinct signaling mechanisms. J Neurosci 29, 5873-83 (2009).

Li L, Hutchins BI, Kalil K. Wnt5a induces simultaneous cortical axon outgrowth and repulsive turning through distinct signaling mechanisms. Sci Signal 3, pt2 (2010).

Lim BK, Cho SJ, Sumbre G, Poo MM. Region-specific contribution of ephrin-B and Wnt signaling to receptive field plasticity in developing optic tectum. Neuron 65, 899-911 (2008).

Liu Y, Berndt J, Su F, Tawarayama H, Shoji W, Kuwada JY, Halloran MC. Semaphorin3D guides retinal axons along the dorsoventral axis of the tectum. J Neurosci 24, 310-8 (2004).

Logan C, Wizenmann A, Drescher U, Monschau B, Bonhoeffer F, Lumsden A. Rostral tectum acquires caudal characteristics following ectopic engrailed expression. Curr Biol 6, 1006-14 (1996).

Lom B, Cogen J, Sanchez AL, Vu T, Cohen-Cory S. Local and target-derived Brain-Derived Neurotrophic Factor exert opposing effects on the dendritic arborization of retinal ganglion cells in vivo. J Neurosci 22 7639-49 (2002).

Luo L, Flanagan JG. Development of continuous and discrete neural maps. Neuron 56, 284-300 (2007).

Lyuksyutova AI, Lu CC, Milanesio N, King LA, Guo N, Wang Y, Nathans J, Tessier-Lavigne M, Zou Y. Anterior-posterior guidance of commissural axons by Wnt-frizzled signaling. Science 302, 1984-1988 (2003).

Mann F, Ray S, Harris WA, Holt CE. Topographic mapping in dorsoventral axis of *Xenopus* retinotectal system depends on signaling through Ephrin-B ligands. Neuron 35, 461-73 (2002).

Marchase RB, Meunier JC, Pierce M, Roth S. Biochemical investigations of retinotectal specificity. Prog Clin Biol Res 15, 73-9 (1977).

Marcus RC, Gale NW, Morrison ME, Mason CA, Yancopoulos GD. Eph family receptors and their ligands distribute in opposing gradients in the developing mouse retina. Dev Biol 180, 786-9 (1996).

Marler KJM, Becker-Barroso E, Martinez A, Llovera M, Wentzel C, Poopalasundaram S, Hindges R, Soriano E, Comella J, Drescher U. A TrkA/ephrinA interaction controls retinal axon branching and Synaptogenesis. J Neurosci 28 12700-12 (2008).

Marotte LR, Vidovic M, Wheeler E, Jhaven S. Brain-derived neurotrophic factor is expressed in a gradient in the superior colliculus during development of the retinocollicular projection. Eur J Neurosci 20 843-7 (2004).

Matsunaga E, Chedotal A. Repulsive guidance molecule/neogenin: A novel ligand-receptor system playing multiple roles in neural development. Dev Growth Differ 46, 481-6 (2004).

Matsunaga E, Nakamura H, Chedotal A. Repulsive guidance molecule plays multiple roles in neuronal differentiation and axon guidance. J Neurosci 26, 6082-8 (2006).

Matsuno T, Ichijo H, Nakamura H. Regulation of the rostrocaudal axis of the optic tectum: histological study after rostrocaudal rotation in quail-chick chimeras. Dev Brain Res 58, 265-70 (1991).

Matsuoka RL, Nguyen-Ba-Charvet KT, Parray A, Badea TC, Chédotal A, Kolodkin AL. Transmembrane semaphorin signaling controls laminar stratification in the mammalian retina. Nature 470, 259-63 (2011).

Maturana HR, Lettvin JY, McCulloch WS, Pitts WH. Physiological evidence the cut optic nerve fibers in a frog regenerate to their proper places in the tectum. Science 130, 1709-10 (1959).

McLaughlin T, Torborg CL, Feller MB, O'Leary DDM. Retinotopic map refinement requires spontaneous retinal waves during a brief critical period of development. Neuron 40, 1147–1160 (2003a).

McLaughlin T, Hindges R, Yates PA, O'Leary DD. Bifunctional action of ephrin-B1 as a repellant and attractant to control bidirectional branch extension in dorsal-ventral retinotopic mapping. Development 130, 2407-18 (2003b).

McLaughlin T, Lim Y-S, Santiago A, O'Leary DDM. EphB receptors in retinal ganglion cells direct dorsal-ventral retinotopic mapping by specific guidance of branches. Soc Neurosci Abstr 35 (2009).

Meyer, RL. Roger Sperry and his chemoaffinity hypothesis. Neuropsychologia 36, 957-80 (1998).

Miskevich F, Zhu Y, Ranscht B, Sanes JR. Expression of multiple cadherins and catenins in the chick optic tectum. Mol Cell Neurosci 12, 240-55 (1998).

Monnier PP, Sierra A, Macchi P, Deitinghoff L, Andersen JS, Mann M, Flad M, Hornberger MR, Stahl B, Bonhoeffer F, Mueller BK. RGM is a repulsive guidance molecule for retinal axons. Nature 41, 392-5 (2002).

Monschau B, Kremoser C, Ohta K, Tanaka H, Kaneko T, Yamada T, Handwerker C, Hornberger MR, Löschinger J, Pasquale EB. Shared and distinct functions of RAGS and ELF-1 in guiding retinal axons. EMBO 16, 1258-67 (1997).

Mui SH, Kim JW, Lemke G, Bertuzzi S. Vax genes ventralize the embryonic eye. Genes Dev 19, 1259-59 (2005).

Mühleisen TW, Agoston Z, Schulte D. Retroviral misexpression of cVax disturbs retinal ganglion cell axon fasciculation and intraretinal pathfinding in vivo and guidance of nasal ganglion cell axons in vivo. Dev Biol 297, 59-73 (2006).

Müller BK, Jay DG, Bonhoeffer F. Chromophore-assisted laser inactivation of a repulsive axonal guidance molecule. Curr Biol 6, 1497–1502 (1996).

Naito J, Chen Y. Morphological features of chick retinal ganglion cells. Anat Sci Int 79, 213-25 (2004).

Nakagawa S, Brennan C, Johnson KG, Shewan D, Harris WA, Holt CE. Ephrin-B regulates the ipsilateral routing of retinal axons at the optic chiasm. Neuron 25, 599–610 (2000).

Nakamoto M, Cheng HJ, Friedman GC, McLaughlin T, Hansen MJ, Yoon CH, O'Leary DD, Flanagan JG. Topographically specific effects of ELF-1 on retinal axon guidance in vitro and retinal axon mapping in vivo. Cell 86, 755-66 (1996).

Nakamura H, O'Leary DDM. Inaccuracies in initial growth and arborization of chick retinotectal axons followed by course corrections and axon remodeling to develop topographic order. J Neurosci 9, 3776-95 (1989).

Nevin LM, Taylor MR, Baier H. Hardwiring of fine synaptic layers in the zebrafish visual pathway. Neural Dev 3, 36 (2008).

Niederkofler V, Salie R, Sigrist M, Arber S. Repulsive guidance molecule (RGM) gene function is required for neural tube closure but not retinal topography in the mouse visual system. J Neurosci 24, 808-8 (2004).

O'Donnell AM, Puri P. The development of excitatory neurons in the chick cloaca. Pediatr Surg Int 26, 111-4 (2010).

O'Leary DDM, Yates P, McLaughlin T. Mapping sights and smells in the brain: Distinct mechanisms to achieve a common goal. Cell 96, 255-69 (1999).

O'Rourke NA, Fraser SE. Dynamic aspects of retinotectal map formation revealed by a vital-dye fiber-tracing technique. Devel Biol 114, 265-276 (1986).

Oohashi T, Zhou XH, Feng K, Richter B, Morgelin M, Perez MT, SU WD, Chiquet-Ehrismann R, Rauch U, Fassler R. Mouse ten-m/Odz is a new family of dimeric type II transmembrane proteins expressed in many tissues. J Cell Biol 145, 563-77 (1999).

Patel NH, Martin-Blanco E, Coleman KG, Poole SJ, Ellis MC, Kornberg TB, Goodman CS. Expression of engrailed proteins in arthropods, annelids, and chordates. Cell 58, 955-68 (1989).

Pfeiffenberger C, Yamada J, Feldheim DA. Ephrin-As and patterned retinal activity act together in the development of topographic maps in the primary visual system. J Neurosci 26, 12873-84 (2006).

Piccolino M, Strettoi E, Laurenzi E. Santiago Ramón y Cajal, the retina and the neuron theory. Doc Ophthalmol 71, 123-141 (1989).

Plas DT, Lopez JE, Crair MC. Pretarget sorting of the retinocollicular axons in the mouse. J Comp Neurol 491, 305-19 (2005).

Poopalasundaram S, Marler KJ, Drescher U. EphrinA6 on chick retinal axons is a key component for p75(NTR)-dependent axon repulsion and TrkB-dependent axon branching. Mol Cell Neurosci 47, 131-6 (2011).

Puelles L. Contributions to neuroembryology of Santiago Ramon y Cajal (1852-1934) and Jorge F. Tello (1880 – 1958). Int J Dev Biol 53 (2009).

Rager G, Rager U. 1 978. Systems matching by degeneration. 1. A quantitative electron microscopic study of the generation and degeneration of ganglion cells in the chicken. Exp Brain Res 33, 65-78 (1978).

Rager G, von Oeynhausen B. Ingrowth and ramification of retinal fibers in the developing optic tectum of the chick embryo. Exp Brain Res 25, 213-27 (1979).

Rager G. Development of the retinotectal projection in the chicken. Adv Anat Embryol Cell Biol 63, 1-90 (1980).

Ramón y Cajal S. Estructura del lóbule óptico de las aves y origen de los nervios ópticos. Rev. Trim. Histol. Norm. Pathol 3-4 (1889).

Ramón y Cajal S. Sur la fine structure du lobe optique des oiseaux et sur I'origine reelle des nerfs optiques. Int. Mschr. Anat. Physiol. 8, 337-366 (1891).

Ramón y Cajal S. Histologie du systeme nerveux de I'homme et des vertebres, Vol 2. Maloine, Paris (1911).

Ramón y Cajal S. *The Structure of the Retina* (compiled and translated by Thorp SA and Glickstein M) pages 149-150, Thomas, Springfield (1972, original 1892).

Rashid T, Upton AL, Blentic A, Ciossek T, Knoll B, Thompson ID, Drescher U. Opposing gradients of ephrin-As and EphA7 in the superior colliculus are essential for topographic mapping in the mammalian visual system. Neuron 47, 57-69 (2005).

Reh TA, Pitts EC, Constantine-Paton M. The organization of the fibers in the optic nerve of normal and tectum-less Rana pipiens. J Comp Neurol 218, 282-96 (1983).

Rétaux S, Harris WA. Engrailed and retinotectal topography. Trends Neurosci 19, 542-6 (1996).

Rockhill RL, Daly FJ, MacNeil MA, Brown SP, Masland RH. The diversity of ganglion cells in a mammalian retina. J Neurosci 22, 3831-43 (2002).

Rodriguez J, Esteve P, Weinl C, Ruiz JM, Fermin Y, Trousse F, Dwivedy A, Holt C, Bovolenta P. SFRP1 regulates the growth of retinal ganglion cell axons through the Frizzled 2 receptor. Nat Neurosci 8, 1301-9 (2005).

Roskies AL, O'Leary DDM. Control of topographic retinal axon branching by inhibitory membrane-bound molecules. Science 265, 799-803 (1994).

Rusoff AC, Easter S. Order in the optic nerve of goldfish. Science 208, 311-2 (1983).

Rusoff AC. Paths of axons in the visual system of perciform fish and implications of these paths for rules governing axonal growth. J Neurosci 4, 1414-28 (1984).

Sajjadi FG, Pasquale EB, Subramani S. Identification of a new eph-related receptor tyrosine kinase gene from mouse and chicken that is developmentally regulated and encodes at least two forms of the receptor. New Biol 3, 769-78 (1991).

Sajjadi FG, Pasquale EB. Five novel avian Eph-related tyrosine kinases are differentially expressed. Oncogene 8, 1807-13 (1993).

Sakaguchi DS, Murphey RK. Map formation in the developing *Xenopus* retinotectal system: An examination of ganglion cell terminal arborizations. J. Neurosci. 5, 3228-3245 (1985).

Sakurai T, Wong E, Drescher U, Tanaka H, Jay DG. Ephrin-A5 restricts topographically specific arborization in the chick retinotectal projection in vivo. PNAS 99, 10795–800 (2002).

Sanchez-Camacho C, Rodriguez J, Ruiz J, Trousse F, Bovolenta P. Morphogens as growth cone signalling molecules. Brain Res Rev 49, 242-252 (2005).

Scalia F, Fite K. A retinotopic analysis of the central connections of the optic nerve in the frog. J Comp Neurol 158, 455-78 (1974).

Scalia F, Arango V. The anti-retinotopic organization of the frog's optic nerve. Brain Res 266, 121-26 (1983).

Schmidt JT, Cicerone CM, Easter SS. Expansion of the half retinal projection to the tectum in goldfish: an electrophysiological and anatomical study. J Comp Neurol 177, 257-77 (1978).

Schmitt AM, Shi J, Wolf AM, Lu CC, King LA, Zou Y. Wnt-Ryk signaling mediates medial-lateral retinotectal topographic mapping. Nature 439, 31-7 (2006).

Scholes J. Nerve fiber topography in the retinal projection to the tectum. Nature 278, 620-4 (1979).

Schulgin. Lobi optici der Vögel. Zoologischer Anzeiger (1881).

Scicolone G, Pereyra-Alfonso S, Brusco A, Pecci Saavedra J, Flores V. Development of the laminated pattern of the chick optic tectum. Int J Dev Neurosci 13, 845-58 (1995).

Sebestény T, Davies DC, Zayats N, Németh A, Tömböl T. The ramification and connections of retinal fibres in layer 7 of the domestic chick optic tectum: a golgi impregnation, anterograde tracer and GABA-immunogold study. J Anat 200, 169-83 (2002).

Shao H, Lou L, Pandey A, Verderame MF, Siever DA, Dixit VM. cDNA cloning and characterization of a Cek7 receptor protein-tyrosine kinase ligand that is identical to the ligand (ELF-1) for the Mek-4 and Sek receptor protein-tyrosine kinases. J Biol Chem 270, 3467-70 (1995).

Shigetani Y, Funahashi JI, Nakamura H. En-2 regulates the expression of the ligands for Eph type tyrosine kinases in chick embryonic tectum. Neurosci Res 27, 211-7 (1997).

Simon DK, O'Leary DDM. Limited topographic specificity in the targeting and branching of mammalian retinal axons. Develop Biol 137, 125–134 (1990).

Simon DK, O'Leary DDM. Responses of retinal axons in vivo and in vitro to position-encoding molecules in the embryonic superior colliculus. Neuron 9, 977–989 (1992a)

Simon DK, O'Leary DDM. Development of topographic order in the mammalian retinocollicular projection. J Neurosci 12: 1212–1232 (1992b).

Simon DK, O'Leary DDM. Influence of position along the medial-lateral axis of the superior colliculus on the topographic targeting and survival of retinal axons. Dev Brain Res 69: 167–172 (1992c).

Simon DK, Roskies AL, O'Leary DDM. Plasticity in the development of topographic order in the mammalian retinocollicular projection. Devel Biol 162, 384-93 (1994).

Spemann, H. Über Correlationen in der Entwicklung des Auges. Verhand. Anat. Ges. 15, 61-79 (1901).

Spemann, H. Neue Tatsachen zum Linsenproblemen. Zool. Anz. 31, 379-386 (1907).

Sperry, RW. The functional results of muscle transposition in the hind limb of the rat. J Comp Neurol 73, 379-404 (1940).

Sperry, RW. The effect of crossing nerves to antagonistic muscles in the hind limb of the rat. J Comp Neurol 75, 1-19 (1941).

Sperry, RW. Transplantation of motor nerve and muscles in the forelimb of the rat. J Comp Neurol 76, 283-321 (1942).

Sperry RW. Visuomotor coordination in the newt (*Triturus viridescens*) after regeneration of the optic nerve. J Comp Neurol 79, 33–55 (1943a).

Sperry RW. Effect of 180 degree rotation of the retinal field on visuomotor coordination. J Exp Zool 92, 263–279 (1943b).

Sperry RW. Optic nerve regeneration with return of vision in anurans. J Neurophysiol 7, 57–69 (1944).

Sperry RW. Restoration of vision after crossing of optic nerves and after contralateral transplantation of eye. J Neurophysiol 8, 15–28 (1945).

Sperry RW. Regulative factors in the orderly growth of neural circuits. Growth (Symposium) 10, 63-87 (1951).

Sperry RW. Chemoaffinity in the orderly growth of nerve fiber patterns and connections. PNAS 50, 703-709 (1963).

Sperry RW. Embryogenesis of behavioral nerve nets. In *Organogenesis*, Eds. Dehaan RL, Ursprung H. Holt ,Rinehart and Winston, New York, NY. 161-86 (1965).

Sperry RW. Models, new and old, for growth of retinotectal connections. In *From Theoretical Physics to Biology*, Ed. Marois M, North-Holland Publishing Company. 191-215. (1975).

Stahl B, Müller B, von Boxberg Y, Cox EC, Bonhoeffer F. Biochemical characterization of a putative axonal guidance molecule of the chick visual system. Neuron 5, 735-43 (1990).

Steurmer C, Easter S. Rules of order in the retinotectal fascicles of goldfish. J Neurosci 4, 1045-51 (1984).

Stieda, L. Studien über das centrale Nervensystem der Vögel und Säugethiere. Z Wiss Zool XIX (1868).

Stone LS. Heteroplastic transplantations of the eyes between the larvae of two species of *Amblystoma*. J Exp Zool 55, 193-261 (1930).

Stone LS. Functional polarization in developing and regenerating retinae of transplanted eyes. Ann NY Acad Sci 49, 856-65 (1948).

Stone LS. Normal and reversed vision in transplanted eyes. Arch Ophthal NY 49, 28-35 (1953).

Stone LS. Polarization of the retina and development of vision. J Exptl Zool 145 85-96 (1960).

Straznicky K, Gaze RM. The growth of the retina in Xenopus laevis: an autoradiographic study. J Embryol Exp Morph 28, 87-115 (1971).

Straznicky K, Gaze RM, Horder TJ. Selection of appropriate medial branch of the optic tract by fibres of ventral retinal origin during development and in regeneration: An autoradiographic study in Xenopus. J Embryol Exp Morph 50, 253-67 (1979).

Straznicky K, Gaze RM. The innervation of a virgin tectum by a double-temporal or a double-nasal eye in Xenopus. J Embryol Exp Morph 68, 9-21 (1982).

Sugiyama S, Funahashi J, Kitajewski J, Nakamura H. Crossregulation between En-2 and Wnt-1 in chick tectal development. Dev Growth Differ 40, 157-66 (1998).

Sun W, Li X, He S. Large-scale morphological survey of mouse retinal ganglion cells. J Comp Neurol 451, 115-26 (2002).

Székely G. Untersuchung der Entwicklung optischer Reflexmechanismen an Amphibienlarven. Acta Physiol Hung 6 (1954).

Tanaka M, Kamo T, Ota S, Sugimura H. Association of Dishevelled with Eph tyrosine kinase receptor and ephrin mediates cell repulsion. EMBO J 22, 847-58 (2003).

Tassew NG, Chestopolava L, Beecroft R, Matsunaga E, Teng H, Chedotal A, Monnier PP. Intraretinal RGMa is involved in retino-tectal mapping. Mol Cell Neurosci 37, 761-9 (2008).

Thakar SG, Henkemeyer M. A cue for vision: How EphB1, EphB2, ephrin-B1, and ephrin-B2 mediate retinocollicular mapping. CSH Meeting on Axon Guidance, Syn Plasticity, & Regen Abstr (2010).

Thanos S, Bonhoeffer F. Investigations on the development and topographic order of retinotectal axons: Anterograde and retrograde staining of axons and perikarya with rhodamine in vivo. J Comp Neurol 219, 420-30 (1983).

Thanos S, Bonhoeffer F. Axonal arborization in the developing chick retinotectal system. J Comp Neurol 26; 155-64 (1987).

Thanos S, Vanselow J, Mey J. Ganglion cells in the juvenile chick retina and their ability to regenerate axons *in vitro*. Exp Eye Res 54, 377-91 (1992).

Thor G, Nitsure N, Hastings H. Consequences for retinal growth when vision occurs in S^2 space. BioSystems 24, 25-30 (1990).

Torborg CL, Feller MB. Spontaneous patterned retinal activity and the refinement of retinal projections. Prog Neurobiol 76, 213-35 (2005).

Trivier E, Ganesan TS. RYK, a catalytically inactive receptor tyrosine kinase, associates with EphB2 and EphB3 but does not interact with AF-6. J Biol Chem 277, 23037-43 (2002).

Twitty VC. Correlation in the development of structures associated with transplanted eyes. Proc Soc Exp Biol and Med 55 (1929).

Twitty VC, Schwind JL. The growth of eyes and limbs transplanted heteroplastically between two species of *Amblystoma*. J Exp Zool 59 (1931).

Twitty VC. Influence of the eye on the growth of its associated structures, studied by means of heteroplastic transplantation. J Exp Zool 61 (1932).

Udin SB, Fawcett JW. Formation of topographic maps. Ann Rev Neurosci 11, 289-327 (1988).

Völgyi B, Abrams J, Paul DL, Bloomfield SA. Morphology and tracer coupling pattern of alpha ganglion cells in the mouse retina. J Comp Neurol 492, 66-77 (2005).

Völgyi B, Chheda S, Bloomfield SA. Tracer coupling patterns of the ganglion cell subtypes in mouse retina. J Comp Neurol 512, 664-87 (2009).

Walter J, Kern-Veits B, Huf J, Stolze B, Bonhoeffer F. Recognition of position-specific properties of tectal cell membranes by retinal axons in vitro. Development 101, 685-96 (1987a).

Walter J, Henke-Fahle S, Bonhoeffer F. Avoidance of posterior tectal membranes by temporal retinal axons. Development 101, 909-13 (1987b).

Walter J, Muller B, Bonhoeffer F. Axonal guidance by an avoidance mechanism. J Physiol (Paris) 84, 104-10 (1990).

Wang Y, Thekdi N, Smallwood PM, Macke JP, Nathans J. Frizzled-3 is required for the development of major fiber tracts in the rostral CNS. J Neurosci 22, 8563-8573 (2002).

Watanabe Y, Nakamura H. Semaphorin signaling in tectal laminar formation. CSH Meeting on Axon Guidance, Synaptogenesis & Neural Plasticity Abstr (2008).

Wathey JC, Pettigrew JD. Quantitative analysis of the retinal ganglion cell layer and optic nerve of the barn owl *Tyto alba*. Brain Behav Evol 33, 279-92 (1989).

Whiting PJ, Schoepfer R, Swanson LW, Simmons DM, Lindstrom JM. Functional acetylcholine receptor in PC12 cells reacts with a monoclonal antibody to brain nicotinic receptors. Nature 327, 515-8 (1987).

Wizenmann A, Brunet I, Lam JS, Sonnier L, Beurdeley M, Zarbalis K, Weisenhorn-Vogt D, Weinl C, Dwivedy A, Joliot A, Wurst W, Holt C, Prochiantz A. Extracellular engrailed participates in the topographic guidance of retinal axons in vivo. Neuron 64, 355-66 (2009).

Wöhrn JC, Puelles L, Nakagawa S, Takeichi M, Redies C. Cadherin expression in the retina and retinofugal pathways of the chicken embryo. J Comp Neurol 396, 20-38 (1998).

Wong RO. Retinal waves: stirring up a storm. Neuron 24, 493-5 (1999).

Yamagata M, Herman JP, Sanes JR. Lamina-specific expression of adhesion molecules in developing chick optic tectum. J Neurosci 15, 4556-71 (1995).

Yamagata M, Sanes JR. Lamina-specific cues guide outgrowth and arborization of retinal axons in the optic tectum. Development 121, 189-200 (1995a).

Yamagata M, Sanes JR. Target-independent diversification and target-specific projection of chemically defined retinal ganglion cell subsets. Development 121, 3763–76 (1995b).

Yamagata M, Weiner JA, Dulac C, Roth KA, Sanes JR. Labeled lines in the retinotectal system: markers for retinorecipient sublaminae and the retinal ganglion cell subsets that innervate them. Mol Cell Neurosci 33, 296-310 (2006).

Yamagata M, Sanes JR. Dscam and Sidekick proteins direct lamina-specific synaptic connections in vertebrate retina. Nature 451, 465-9 (2008).

Yamagata M, Sanes JR. Synaptic localization and function of Sidekick recognition molecules require MAGI scaffolding proteins. J Neurosci 30, 3579-88 (2010).

Yates PA, Roskies AL, McLaughlin T, O'Leary DD. Topographic-specific axon branching controlled by ephrin-As is the critical event in retinotectal map development. J Neurosci 21, 8548-63 (2001).

Yates PA, Holub AD, McLaughlin T, Sejnowski TJ, O'Leary DDM. Computational modeling of retinotopic map development to define contributions of EphA-ephrinA gradients, axon-axon interactions, and patterned activity. J Neurobiol 59, 95–113 (2004).

Yoon MG. Retention of the original topographic polarity by the 180 degrees rotated tectal reimplant in young adult goldfish. J Physiol 233, 575-88 (1973).

Yoon MG. Readjustment of retinotectal projection following reimplantation of a rotated or inverted tectal tissue in adult goldfish. J Physiol 252, 137-58 (1975).

Yoshikawa S, McKinnon RD, Kokel M, Thomas JB. Wnt-mediated axon guidance via the *Drosophila* Derailed receptor. Nature 422, 583-588 (2003).

Zhang JH, Cerretti DP, Yu T, Flanagan JG, Zhou R. Detection of ligands in regions anatomically connected to neurons expressing the Eph receptor Bsk: potential roles in neuron-target interaction. J Neurosci 16, 7182- 92 (1996).